

**Vessel-on-a-Chip Model: Nanoparticle Trafficking in Blood Vessels**

by

Madhumita Suresh

A Thesis submitted to the Faculty of Graduate Studies of

The University of Manitoba

in partial fulfillment of the requirements of the degree of

**MASTER OF SCIENCE**

Rady Faculty of Health Sciences

College of Pharmacy

University of Manitoba

Winnipeg

Copyright © 2022 by Madhumita Suresh

## ABSTRACT

Nanoparticles (NPs) are engineered particles in the nanometer range used as carriers to deliver drugs to the target sites and avoid off-target drug accumulation, a concept applied for several decades in tumor targeting. Most NPs developed for cancer therapy are intravenously administered where the endothelial barrier lining the lumen of the blood vessels is the first barrier they interact with before extravasating into the target tissues. Little is known about the interaction of NPs with the endothelial barrier under conditions simulating angiogenic blood vessels of the tumor microenvironment, namely the shear stress on the endothelial cells (ECs) due to blood flow and the chromosomal abnormalities of this special population of ECs. We hypothesize that the interaction and the impact of NPs on the ECs are influenced by the shear stress and the chromosomal instability or aneuploidy of ECs. As conventional models are static, they fail to account for the dynamism seen physiologically, resulting in discrepancies between *in vitro* and *in vivo* experiments. Therefore, we will rely on microfluidic cell models (organ-on-a-chip models) that expose the cells cultured in microscale channels to fluids at highly controlled and replicable flow conditions mimicking *in vivo* scenarios while using minimum resources. We have used vessel-on-a-chip models to evaluate a novel class of indium-based quantum dots (QDs) and compared the results to conventional cadmium-based QDs. Overall, our results support our hypothesis that dynamic conditions and cell aneuploidy result in different cell phenotypes resulting in different cell responses, mainly cell viability and cell uptake of QDs. Results in this study are believed to direct future research lines towards minimizing the discrepancies between *in vitro* and *in vivo* responses and better defining cell responses of NPs using physiologically relevant *in vitro* cell-based assays.

## ACKNOWLEDGEMENT

I found interest in nanomedicine, which has taken me from Newfoundland to Atlanta and back to Canada to the University of Manitoba. The interest in nanoparticles sparked in my initial stint at Mercer University, Atlanta, has grown and blossomed to fruition here at the College of Pharmacy, University of Manitoba. From a nerdy clinical dietitian turned full-time mother to an aspiring nanoscientist, my life has radically transformed in the past two years.

I owe this entirely to my supervisor, Dr. Hagar Labouta, to whom I will be eternally grateful. I will fall short of words to express how instrumental she has been in every little success I had here. Her wise words of advice, constant guidance, and unfailing encouragement and determination have truly empowered me. She has taught me how to collect my thoughts, process them critically and deliver them collaboratively. In the endless challenges thrown at us by COVID-19 and lockdown, her undaunted efforts to keep up the team spirit and carry on with work to our best in these challenging times have been quite contagious. She is truly my role model as a mom and as a woman in science, and I am thankful to her for this wonderful opportunity to watch and learn how to channel my skills and bring out my best under her supervision.

In these two years, I have also grown in self-confidence and life skills, and this holistic personal growth would be impossible without my loving family. I have always had two strong pillars of support through good and challenging times in my lovely mother-in-law and my beloved husband. They have both encouraged me and believed in me when I did not. The very reason I pursued my Master's is thanks to my dear husband, Patanjali Tatikola; he always had my back and nudged me forward every time he sensed me slackening!

Words cannot describe my gratitude for my mother-in-law, Dr. Kanakalakshmi Tatikola, who means the world to me. She has always supported me as a mom rather than a mother-in-law and inspired and motivated me. It warms my heart to say what immense, endless love and indomitable spirit of sacrifice she has modeled from the day I have known her. I have always had a mentor and confidante in her and a reassuring hand of blessings over her littles. Her reassuring presence, especially with a toddler in tow and a baby on the way at the peak of my project, has been a Godsend! I love you, mom!

I would gratefully acknowledge our past lab member, Dr. Shahla Shojaei. I am fortunate to have had a chance to work with Shahla as she shared her knowledge and provided significant input for my project. I am thankful to her for her training and guidance with cell-culture techniques, and I greatly benefitted from her academic experiences, which have helped me design my experiments and manage my time wisely. Her inputs and insightful discussions on my project have enriched me and built my confidence throughout my degree.

I sincerely thank my committee members, Dr. Geoff Tranmer, Dr. Donald Miller, and Dr. Dake Qi, for being the most supportive advisors one could ask for. Their constant feedback, valuable remarks, and reflective questions regarding my project and guidance and direction have helped me shape my project and delve deeper each time, significantly honing my research acumen.

I sincerely thank Dr. Max Anikovskiy and his team at the University of Calgary for their invaluable discussions that have helped me with my project.

I sincerely thank Dr. Pingzhao Hu from the Department of Biochemistry and Medical Genetics, University of Manitoba, for analyzing the data, which is crucial for my thesis. I thank them for the time and insightful knowledge that they shared with me.

I thank our team of smart undergraduate research students - Tushar Upreti, Mohammad Kiumarsi, and Simran Dhaliwal, for every little help they forwarded me in the lab and for sharing their valuable feedback regarding my project.

I thank the University of Manitoba, NSERC, Research Manitoba, and my supervisor for taking care of my financial aid. It has been a pleasure being a part of the UofM student community and a member of the Labouta lab.

## **DEDICATION**

I dedicate my work to my loving parents - Dr. G.Suresh and Mrs. Lakshmi - I would not exist without them.

I dedicate my work to my amazing mother-in-law, who has held my hand and taught me life.

I am immensely grateful for all their tolerance, abundant blessings, and endless love, and I hope I can be that person for my kids!

My work is forever dedicated to my children: Divija and Lalithaditya.

You mean the world to me and remind me to strive harder and be better for your sakes!

## TABLE OF CONTENTS

ABSTRACT.....	1
ACKNOWLEDGEMENT .....	2
DEDICATION.....	4
LIST OF TABLES .....	7
LIST OF FIGURES .....	8
CHAPTER 1: INTRODUCTION, RATIONALE, HYPOTHESIS, AND OBJECTIVES .....	10
1. INTRODUCTION: .....	10
1.1. Nanomedicine and Nanoparticles (NP) in tumor targeting:.....	10
1.1.1. Quantum Dots .....	10
1.2. Nanoparticle - Endothelial Cell Interactions:.....	11
1.2.1. Microvasculature and the Endothelium .....	12
1.2.2. Vascular Biomechanics: Shear stress-induced phenotypical changes in the endothelial cells	14
1.2.2.1 Microfluidic vessel-on-a-chip models.....	15
1.2.3. Genotypical Changes: Aneuploidy of tumor endothelial cells.....	17
1.2.4. State of the art on NP-EC interactions .....	19
1.3. Analysis of Impact of NP on the Endothelium: .....	21
1.3.1. Cell viability & impact on Intracellular machinery .....	21
1.3.2. Cell uptake by Confocal Imaging .....	23
1.3.3. Cell Transcriptome Analysis.....	24
2. RATIONALE.....	29
3. HYPOTHESES .....	30
4. AIMS.....	30
CHAPTER 2: MATERIALS AND METHODS .....	32
1. Designing Indium-Based Quantum Dots: .....	33
1.1 Synthesis of Indium Phosphide/Zinc Sulphide Quantum Dots .....	33
1.2 Transfer of InP/ZnS QDs into Water via Ligand Exchange: .....	35
2. Characterization: .....	36
3. Colloidal Stability of MPA-Capped InP/ZnS QDs in Water and Culture Media: .....	36
4. Cell Culture:.....	37
5. Cell Viability Assay:.....	37
6. Dynamic Vessel-On-A-Chip Experiments.....	38

6.1	Developing a vessel-on-a-chip model:.....	38
7.	HUVEC Cell Morphology .....	41
8.	Cell Uptake by Confocal Microscopy.....	42
8.1	Sample Preparation and Immunofluorescence staining: .....	42
8.2	Confocal Imaging:.....	43
9.	Transcriptomic Analysis .....	43
9.1	Pathway Enrichment Analysis: .....	44
Chapter 3: RESULTS AND DISCUSSION .....		45
1.	Quantum dots – synthesis, composition, and physicochemical properties: .....	45
2.	Colloidal stability of MPA-capped InP/ZnS QDs in water and culture media: .....	48
3.	Cell models: .....	52
4.	Cytotoxicity of Quantum Dots:.....	54
5.	Development of Dynamic Vessel-on-a-Chip Model: .....	58
6.	Nanoparticle – Endothelial cell interactions: .....	59
6.1	Cell uptake of QDs using confocal microscopy:.....	59
7.	Transcriptome Analysis: .....	64
7.1	Effect of exposure of Euploid HUVEC cells to dynamic conditions:.....	66
7.2	Effect of Induction of Aneuploidy in HUVEC cells under Static Conditions: .....	70
7.3	Effect of Exposure of Aneuploid HUVEC Cells to Dynamic Conditions: .....	73
7.4	Effect of Induction of Aneuploidy on HUVEC cells under Dynamic Conditions:.....	76
7.5	Effect of CdSe/ZnS QDs on Euploid HUVEC Cells under Static Conditions:.....	79
7.6	Effect of InP/ZnS QDs on Euploid HUVEC Cells under Static Conditions:.....	82
7.7	Effect of CdSe/ZnS QDs in Euploid HUVEC cells under dynamic conditions:.....	84
	.....	88
7.8	Effect of Exposure to InP/ZnS QDs on Euploid HUVEC cells under Dynamic Conditions: .	88
7.9	Effect of Exposure to CdSe/ZnS QD on Aneuploid HUVEC Cells in Static Conditions:.....	91
7.10	Effect of Exposure to CdSe/ZnS QDs on aneuploid HUVEC cells under dynamic conditions	94
7.11	Effect of InP/ZnS QDs on Aneuploid HUVEC cells under static conditions: .....	96
7.12	Effect of InP/ZnS QDs in aneuploid HUVEC cells in dynamic conditions:.....	99
CHAPTER 4 – SUMMARY.....		103
BIBLIOGRAPHY .....		110

## LIST OF TABLES

Table 1	Molar concentrations of mercaptopropionic acid (MPA, MW 106.14) and tetramethylammonium hydroxide (TMAH, MW 181.23) used in the ligand exchange reaction to prepare water-dispersible quantum dots	35
Table 2	Groups for Flow Experiment on Vessel-on-a-chip model	42

## LIST OF FIGURES

Figure 1:	Hierarchy of Blood Vessels	12
Figure 2	Cross-Section of Blood Vessels	13
Figure 3	Quantum dots synthesis setup	35
Figure 4	(A) Freshly prepared InP/ZnS QDs suspended in chloroform, (B) Prepared QDs show fluorescent under UV light	35
Figure 5	Structure of 3-mercaptopropionic acid	36
Figure 6	Capping InP/ZnS QD with 3-mercaptopropionic acid	37
Figure 7	Vessel-on-a-Chip with Normal HUVEC	41
Figure 8	Vessel-on-a-Chip with Monastrol treatment	41
Figure 9	Vessel-on-a-chip model connected to the flow system	42
Figure 10	Size of InP/ZnS QDs. (A) TEM image of InP/ZnS QDs, (B) Histogram of InP/ZnS QD diameter.	48
Figure 11	Fluorescence curve comparing MPA-capped InP/ZnS QD capped with MPA to conventional CdSe/ZnS QD	49
Figure 12	Stability of MPA capped InP/ZnS QD in water over 40 days at 37°C.	51
Figure 13	Stability of MPA capped InP/ZnS QD in EGM-2 media with supplements over 31 days at 37°C.	52
Figure 14	(A) Normal and aneuploid HUVEC cells with DAPI stained nuclei at different magnifications, (B) Quantification of abnormal nuclei after monastrol treatment for 20 hours, (C) Monoester formation characteristic of mitosis inhibition by monastrol.	54
Figure 15	Comparing bioluminescence of CdSe/ZnS QDs and InP/ZnS QDs dispersed in culture media for interference, ns denotes statistical non- significance ( $p > 0.05$ ).	56
Figure 16	ATP Control Assay	56
Figure 17	Control groups with normal and aneuploid HUVEC cells	57
Figure 18	Viability of HUVEC cells in the presence of CdSe/ZnS and InP/ZnS QDs.	58

Figure 19	Bright-field images of HUVEC cells in a vessel-on-a-chip model under different conditions (static condition, dynamic flow, and cell aneuploidy) without and following QD exposure	63
Figure 20	Confocal images of HUVEC cells of HUVEC cells in a vessel-on-a-chip model under different conditions (static condition, dynamic flow, and cell aneuploidy) without and following exposure to QDs.	64
Figure 21	Effect of the dynamic conditions on the Euploid HUVEC cell transcriptome.	70
Figure 22	Effect of aneuploidy induction on the cell transcriptome of HUVEC under static conditions.	73
Figure 23	Effect of the dynamic conditions on Aneuploid HUVEC cell transcriptome.	76, 77
Figure 24	Effect of induction of aneuploidy on HUVEC cell transcriptome under dynamic conditions	79, 80
Figure 25	Effect of exposure to CdSe/ZnS QDs on Euploid HUVEC cell transcriptome under static conditions.	82
Figure 26	Effect of exposure to InP/ZnS QDs on Euploid HUVEC cell transcriptome under static conditions.	84, 85
Figure 27	Effect exposure to CdSe/ZnS QD on Euploid HUVEC cell transcriptome under dynamic conditions.	88, 89
Figure 28	Effect of exposure to InP/ZnS QDs on Euploid HUVEC cell transcriptome under dynamic conditions.	91, 92
Figure 29	Effect of exposure to CdSe/ZnS QDs on Aneuploid HUVEC cell transcriptome in a static condition.	94
Figure 30	Effect of exposure to CdSe/ZnS QD on aneuploid HUVEC cell transcriptome under dynamic conditions.	97
Figure 31	Effect of exposure to InP/ZnS QDs on aneuploid HUVEC cell transcriptome in a static condition.	99, 100
Figure 32	Effect of exposure to InP/ZnS QDs on aneuploid HUVEC cell transcriptome under dynamic conditions.	102, 103

## **CHAPTER 1: INTRODUCTION, RATIONALE, HYPOTHESIS, AND OBJECTIVES**

### **1. INTRODUCTION:**

#### **1.1. Nanomedicine and Nanoparticles (NP) in tumor targeting:**

Nanotechnology applications in the medical sciences encompass developing diagnostics and therapies targeting diseased sites (e.g., tumor or inflamed tissue) and avoiding off-target accumulation. Nanoparticles (NPs) are engineered particles in the nanometer range with size-dependent properties. The NP core can have different compositions – lipid, protein, polymeric, or inorganic. By engineering the design properties of NPs, e.g., size and surface chemistry, NPs can have a longer systemic circulation time, bypassing the first-pass metabolism, thereby requiring lower doses of the loaded drug to achieve better therapeutic outcomes.<sup>1-4</sup> The design properties of NPs can also be tailored to control the rate, time, and location of drug release, thereby improving the safety, efficacy, and transport across biological barriers.<sup>1,3,4</sup> These factors are especially important for delivering potent drugs such as chemotherapeutic agents.

Most clinically approved NP-based therapies are used for tumor targeting and are administered intravenously.<sup>5,6</sup> Based on their size, circulating NPs exit the leaky angiogenic tumor vessels and accumulate in the tumor tissues due to the poor lymphatic drainage that characterizes the microenvironment in many human solid tissue cancers. This phenomenon is called the enhanced penetration and retention (EPR) effect.<sup>2</sup> Some examples of marketed NP products are Doxil®, a PEGylated (polyethylene glycol-coated) liposomal formulation of doxorubicin, nanocrystal drug Rapamune, an immunosuppressant to prevent organ rejection of kidney transplants in recipients, inorganic iron oxide NPs coated with amino silane called Nanotherm, which is used in local thermal ablation of tumors.<sup>5-7</sup>

##### **1.2.2.1 Quantum Dots**

Quantum dots (QDs) are inorganic, metallic nanoparticles with different compositions and significant biomedical applications. Their size ranges from 2 – 10 nm in diameter, and they exhibit size-dependent properties.<sup>8-10</sup> QDs are photostable, auto-fluorescent, and not subject to photo-bleaching.

QDs are nanoscale clusters of semiconductor atoms forming the core and the shell, and the surface is functionalized with a polymeric capping agent. The core constitutes semiconductor material such as cadmium selenide (CdSe) or indium phosphide (InP). The ions in the core compound do not exhibit a detectable photoluminescent emission spectrum; however, the epitaxial growth of shells using semiconductors with wider bandgaps, typically zinc sulphide (ZnS) or zinc selenide (ZnSe), surrounds and stabilizes the core by sharing electrons with the core compound ions. Thereby the quantum yield of photoluminescence is increased.<sup>11,12</sup>

Cadmium-based QDs have been prevalent for a long time but are controversial for biological applications.<sup>13-16</sup> Cadmium<sup>17</sup> and cadmium-based QDs<sup>18-22</sup> are known for their toxicity to cells resulting in inhibition of cell proliferation and differentiation, apoptosis, damage of DNA repair mechanism, mitochondrial toxicity, and chromosomal aberrations and mutations.<sup>17,20,23</sup> Hence, several attempts were conducted to coat the QDs to reduce toxicity.<sup>13,24-26</sup> Nevertheless, there is still a potential for leaching Cd ions from packing defects on the QD surface, resulting in cellular toxicity.<sup>12</sup>

QDs with indium phosphide (InP) core and zinc sulphide (ZnS) shell were therefore proposed as a safe alternative for cadmium-based QDs (toxic), particularly for cancer diagnosis.<sup>11,27-29</sup> The InP core has a very poor visible fluorescence emission, and the emission spectrum becomes visible by adding multiple ZnS shells. The ZnS shells enhance the optical properties as the core ions share electrons with the Zn ions of the shell, increasing the bandwidth for the movement of excitons. The core-shell assembly as initially prepared is hydrophobic and is dispersed as a colloid in organic solvents like hexane or chloroform.<sup>12</sup> The QD then requires surface modification by an amphiphilic capping agent serving two purposes – to render the QDs dispersible in aqueous media by addition of ionizable functional groups to the surface and to render it suitable as a drug carrier/vehicle by covalent functionalization of the nanocrystal with antibodies, drugs, nucleic acids or other biomolecules.<sup>29</sup>

## **1.2. Nanoparticle - Endothelial Cell Interactions:**

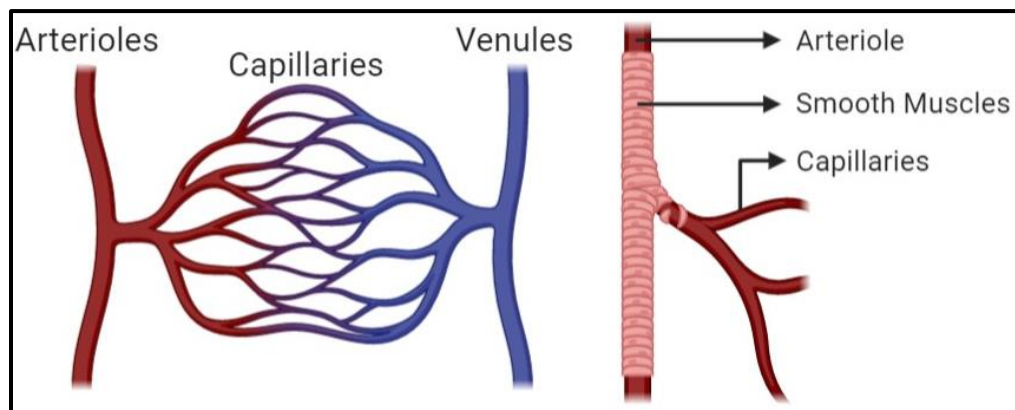
Irrespective of the administration site for any NP – be it transdermal, oral, pulmonary, or intravenous, they eventually end up in the blood circulation (specifically in the microcirculation) before reaching their target sites. Further, most applications of NPs involve intravenous

administration. The cells lining the blood vessel walls constitute the first barrier the NPs cross to reach the target site. So, it is vital to understand the vasculature and the morphology of cells associated with it to understand better the impact of those NPs on the endothelium lining the blood vessels before reaching the target site of action.

### 1.2.2.2 Microvasculature and the Endothelium

The blood vessels form a vast network that supplies the tissues and organs with vital oxygen and nutrients that nurture and sustain the body. The hierarchy of blood vessels (Figure 1) begins with arteries. Each artery branches out into several arterioles, meta-arterioles, precapillary sphincters, and true capillaries. All gaseous and nutrient exchange occurs at the capillary level. Capillaries converge to form small venules – both are the primary exchange vessels. The venules converge to form collective venules that further combine to form veins.

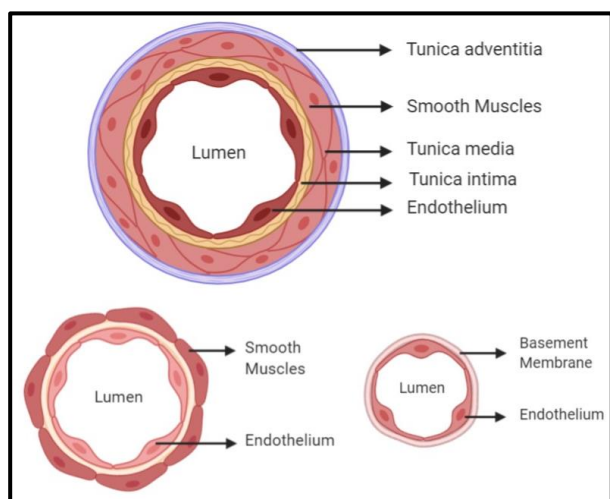
**Figure 1: Hierarchy of Blood Vessels** - Hierarchically, blood vessels progress from the heart and branch out as arterioles and into capillaries that converge to form venules that further converge to form veins. Except for capillaries, all higher-order vessels are covered with smooth muscle layers.



A cross-section of blood vessels (Figure 2) shows that primary vessels - arteries, and veins consist of 3 layers: the outer tunica adventitia, the middle tunica media, and the innermost layer, the tunica intima. In the subsequent branches, the thickness of the outer and middle layers gradually decreases. The innermost tunica intima is the only layer in the capillaries and small venules where

gas and nutrients exchange with the tissues. Hence, the endothelium is the most vital layer, and the other outer layers essentially offer structural support.<sup>30,31</sup>

**Figure 2: Cross-Section of Blood Vessels** Cross-section of all major to minor vessels shows a progressive decrease in the number of layers of cells. Major vessels like arteries and veins have five layers – innermost endothelium, tunica intima, tunica media, smooth muscles, and tunica adventitia. Minor vessels like arterioles and venules have just the smooth muscles and endothelium, while capillaries have only a layer of endothelial cells covered by the basement membrane.



The tunica intima comprises a monolayer of endothelial cells (EC) and lines the innermost lumen of the entire circulatory system. The endothelial cells support tissue growth and repair by sustaining blood supply to tissues and regenerating the microvasculature by angiogenesis. ECs have a variety of functions. The endothelium maintains vascular homeostasis and regulates local cell growth, and the extracellular matrix acts as a barrier between blood and organs and is responsible for transferring nutrients, hormones, and white blood cells in anti-inflammatory responses. It participates in wound repair processes, regulation of blood pressure, blood flow, and coagulation and has crucial roles in the pathophysiology of several diseases.<sup>32,33</sup>

*In vivo* and *ex vivo* animal models have been used to represent the physiology of various organ systems, but their EC phenotype is different from human ECs.<sup>34</sup> In some studies, *in vitro* 2D and 3D cell cultures, were shown to replicate the microvasculature.<sup>35-37</sup> Several *in vitro* models were

therefore developed. These models have helped develop insights into the molecular mechanism of angiogenesis and vasculogenesis, the degree of differentiation into arteries or veins, and the interaction between drug molecules and the cells.<sup>38</sup>

It is important to develop bio-relevant platforms that mimic the natural dynamic physiology of human blood vessels and use endothelial cells of human origin to translate developed therapies and diagnostics, especially those intended for intravenous administration. One of the primary cells extensively used as an *in vitro* model to study endothelial cell functions is the human umbilical vein endothelial cells (HUVEC).<sup>39</sup> HUVEC models have been useful for the *in vitro* study of cardiovascular pathophysiologies, such as platelet adhesion to the endothelium, endothelial damage and repair, and the potential impact of atherosclerosis in early and progressive stages.<sup>39</sup> However, these *in vitro* models do not accurately picture the actual pathophysiology that can be visualized *in vivo* – both dimensionally and dynamically. Conventional *in vitro* static models consist of well-plates, test tubes, or slides/coverslips in petri-dishes on which studies are conducted. These do not account for the 3D structure of the vessels, the mechanical forces on the endothelium, and the fluid dynamics in the human blood vessel due to constant laminar blood flow. With the advent of organ-on-a-chip models for *in vitro* studies,<sup>40</sup> demerits of conventional methods could be overcome; this is described in detail in the following sections.

### **1.2.2.3 Vascular Biomechanics: Shear stress-induced phenotypical changes in the endothelial cells**

ECs are subject to wall shear stress (WSS), the unidirectional laminar force exerted by blood flow on the endothelial cells. According to Poiseuille's law, shear stress ( $\tau$ ) is defined as

$$\tau = \frac{4Q\eta r^3}{\pi} \quad (\text{Equation 1})$$

where Q is the fluid flow rate, and  $\eta$  is the fluid viscosity.

WSS is considered a biomechanical stimulus that is responsible for the angiogenic and vasculogenic functions of ECs, as the laminar force exerted by the blood flow on the ECs, activates the biomolecules and receptors responsible for cell growth, arrangement, branching, and so on to be able to function and thrive and provide structural support to the blood vessels.<sup>41,42</sup> The magnitude of WSS and type of flow also alter the phenotype of the cells and impact the expression of surface receptors and other effects on the EC genetic machinery.<sup>43-45</sup> Acute shear stress in the

blood vessels activates signaling cascades in ECs, with the consequent acute release of nitric oxide and prostacyclin. It also triggers responses similar to inflammatory cytokines to adapt to chronic shear stress. It also adapts by structural remodeling and flattening to minimize shear stress.<sup>43</sup> Chronological increase in WSS, as in pathological vascular conditions such as hypertension, can be detrimental to the endothelial phenotype tissue. These conditions could result in thrombus formation due to aggregation of platelets or atherosclerosis and further worsen the already existing high shear stress impacts.<sup>46</sup>

The shear stress ranges from the low value of  $< 1$  dyne/cm<sup>2</sup> in the normal physiology of large veins and tends to be highest in small arterioles, reaching 60 to 80 dynes/cm<sup>2</sup>.<sup>43,44,47-49</sup> Shear stress in tumor is within the range of 0.1 dyn/cm<sup>2</sup> to 1-40 dyn/cm<sup>2</sup>, whereas in normal physiological conditions, the shear stress is 1-4 dyn/cm<sup>2</sup> in the veins, 10-20 dyn/cm<sup>2</sup> in the capillaries and 4-30 dyn/cm<sup>2</sup> in arteries.<sup>47,48</sup>

#### **1.2.2.4 Microfluidic vessel-on-a-chip models**

Translating medical research from benchtop to bedside involves three significant steps: in vitro, in vivo, and clinical trials. This process is time-consuming, utilizes plenty of resources, and does not always guarantee a successful human translation due to anatomical and physiological differences. This issue is addressed to a vast extent by microfluidics, a technology that manipulates small volumes ( $10^{-9}$  to  $10^{-18}$  liters) of fluids (droplets, microchannels, jets, and thin water films) where at least one dimension of the fluid studied falls below a millimeter.<sup>50,51</sup>

The use of microfluidic channels enables physiological relevance of the fluid flow properties and can be explained by understanding the different flow regimes in channels. Fluid flow can be laminar or turbulent. Laminar flow involves the smooth or regular flow of particles in parallel paths within the fluid. Thus, laminar flow is also known as streamline or viscous flow. Contrary to laminar flow, turbulent flow is characterized by the irregular movement of fluid particles. In turbulent flow, the fluid particles do not flow in parallel layers. There is a great deal of lateral mixing and disruption between the layers. At the macroscale, the fluid flow properties are generally turbulent and not predictable. However, at the micro-scale, fluid properties and characteristics differ vastly from macroscale – fluid viscosity and capillary flow dominate microchannels, and fluids maintain laminar flow, mimicking physiological conditions. We could

further explain this using the Reynolds number ( $R_e$ ) to categorize the flow type in the channels.  $R_e$  is the ratio of the inertial forces to viscous forces in a fluid flow; it is a dimensionless number.<sup>52,53</sup> It is defined as

$$R_e = \frac{\rho VL}{\mu} \quad (\text{Equation 2})^{52}$$

where  $\rho$  is the fluid density,  $V$  is the flow velocity,  $L$  is the length or diameter of the channel (the smallest dimension), and  $\mu$  is the dynamic viscosity of the fluid. The flow is laminar when  $R_e$  is below 100, and generally, no turbulence occurs until the  $R_e$  is in the range of 2000. At least one dimension in microfluidic platforms is in  $\mu\text{m}$ ; the  $R_e$  is less than 100 and possibly below 10<sup>52-54</sup>. Laminar flow mimics physiological conditions and makes the fluid properties and molecular transportation predictable, allowing for precise flow through the microchannels.<sup>54-56</sup>

The microscale dimensions also enable cellular and molecular level studies with minimal samples and reagents to obtain high resolution and sensitivity results, especially useful when handling rare samples. Its high-throughput capabilities maximize output using minimum resources, resulting in optimal usage of resources and less wastage. Furthermore, their minimal use of space and time is undoubtedly helpful.<sup>57</sup>

Organ-on-a-chip models are micro-engineered biomimetic systems containing microfluidic channels in which viable human cell lines are cultured under conditions that replicate the microstructure of organs and tissues and the dynamic environment, thereby, the pathophysiology of organs/tissues *in vitro*. This technology was further explored in recent years to develop valuable data on the toxicity, efficacy, and interactions of drugs with cells by modeling organs such as the lungs, the kidneys, the skin, the gastrointestinal system, and many more. These platforms model healthy and diseased states and can be low-cost, high-throughput alternatives to conventional animal models for pharmaceutical studies.<sup>58-63</sup>

Different organ-on-a-chip models have been developed using various techniques to carry endothelial cells of different origin, co-cultured with tumor or other organ cells<sup>61,64,65</sup> such as tumor-on-a-chip<sup>66,67</sup>, lung-on-a-chip<sup>68-70</sup>, retina-on-a-chip<sup>71</sup>, blood-brain barrier<sup>35,72-74</sup>, placenta<sup>34,75-79</sup> and so on. Vessel-on-a-chip models are specific platforms that are stand-alone representative of blood vessels. They consist of channel vessels with endothelial cells of any

origin, cultured using 2D or 3D methods.<sup>80,81</sup> Recent developments in this field of microfluidics have shown increased interest in studying blood vessels by themselves, and we, therefore, have come across several models lately.<sup>58,82-84</sup> Fabricated polycarbonate film channels<sup>82</sup>, cell patterning<sup>85</sup>, sacrificial molds<sup>86</sup>, 2D and 3D bioprinting<sup>80</sup>, hydrogel scaffolding<sup>58,86</sup> are some state-of-the-art microfluidic vessel models that are currently being studied. These models are used to study several aspects of vasculature from angiogenesis and vasculogenesis<sup>87,88</sup>, effects of shear stress and fluid dynamics within the vascular blood flow<sup>48,55</sup>, studying tumor vasculature<sup>21,58,66,89</sup>, studying other pathophysiological conditions in vasculature<sup>83,90-93</sup>, outcomes of NP interactions with vascular ECs<sup>36,94-100</sup>, and many more. These models are mostly the first of their kind and explore single parameters in depth. In our vessel-on-a-chip model, we plan to incorporate a simple flow system with HUVEC cells (with or without chemically induced aneuploidy) and subject it to shear stress or static conditions, and test for cellular uptake of QDs and compare the outcome to similar conditions without exposure to QDs. Although several individual models exist, as stated in various literature sources, no vessel-on-a-chip model exists for testing the impact of NPs on euploid and aneuploid ECs (discussed in the next section) under conditions of shear stress.

#### **1.2.2.5 Genotypical Changes: Aneuploidy of tumor endothelial cells**

*In vitro* studies typically employ normal euploid cells to test the various hypotheses of biological applications. Euploidy is defined as the condition in which a haploid (2n) number of chromosomes exists in the genes, and this is what we see in normal primary cells. However, circumstantially if there is a variation in this number, and more or less than two chromosomes are present, it is termed aneuploidy. Aneuploidy is a state characterized by the presence of aberrations in either the whole number of chromosomes (more or less than usual) or, by extension, the gains or losses in chromosome arms.<sup>101</sup> It is a consequence of chromosomal instability, a consistently high rate of gain or loss of chromosomes (whole or arms) seen in human cells, and missegregation of chromosomes.<sup>102</sup> Although it occurs commonly in several birth anomalies, aneuploidy is also a prominent marker for cancer.<sup>102,103</sup> Recently, aneuploidy was also proposed to lead to chromosomal instability suggesting a positive feedback loop resulting in increasing levels of aneuploidy.<sup>104,105</sup>

The innermost lumen consists of ECs with a regular spindle-shaped structure without many cytoplasmic projections in a healthy vasculature. The EC layer is covered by a basement membrane

(BM) (a layer rich in collagen, laminin, and fibronectin) and Pericytes (vital for the vessels' structural and functional stability and control). In tumor tissues, the ECs recruited to form the tumor vasculature are deficient in these structural and functional characteristics showing poor barrier function and fewer pericytes, causing gaps or leaks called fenestrae. There is also a defective hierarchical arrangement of vessels, irregularity in size, shape, and vasculogenesis. Genetic expression profiling of normal versus tumor ECs revealed distinct tumor endothelial markers known as "Mobile" RNA or miRNA, which varied amongst primary tumors and metastases. The role of this miRNA is to act as a recruiting agent that moves back and forth from tumor ECs to normal ECs via gap junctions or exosomes. Its functions are: to promote angiogenesis of tumor ECs, intravasation, extravasation, and secondary extravasation to metastasize.<sup>106</sup>

Little is understood about the microvasculature in a tumor-microenvironment at the genetic level. Until recently, it was assumed to be diploid or euploid like normal vascular ECs. However, there is clear evidence from recent studies indicating that the tumor ECs are not just aberrant in their phenotype and function, but this abnormality extends to the aneuploid nucleus as well.<sup>103-105,107-110</sup> Therefore, chemically induced aneuploidy in lab conditions allows us to simulate a tumor-like microvascular environment to study these factors in detail.<sup>110-114</sup>

Despite evidence on aneuploid tumor ECs, *in vitro* models have commonly employed primary endothelial cells (euploid) for screening the impact of NPs.<sup>20,115,116</sup> The impact of NPs on and their interaction with aneuploid endothelial cells were overlooked in previous work and have not been considered to date. Using aneuploid cell models for screening NPs, this novel approach will pave the way for a more in-depth understanding of NP-aneuploid EC interactions. This approach accurately depicts the impact of NPs on aneuploid ECs in cancer patients and will enable the design of NPs with expected behavior in angiogenic tumor vessels. As this area is still uncharted territory, our study will be a one-of-its-kind initiative in this direction.

There have been several studies on chemicals that can induce aneuploidy in cells. Most chemicals studied in the late 1980s affected the metaphase or anaphase<sup>117,118</sup> of mitotic cell division, and more recent studies show that several drugs or chemicals can inhibit mitosis at each stage of mitosis.<sup>119,120</sup> Monastrol is one such mitotic inhibitor used to produce a controlled inhibition of

cell division which is reversible. Studies have especially been using monastrol to induce aneuploidy<sup>101,121</sup> where the mitosis is inhibited at metaphase, and the cell division is slowed down long enough to study the outcomes of aneuploidy, and several further observations can be made using these cells. This method is very useful for our study as we can use the same euploid cell model and induce aneuploidy in the cells for relevant comparison.

#### **1.2.2.6 State of the art on NP-EC interactions**

Several studies focus on investigating the interaction of NPs with cells.<sup>122</sup> These studies are limited to assessing the therapeutic effect or the targeting accuracy and the cytotoxicity of NPs on the cells. Since the ECs form a selective barrier between the blood and tissues and since most applications of NPs involve intravenous administration, the interaction between the NPs and the ECs needs to be investigated and is considered the fundamental basis for the application of NPs.<sup>123</sup>

The physicochemical properties of the NPs, such as size, composition, and surface properties, were shown to have a variable impact on the EC viability and cell uptake under static conditions.<sup>124-126</sup> For instance, cyclic RGD functionalized polymeric NPs associated more with HUVEC cells than control non-functionalized NP counterparts.<sup>126</sup> In another study, Caco-2 cells exposed to a series of polystyrene NP formulations, 100 nm vitamin E TPGS-coated NPs exhibited approximately more than two-fold greater uptake than 50 nm NPs and more than one-fold greater uptake than 500 nm NPs, respectively. Contrary to popular belief that cell uptake of NPs increases on decreasing their particle sizes, this study showed an optimum size range around 100 nm for relatively high cell uptake.<sup>127</sup>

Apart from these physicochemical properties of the NPs, such as size, composition, and surface properties, the serum concentration of NPs, environmental conditions such as cell type<sup>116</sup>, WSS<sup>128,129</sup>, and flow type<sup>95,130</sup> were also found to impact this interaction. Therefore, conventional *in vitro* methods used for NP evaluation lack bio-relevance since they disregard the dynamic conditions.<sup>131-133</sup> Recently, the use of microfluidics has enabled the development of better *in vitro* testing platforms that mimic the dynamic physiological environment.<sup>84,134,135</sup> Scientists have demonstrated the urgent need for developing such dynamic models to translate nano-therapies from bench to bedside with accurate and timely screening.<sup>84</sup>

Studies conducted under flow conditions showcase the hemodynamic conditions prevalent in the blood vessels, which profoundly impact cell morphology and the outcome of NP interactions with cells.<sup>130</sup> Several biomimetic microfluidic models were developed to simulate different physiological and pathological conditions.<sup>134</sup> Among those models, co-culture models, including vascular endothelial cells, were developed to test NPs in conditions that mimic different organ systems such as the placenta<sup>136</sup>, the lung<sup>137</sup>, the cardiovascular system<sup>138</sup>, and tumor microsystems<sup>139</sup>.

A 3D lung-on-a-chip model was developed and studied by Zhang et al.<sup>137</sup>. This model has two parallel microchannels lined with human pulmonary alveolar epithelium and HUVEC cells separately and a middle channel filled with 3D Matrigel. HUVEC cells were subjected to dynamic physiological fluid flow conditions with a flow rate of 10  $\mu\text{l/hr}$ , corresponding to a shear stress of 0.0035  $\text{dyn/cm}^2$ , to mimic the fluid flow *in vivo*. This model was used to study the impacts of acute pulmonary exposure to different concentrations of ZnO, and TiO<sub>2</sub> NPs delivered to epithelial cells. The alterations in alveolar-capillary integrity, barrier function, and junction protein expression due to NP exposure as well as stress responses, namely ROS and apoptosis of both cells, were examined. Collectively, their results showed that cell-cell interactions, cell-matrix interactions, and vascular mechanical cues collectively promote barrier function. Under these conditions, ZnO NPs were found to be relatively more cytotoxic and more permeable to the barrier as compared to TiO<sub>2</sub> NPs.

A vessel-on-a chip model comprised of HUVEC cells was used to mimic conditions of atherosclerosis characterized by permeable microvessels. Permeabilization of the endothelial barrier was induced using tumor necrosis factor  $\alpha$  (TNF- $\alpha$ ).<sup>138</sup> This pathological model was used to study the translocation of lipid-polymer hybrid NPs, where Gold nanocrystals (Au NC) functionalized with Cy5.5 were coated with PLGA and a lipid mixture of DSPE-PEG2000 and DSPC, across the endothelial barrier. Control vessel-on-a-chip model (not treated with TNF- $\alpha$ ) was used to simulate healthy conditions with tightly connected endothelial barrier. This lipid-polymer hybrid NPs were infused in the upper channel at a flow rate of 8  $\mu\text{l/min}$  (1  $\text{dyn/cm}^2$ ), and samples were withdrawn from the lower channel, maintained at a flow rate of 2  $\mu\text{l/min}$ , every 10 min up to 1 hour to measure the concentration of translocated NPs. The percentage NP translocation across the endothelium was calculated using the ratio of fluorescence intensity of

sampled NPs from the lower channel to that of the infused NPs in the upper channel. Overall, endothelialized microchip with controllable permeability could be developed to probe nanoparticle translocation across an endothelial cell layer. These results were then validated using *in vivo* rabbit models. They concluded that the translocation of NPs across the atherosclerotic endothelium is favored at sites with increased endothelial permeability.

In cancer-on-a-chip platforms,<sup>139</sup> modeled by Vu et al. in 2019, in a microfluidic 3D tumor microvasculature model, HUVEC cells and cancer cells (MDA MB-231) demonstrate uptake of NPs due to the EPR effect. HUVECs were treated with a selective TRPV4 agonist to create “tunable” leakiness in the adherens junctions. NPs with different sizes and surface chemistries were tested for extravasation across the endothelial barrier and accumulation in the tumor tissues. The particle size of 40 nm was most favored compared to 70 and 130 nm NPs to penetrate the cell barrier. Comparing 70 nm NPs with carboxylic and tertiary amine surface chemistry, carboxylic acid was more favored in penetrating the cell barrier and avoiding unwanted endothelial interactions, thus concluding that NP interactions with the vasculature do not solely depend on particle size but also their surface characteristics.

In summary, there is existing evidence demonstrating the impact of the dynamic conditions on NP interactions with cells. Microfluidic organ-on-a-chip models were shown to replicate physiological and pathological conditions but their use in evaluation of NPs is still at the early stage.

### **1.3. Analysis of Impact of NP on the Endothelium:**

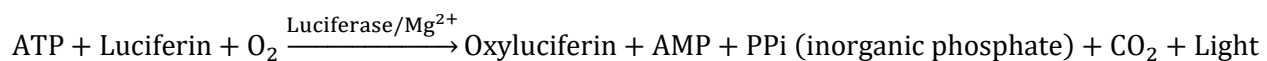
To fully understand the impact of NPs on the ECs, the cells upon exposure to NPs can be evaluated for cell viability, cell uptake of NPs, and cellular changes at the genome level, the cell transcriptome.

#### **1.2.2.7 Cell viability & impact on intracellular machinery**

Cell viability is the ratio of healthy, live cells in a population exposed to a specific environmental condition compared to a control group.<sup>140,141</sup> It is essential to determine cell viability to determine whether the environmental conditions are conducive to cell survival. Several factors like disease state, exposure to toxins, and external stressors can uniquely impact cell viability.<sup>141</sup>

In the case of cancer or aneuploidy in general, <sup>119</sup> cells exhibit enhanced viability, enabling them to proliferate abnormally and evade apoptosis, while exposure to toxic metals or degenerative diseases is characterized by progressive cell loss. Injury and infection also negatively impact cell survival, resulting in necrotic or apoptotic cell death.<sup>20,142</sup> Hence, we can say that there is a crucial link between cellular health and disease which necessitates the measurement of cell viability under different experimental conditions.

Several techniques have been developed for determining cell viability.<sup>22,141,143</sup> Live/dead cell counting assay is one such method to assess cell viability. These tests use either cell-permeable or impermeable dyes or both together to label viable or dead cells in a sample. A good example is trypan blue, a cell impermeable azo dye that cannot penetrate the cell membranes of healthy cells. Only dying cells with damaged membranes take it up, enabling us to count the number of dead (blue) and living (colorless) cells using a hemocytometer.<sup>141</sup> On the other hand, adenosine 5'-triphosphate (ATP) is a major energy source for cellular processes. ATP is thus considered a good biomarker for cell viability testing. Bioluminescence measurement of ATP has been previously described indicating a linear relationship between viable cell number and measured luminescence using the following luciferin-luciferase reaction <sup>21,141,144,145</sup>:



While studying NP – EC interactions, screening the cells for possible toxicity is required to determine a safe concentration to study the impact of NP on ECs. However, there is a chance for NPs to interfere with the screening agents. Hence, it is good to conduct an interference test for NPs under investigation before running the assay to eliminate interference errors. Further screening colloidal stability of NPs in the cell culture media is essential to confirm NP stability, in addition to the use of suitable controls.<sup>21,146</sup> Positive (exposed to a cytotoxin) and negative controls (exposed to buffer) should be used to depict dead or alive cells. Positive controls are mandatory to validate the assay protocol itself by comparing both extreme outcomes (cell death and cells thriving) as previously established by our group.<sup>21</sup> It is also required to calibrate the protocol rather than normalizing the cytotoxicity data solely based on the untreated group alone.

Colloidal stability of NPs is first determined over an extended period to ensure that the NP is stable in the presence of the culture media and the fluorescence properties are not affected by the

components in the media. Tracking the fluorescence of the NPs suspended in the media is done over an extended period, possibly weeks, to ensure their stability. An interference test is done for NPs and the assay reagents to eliminate the potential interaction of NPs with the assay reagents due to the high absorptive power of the NPs (particles with high surface area and high surface energy) or optical interference between the NPs and the assay readings.<sup>21</sup>

#### **1.2.2.8 Cell uptake by Confocal Imaging**

The cell membrane protects the intracellular components from the surrounding environment and potential intoxicants. However, for many NPs, their safe entry into the cells is an important step for their diagnostic or therapeutic effect. In either case, cell uptake of NPs is an important outcome of NP-cell interaction that needs to be investigated to quantify and understand cell responses to NPs. Cell uptake occurs through endocytosis, which could be of 3 types – phagocytosis, pinocytosis, and receptor-mediated endocytosis.<sup>123</sup> This is governed by the physicochemical properties of the NPs and the cell type. Different techniques exist for determining cell uptake of nanoparticles, including SEM, TEM, confocal microscopy, and so on.<sup>147</sup> Of all these methods, the development of confocal imaging has been considered a great addition to the field by allowing for obtaining 3D information of the location of the NPs on or within the cell, based on optical sectioning.<sup>148</sup>

Cell uptake of QDs has been investigated in several *in vitro* studies using different cell types under static conditions, based on their intrinsic fluorescent properties that enable tracking without the need for labeling that might change the surface properties in case of other NPs.<sup>18-20,149-161</sup>

Pollinger et al. studied NP targeted delivery in age-related macular degeneration and diabetic retinopathy. Here Mueller cells and astrocytes represented glial cells (off-target cells), and human dermal microvascular endothelial cells (HDMECs) were the model for retinal capillary endothelium. *In vitro* study of the uptake of CdSe/ZnS QD surface modified with cyclo(-Arg-Gly-Asp-D-Phe-Cys) [cyclo(RGDfC)] showed negligible uptake in off-target cells and strong  $\alpha\beta3$  integrin-mediated interaction with HDMEC. These results were comparable to retinal cells harvested from *in vivo* mice administered with 200 pmol of QD and sacrificed after 1 hour of circulation of the QD. The study confirmed that cyclo(RGDfC)-decorated NPs were ideal for targeting endothelial cells in the posterior eye under physiological conditions.<sup>152</sup> Jiang et al. studied the uptake of amino functionalized CdSe/ZnS QD into HUVECs grown in parallel plates under

flow conditions and into zebrafish vessels. They observed that surface charge and blood flow modulate QD-EC association and uptake in both *in vitro* and *in vivo* conditions.<sup>154</sup>

Samuels et al. studied the uptake of negatively charged thioglycolic acid (TGA) -stabilized CdTe QD (2.7 nm and 4.7 nm) by HUVEC cells in microfluidic channels demonstrating the critical role of shear stress in NP uptake. Here, vascular inflammation related to endothelial damage was simulated by either treating with tumor necrosis factor- $\alpha$  (TNF- $\alpha$ ) or compromising the cell membrane using low Triton X-100 concentration. Both groups were exposed to low, medium, and high SS rates (0.05, 0.1, and 0.5 Pa, respectively). The results showed that a shear stress rate of 0.05 Pa recorded the maximum NP uptake by cells, and this was irrespective of the method of induction of endothelial damage as it had no significant influence on NP uptake.<sup>151</sup>

Most of these studies examined cadmium-based QDs, very few investigated the uptake of InP/ZnS QDs into human endothelial cells under static conditions. It is expected that InP/ZnS QDs would have different uptake than CdSe/ZnS ones despite having the same shell because of the easy dissociation of Cd ions in the presence of aqueous phase combined with cadmium's inherent toxicity rendering the quantum dot cytotoxic to the cells, and could also impact the cell membrane integrity affecting QD internalization.<sup>157</sup>

However, not many cell uptake studies for InP/ZnS QDs under dynamic conditions *in vitro* have been investigated to date. Our study can be considered a novel and pioneering step due to the lack of knowledge on NP interactions with aneuploid cells. Understanding the interaction of NPs with aneuploid cells will enable us to design nano-diagnostics and delivery systems informed by the tumor tissue's microenvironment and have a high potential for clinical translation in cancer.

#### **1.2.2.9 Cell Transcriptome Analysis**

A powerful approach to determine how human cells, including human endothelial cells, respond to a particular biomechanical environment or biotic conditions is to determine how these applied conditions change the expression of its genome.<sup>162,163</sup> The large-scale profiling of NP exposure-induced gene expression alterations in the cells sets the stage for a mechanistic understanding of the behavior of NPs, including targeting, cell uptake, mechanistic toxicological understanding, and so on.<sup>164</sup> Transcriptome analysis is the study of the transcriptome or the RNA transcripts produced

by a genome in a particular cell using high-throughput techniques. A transcriptomic analysis is the latest approach to understanding the intricate functions of mRNA and proteins within the cell. <sup>165</sup>

The whole transcriptome has been studied since the early 1990s, and technological advances have made major transformations in the field. There are two major techniques: microarrays and next-generation sequencing (NGS), known as RNA sequencing (RNA-Seq). Microarray helps to quantify the RNA data in a predetermined sequence of genes. RNA-Seq, on the other hand, uses high-throughput sequencing to capture all sequences present in the transcriptome. Some advantages of microarrays over RNA-Seq are that it is a highly specific assay, less labor-intensive, with more than 90% accuracy. Microarrays, however, also have limitations. A higher quantity of RNA is required, about 1µg, while RNA-seq requires only about 1ng of RNA. A reference genome transcript is required for further analysis of data which is not required for RNA-Seq. Microarrays depend on fluorescence detection of arrays of gene sequence while RNA-Seq detects single nucleotide polymorphism, and lastly, microarrays require confirmation with RT qPCR, whereas it is not mandatory for RNA-Seq data. Hence, we can say that although the technology has advanced with time, microarrays are still relevant and will be a useful and economical alternative to RNA-Seq. <sup>163</sup>

Transcriptomic results in combination with bioinformatics tools provide comprehensive information on the gain or loss of cellular function and thereby the change in the cell's overall behavior. This helps identify specific pathways and cellular processes that respond when the cell is subjected to different conditions. In general, the main purpose of the transcriptomic analysis is to compare specific cell samples in pairs to study certain biological questions. It is important to know and understand how the cells are impacted in structure, proliferation, and metabolism in normal physiological conditions before looking at how any changes to these conditions will affect the cell transcriptome. This will further help understand which specific genes contribute to the affected pathways by identifying the up or down-regulation of these genes and the magnitude of change.

Among the different expression (transcript) profiling techniques, microarray sequencing is a high throughput method that uses high-density microscopic array elements, planar glass substrates, low reaction volumes, multicolor fluorescent labeling, high binding specificity, high-speed

instrumentation for detection, and sophisticated software for data analysis. Specifically, microarrays consist of short nucleotide oligomers or 'probes' fixed on a solid substrate in a chip in small, microscopic spots. The abundance of RNA transcripts isolated from the cells is determined by hybridizing fluorescently labeled transcripts to these probes. The fluorescence intensity at each probe location on the array indicates the transcript abundance for that probe sequence. The signal intensity is normalized to controls and reference samples, indicating whether a particular gene increased, decreased, or showed regular expression. The Final output summarizes each gene included in the microarray and whether the gene is up or downregulated. When several samples are tested in this manner, we can establish a gene expression profile using the microarrays for any given diseased or abiotic state or an exposure condition under investigation. It is also considered a high precision tool for understanding the finer nuances of cell functions and the mechanistic understanding of the cellular functional outcomes in the presence of mechanical stressors and external agents.<sup>166-168</sup> For instance, hemodynamic factors such as laminar shear stress impact the phenotype of endothelial cells upregulating factors such as endothelial nitric oxide synthase (eNOS) and thrombomodulin (TM) that confer potent antithrombotic, antiadhesive, and anti-inflammatory properties to the endothelium.<sup>169</sup> On the contrary, toxic factors like turbulent flow, proinflammatory cytokines, or advanced glycation end products<sup>169</sup> are detrimental to normal endothelial function.

### **1.3.3.1 Transcriptomics for screening nanoparticle-induced cellular outcomes**

Transcriptomics has been recently employed as a useful tool in several nanomedicine-related works, particularly for screening the impact and potential cytotoxicity of NPs.<sup>170-172</sup>

Techniques for detecting cell viability, stress response, inflammatory response have been used conventionally for NP cytotoxicity screening.<sup>173</sup> This could include detecting mitochondrial activity via MTT assay, detecting LDH release upon necrosis, Annexin V for staining apoptotic and necrotic cells, detecting intact lysosomes by neutral red uptake, and detecting ATP release by live cells, detection of apoptosis marker Caspase-3, and so on. The stress response is detected by measuring reactive oxygen species and Inflammatory response by enzyme-linked immunosorbent assay (ELISA).<sup>173</sup> These techniques only focus on the macromolecular consequences of biochemical processes. However, with time and technological advancements, several refined techniques classified under '-omics' nomenclature such as genomics, proteomics, metabolomics,

transcriptomics, lipidomics, cytomics, metallomics, ionomics, interactomics, and phenomics have been developed.<sup>174</sup> Omics studies allow for exploration of the genome, transcriptome, and proteome in a broader sense with greater sensitivity and resolution, giving us a new direction for research.<sup>172,175,176</sup> It provides solutions for target discovery and validation, drug toxicity and safety assessment, pharmacology, molecular diagnosis and prognosis, and personalized healthcare, among other implications. The only major limitation of omics is that they are vast and require other analytical tools like bioinformatics to interpret the data. Transcriptomics and appropriate bioinformatics tools together are useful in investigating toxicity or therapeutic mechanisms and cellular responses induced by NPs from environmental, occupational, and pharmacological sources.

Currently, several databases exist with various human transcriptome samples. One such database of interest is the NanoMiner, in which about 400 human transcriptome samples (microarray) exposed to various types of nanoparticles are documented.<sup>177</sup> Expression profiles can be plotted for genes of interest, clustering samples within datasets, finding differentially expressed genes in general, and locating particular genes of interest that are differentially expressed, analyzing enriched Kyoto Encyclopedia of Genes and Genomes (KEGG) pathways and Gene Ontology (GO) terms for the detected genes, searching the expression values and differential expressions of pathways or GO's of interest are all possible with this data resource.<sup>177</sup>

Lim et al., in 2012, studied the impact of sub-lethal concentrations of 5nm and 100 nm silver (Ag) NPs on inflammatory and stress genes in human macrophages to understand the risks of Ag NP exposure using the cDNA microarray analysis technique. The microarray analysis showing a significant elevation in protein levels of hemoxygenase-1(HO-1), heat shock protein-70 (HSP-70), and interleukin-8 (IL-8) together with Western blot analysis demonstrated that low level and early-stage exposure to 5nm Ag NP and not 100nm Ag NP inflammatory and stress responses in our immune system.<sup>178</sup>

Akbari et al. developed a novel data mining method to screen long non-coding RNA (lncRNAs) that are responsible for the regulation of apoptosis in colorectal cancer and validated the data *in vitro* by inducing apoptosis in Caco-2 cells with the help of Ag@Glu-TSC nanoparticles (silver@glutamic acid – thio semicarbazide) at a half-maximal inhibitory concentration (IC 50) of 500 µg/ml.<sup>179</sup> They examined a list of 48 genes obtained from the literature survey, and using the

Enrichr software, narrowed it down to 12 common genes involved in the apoptotic pathway. Among them, six genes were identified to have been down-regulated in tumor tissues, and eight lncRNAs were identified as being associated with 5 of these genes. Four of these genes were later found to be significantly upregulated in the *in vitro* study on Caco-2 cells with NP treatment to induce apoptosis.<sup>179</sup>

Zinc oxide NPs have been identified as having an anti-carcinogenic effect against human chronic myeloid leukemia cells (K562 cells). However, as the transcriptomic approach was never used before to assess the type of apoptosis induced in these cells by the NP, this study was undertaken by Alsagaby et al.<sup>180</sup>. The cell viability assay (MTT) - a time-dependent analysis, showed an inverse relationship between time and cell viability. Dissolution analysis of ZnO in the presence of culture medium also showed dose and time-dependency in the release of Zn ions. FACS analysis for determining the type of cell death was done with a concentration of 40 µg/ml of ZnO NPs for 15 and 72 hours and showed an increase in apoptotic population with time—cell viability of 73% versus control at 98% for 15 hours and a mere 5.2% versus 84% for the control group at 72 hours. These results were compared to results from the microarray-based transcriptomic analysis. The differential expression of apoptosis genes indicated they are pro-apoptotic. Using the DNA microarray approach, they were able not just to confirm the results of other tests but also to identify the possible molecular mechanisms by which the NPs are toxic to the cells,<sup>180</sup>

Gurunathan et al. studied the effects of Graphene Oxide – a 2D carbon sheet with a single-atom thickness with many nanotechnological uses. To establish concrete scientific evidence on the cytotoxicity of graphene oxide in HEK29 cells, the group studied cells exposed to the nanomaterial at different concentrations for several hours using cell viability and proliferation assays. However, meanwhile, the transcriptomic analysis points out the mechanism of action to be apoptosis and the biological processes involved.<sup>181</sup> Similarly, they also worked on a similar study with Pt NPs, which induced apoptosis inflammation and are generally cytotoxic to monocytic leukemia cells.<sup>182</sup>

Lastly, a study by Chen et al. on murine endothelial dysfunction and transcriptome is worthy of mention as they were studying how it is induced by black phosphorus QD (BP QD) and nanosheets (NS).<sup>183</sup> The group studied HUVECs as a model for endothelial function and mouse aortas after exposure to BP QDs and BP NS. In HUVECs, BPNSs were found to inhibit *in vitro* angiogenesis at non-cytotoxic concentrations. It also triggered platelet aggregation and decreased nitric oxide

production due to eNOS dysregulation pointing towards endothelial dysfunction. Although BPQD and BP NS both inhibit eNOS, BPNSs also down-regulate eNOS expression. In mouse aortas, though they found no pathological damage, both nanomaterials cause sufficient vascular risks. RNA-Seq was done to confirm these observations, and they found that BP QD and BP NS triggered eNOS pathways differently and thereby triggered eNOS dysregulation. They concluded that although BP NS and BPQD shared similar physico chemical properties, their differences in morphology could have contributed to the differential vascular outcomes.<sup>183</sup>

Some of the most significant works done in transcriptomics research involve several types of human cells, including endothelial cells and even some types of cancer cell lines. In following these studies, we are also highly motivated to determine the relationship we have established here between cells and nanoparticles and how the impact on their transcriptome can reveal or confirm conventional findings and give direction towards which metabolic pathways and cellular functions are affected and how. This kind of information helps to build better nanomaterials that are biologically safe and compatible. However, one common deficit seen in all these studies is that they are conducted under static conditions. However, the human body, being a dynamic entity, is not satisfactorily replicated. Recently, the impact of InP/ZnS QDs on the cell transcriptome has only been investigated using *Saccharomyces cerevisiae* (yeast)<sup>184</sup> and under static conditions in HeLa cells<sup>185</sup>. Investigating the effect of InP/ZnS QDs on the transcriptome of human cells under dynamic physiological conditions under euploid versus aneuploid conditions has not been undertaken in this study to date.

## **2. RATIONALE**

Most applications of NPs in tumor targeting involve intravenous administration.<sup>1</sup> The NPs are designed to extravasate through the fenestrae in the discontinuous tumor endothelium.<sup>2</sup> Tumor endothelium is also the target for several designed NPs and therapies.<sup>4,36,186,187</sup> This highlights the significance of studying the EC responses to NPs.

Interaction of NPs with the ECs and their impact on ECs are governed by hemodynamic factors such as WSS, but the exact mechanism is not fully understood.<sup>43,49</sup> NPs designed for tumor targeting have been conventionally evaluated *in vitro* under static conditions. This fails to mimic

the dynamic *in vivo* environment, making the results from static studies irrelevant to the actual physiological scenario.<sup>16,188</sup> Further, the effect of aneuploidy of tumor ECs on their responses to NPs has not been studied to date.

We will compare outcomes of tumor vasculature (HUVECs with induced aneuploidy) exposed to NPs to that of normal vasculature exposed to NPs. These outcomes include cell viability, cell transcriptome, and cell uptake of NPs. To define the role of a dynamic environment in defining cell responses, we compare these cell responses in the presence and absence of biologically relevant fluid flow conditions.

The QDs are being used as a model NP with great biomedical potential due to their fluorescent properties, facilitating their characterization and tracking.<sup>8-10</sup> We compare EC responses to Cd-based and In-based QDs to understand how CdSe/ ZnS QDs interact with cells and the cytotoxicity of cadmium-based QD to cells and study the proposed study alternative QD made out of Indium Phosphide to compare the NP-EC interactions.

### **3. HYPOTHESES**

We hypothesize that biomechanical stressors, namely wall shear stress (WSS) and cell aneuploidy, can alter the cell phenotype and regulate receptor expression, thus dictating NP interaction with endothelial cells. We also hypothesize that InP/ZnS QDs are less toxic to endothelial cells than CdSe/ZnS QDs.

### **4. AIMS**

The overarching goal of this thesis work is to understand the impact of wall shear stress and cell aneuploidy on the interaction of NPs with ECs, namely cell transcriptome and cell uptake. To achieve this goal, we have two specific aims.

- i. To design and characterize quantum dots with different engineered properties, namely core composition and surface properties.**

Cadmium-based QDs are conventionally studied, and extensive data exists on their cytotoxic nature. However, these studies also precluded their further use in *in vivo* studies owing to their

cytotoxic nature.<sup>12,17,20,23</sup> Recently, indium based QDs were proposed as a novel alternative with lower cell toxicity.<sup>11,27-29</sup> To render them dispersible in aqueous media for use in biological studies, InP/ZnS QDs were capped using the polymer 3-Mercaptopropionic acid (MPA) in this study. QDs were characterized for size and zeta potential using TEM and dynamic light scattering, respectively. Stability was tracked over a month using fluorescence and absorbance measurements to ensure colloidal stability in water and culture media.

**ii. To assess the interaction of NPs with healthy and aneuploid endothelial cells at static and dynamic conditions using a vessel-on-a-chip model.**

We investigated NP interaction with human umbilical vein endothelial cells (HUVEC), being well-studied primary cells to simulate the microvasculature.<sup>20,115,189,190</sup> We have cultured these cells under different conditions in a microfluidic chip. The microfluidic chip has a channel height of 0.2mm, a channel length of 50 mm, a width of 5 mm, and Reynold's number of about 8, making the fluid flow inherently laminar. We used cell culture media with modified dynamic viscosity to mimic blood (3.0 cP) with 3% of 500,000 MW Dextran.<sup>191</sup> We exposed the cells to a shear stress of 1 dyne/cm<sup>2</sup>. This shear stress lies within the normal physiological range (1-5 dyn/cm<sup>2</sup>) of shear stress as seen in veins.<sup>47,48</sup>

Monastrol, a small, cell-permeable molecule, has been studied as a tool to inhibit the Eg5-Kinesin motor protein that aids cells in mitosis.<sup>192</sup> When Euploid primary cells like HUVEC are treated with monastrol, it renders the cells chromosomally unstable, inducing aneuploidy, albeit temporarily, as monastrol actions on the cells are reversible.<sup>193</sup>

## CHAPTER 2: MATERIALS AND METHODS

### MATERIALS

Indium (III) chloride ( $\text{InCl}_3$ , powder ampouled under argon, 99.999%, ultra-dry), zinc chloride ( $\text{ZnCl}_2$ , anhydrous, 98+%), tris(diethylamino)phosphine ( $[(\text{DEA})_3\text{P}$ , hexaethyl phosphorus triamide], 97%, 2.5mM), sulphur powder, sublimed (99.5%), tri-n-octyl phosphine (TOP, technical grade, 90%), zinc stearate ( $\text{ZnO}$  12.5-14%), 1-octadecene (technical grade, 90%) chloroform (spectrophotometric grade, 99.5%), tetramethylammonium hydroxide pentahydrate (TMAH, 98%) were purchased from Alfa Aesar. Oleylamine (cis-1-amino-9-oleylamine, technical grade, 70%) and gelatin solution in water (tissue culture grade) were purchased from Sigma-Aldrich. 3-mercaptopropionic acid (MPA, 99+%) was purchased from Acros Organics, Human umbilical vein endothelial cells (HUVEC), the culture media EBM-2 – Endothelial cell basal medium (Clonetics), EGM-2 SinglQuot Kit (supplements and growth factors: Hydrocortisone, hFGF, VEGF, R3-IGF, Ascorbic acid, hEGF, GA-1000, Heparin), ViaLight™ Plus<sup>194</sup> cell proliferation and cytotoxicity bioassay kit and ATP Standards were purchased from Lonza™. Fetal Bovine Serum (FBS), monastrol, cell-permeable mitosis inhibitor; trypsin 0.25% trypsin, 0.1% EDTA in HBSS without calcium, magnesium, and sodium bicarbonate; trypsin neutralizer solution (1X); 96 well-plate, tissue culture treated, sterile (Falcon); black 96 well plate, clear-bottom, unsterile (Falcon); Centrifuge tubes (50ml, 15 ml, 1.5 ml) were purchased from Corning™. Triton-X -100, electrophoresis grade; Dulbeccos Phosphate Buffered Saline - DPBS (1X); Invitrogen™: E-cadherin, Alexa Fluor 647, Concanavalin Alexa Fluor conjugate 647, Concanavalin Alexa Fluor conjugate 488, DAPI, ZO-1, Qdot® 605 ITK™<sup>195</sup>, and ethanol, anhydrous were supplied by Fisher™. Dimethylsulfoxide (DMSO) is from ATCC, 500,000 MW Dextran powder is from Spectrum Chemicals. Bovine Serum Albumin (BSA) is from HyClone™. RNeasy® Mini Kit (50) is from Qiagen. Nitrogen gas, compressed, was supplied by ConAir. Microfluidic chips, iBidi μ-Slide I<sup>0.2</sup>,<sup>196</sup> were purchased from iBidi™ (Germany).

## METHODS:

### 1. Designing Indium-Based Quantum Dots:

#### 1.1 *Synthesis of Indium Phosphide/Zinc Sulphide Quantum Dots*

QDs with an indium phosphide (InP) core and a zinc sulphide (ZnS) shell were synthesized following a protocol adapted from Tessier et al.<sup>28</sup> Briefly, 130 mg of InCl<sub>3</sub> (0.45 mM), 340 mg of ZnCl<sub>2</sub> (2.37 mM), and 5.0 ml of oleylamine (15.25 mM) were combined in a 50ml round bottom flask while stirring and purging with Nitrogen gas as shown in Figure 3. The temperature was maintained at 120°C for 30 minutes and then further increased to 180°C. Next, 0.45ml of tris(diethylamino)phosphine (2.5mM) was injected, and the temperature was maintained at 180°C, and indium phosphide cores could grow for 30 minutes.

For the first zinc sulphide shell, 1 ml of TOP-S (0.72 g of sulphur powder in 10 ml of trioctylphosphine) was slowly injected into the reaction mixture. After one hour, the temperature was increased to 200°C; 1 g of Zn Stearate (1.6mM) in 4 ml of Octadecene (ODE) (6.25 mM) was added under stirring for 30 min before a subsequent increase in the temperature to 220°C. A second shell formation was initiated by adding 0.7 ml of TOP-S and stirring for 30 minutes. This mixture was further heated to 240°C, and 0.5g of Zn Stearate (0.8mM) in 2 ml of Octadecene (ODE) (6.25 mM) was added to it. Finally, the temperature was raised to 260°C and maintained for 1 hour before cooling down to around 60°C and stopping nitrogen purge. The InP/ZnS QDs were suspended in 20 ml of chloroform. Figure 4 shows a freshly prepared batch of QDs suspended in chloroform and its fluorescence under UV light. The QDs are then precipitated and washed thrice with around 50 ml of 95% ethanol on ice by centrifuging at 4000 rpm for 20 minutes.

The QD pellet thus obtained was resuspended in 40 ml of chloroform to obtain a QD stock. To render prepared QDs suitable for biological applications, we followed ligand-exchange reactions to transfer them to bio-compatible solvents.

**Figure 3: Quantum dots synthesis setup** – Round-bottomed flask is connected to a condenser, heated on a mantle with a feedback thermometer, and purged with  $N_2$  gas. The chemicals are constantly mixed with a magnetic glass stir-bar resistant to high temperatures (above  $250^\circ\text{C}$ ). The inlets of the round-bottom flask connected to the thermometer and gas are each sealed with a septum. The chemicals are injected through the septa during synthesis. Gas flow and water flow through the condenser are constantly monitored owing to high temperatures.

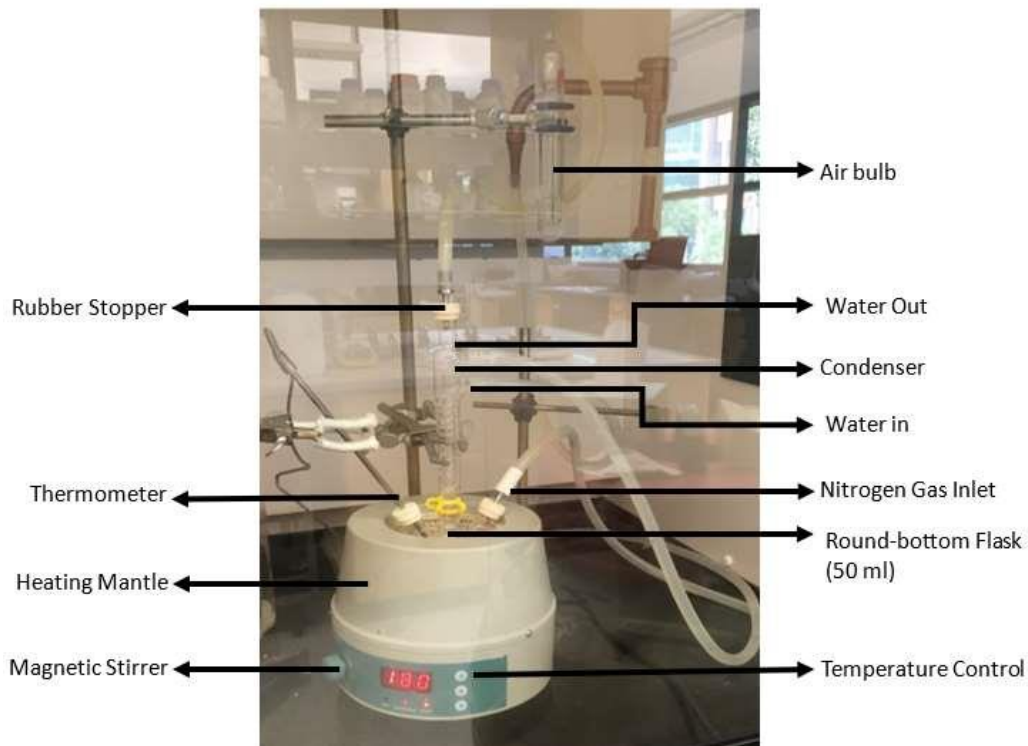
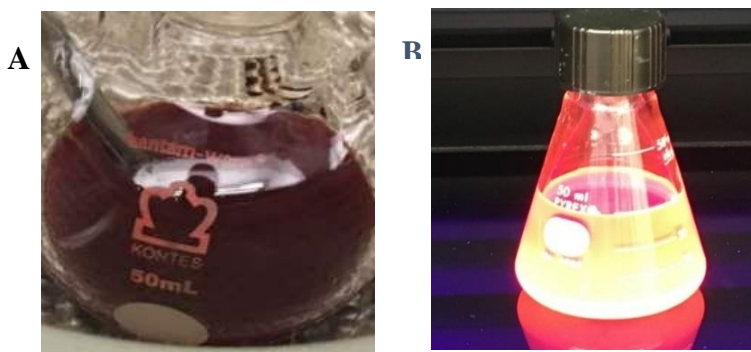


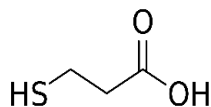
**Figure 4:** (A) Freshly prepared InP/ZnS QDs suspended in chloroform, (B) Prepared QDs show fluorescent under UV light.



## 1.2 Transfer of InP/ZnS QDs into Water via Ligand Exchange:

To render QDs water-dispersible, they were functionalized with 3-mercaptopropionic acid (MPA) (Figure 5) following a ligand exchange reaction by Pong et al.<sup>197</sup>

**Figure 5: Structure of 3-mercaptopropionic acid**

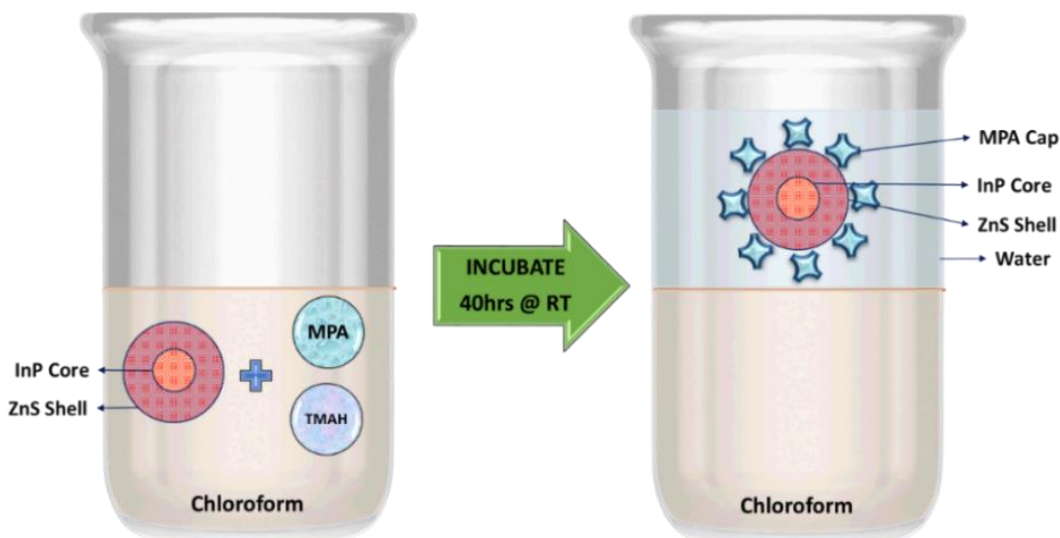


A mixture of 3-mercaptopropionic acid (MPA) and tetramethylammonium hydroxide (TMAH) taken in a 1:1 molar ratio was dissolved in 2 ml chloroform. (Table 1). The solution was incubated for an hour, during which it separated into two phases and two distinct layers formed. The top aqueous layer was discarded, and 100 $\mu$ l of InP/ZnS QDs were added to the bottom layer, and the mixture was allowed to incubate in the dark for 40 hours. Next, 1 ml of distilled water was added, and the mixture was stirred vigorously until the InP/ZnS QDs transferred into the aqueous phase, which was then separated. Finally, QDs were washed thrice with ethanol by centrifugation at 4000 rpm for 10 min, then dried the pellet under nitrogen to remove the remaining organic solvent and resuspension in distilled water. Aqueous dispersions of QDs were kept in the dark at room temperature till further characterization.

**Table 1:** Molar concentrations of mercaptopropionic acid (MPA, MW 106.14) and tetramethylammonium hydroxide (TMAH, MW 181.23) used in the ligand exchange reaction to prepare water-dispersible quantum dots. For all formulations (QD-1 to QD-4), a molar ratio of 1:1 was maintained.

Formulation code	Molar Concentration (mM)	
	MPA	TMAH
QD-1	0.057	0.055
QD-2	0.28	0.27
QD-3	0.57	0.55
QD-4	0.86	0.83

**Figure 6: Capping InP/ZnS QD with 3-mercaptopropionic acid** – The InP/ZnS QD suspended in chloroform is treated with 3-mercaptopropionic acid (MPA) and tetramethylammonium hydroxide (TMAH) mixture and incubated for 40 hours at room temperature to get water-dispersible InP/ZnS QDs capped with MPA.



## 2. Characterization:

We characterized the prepared QDs for particle size using transmission electron microscopy (TEM), and images were analyzed using ImageJ software. The zeta potential of QDs was measured using Zeta-Potential Analyzer – Zeta PALS (Brookhaven™ Instruments) before and after capping. Fluorescence correlation spectroscopy (FCS) was conducted on an Alba IV confocal spectroscopy and imaging workstation (ISS Inc.) to determine the concentration of QD dispersions. The fluorescence spectra of QDs were recorded using a BiotekGen5 Micro Plate Reader. The excitation wavelength was set to 500nm, and the emission was measured from 550nm to 700 nm.

## 3. Colloidal Stability of MPA-Capped InP/ZnS QDs in Water and Culture Media:

Fluorescence measurements were used to track the colloidal stability of MPA-capped InP/ZnS QDs (QD-1, QD-2, QD-3, and QD-4, Table 1) in distilled water at room temperature and in EGM-2 culture media (with supplements - bovine brain extract with heparin, human endothelial growth factor (EGF), hydrocortisone, gentamicin, amphotericin B, 2% fetal bovine serum (FBS)) at 37°C for 30 days and 41 days, respectively.

#### **4. Cell Culture:**

Primary human umbilical vein endothelial cells (HUVEC) were cultured in 75-cc T-flask using 10 ml of EGM2 media supplemented with growth factors at 3% concentration at 37°C and 5% CO<sub>2</sub>. The reconstituted media with 2% FBS, growth factors, supplements (bovine brain extract with heparin, human endothelial growth factor (EGF), hydrocortisone, gentamicin, amphotericin B, 2%) had a shelf-life of up to 2 weeks and were utilized immediately. The growth of the cells was monitored under a light microscope, Olympus CKX41. Media were changed on alternate days until cells reach 90% confluency in the flask before cell detachment.

Cells were detached from the flask by adding 2.5 ml of trypsin and incubating for 5-7 min at 37°C and 5% CO<sub>2</sub>. Trypsin neutralizing solution (5% fetal bovine serum in phosphate-buffered saline without calcium and magnesium) of about twice the trypsin was added to neutralize the effect of trypsin. The cell suspension was centrifuged at 200 G for 5 minutes, and the cell pellet was resuspended in media. The cells are counted, and the concentration was readjusted with media to approximately 0.5 to 2x10<sup>6</sup> cells/ml.

To cryopreserve the passages by backing them up for later use, we added 80% complete media, 10% FBS, and 10% DMSO to the cell suspension while maintaining the temperature of the cryovials at 4°C using an ice bath. The cryovials were immediately transferred to -20°C for 2 hours, followed by -80°C for 12-24 hours before transferring the vials to liquid nitrogen. The cells were used in passages 9-12.

#### **5. Cell Viability Assay:**

The potential cytotoxic effects of CdSe/ZnS and InP/ZnS QDs on normal and aneuploid HUVEC were investigated using ViaLight™ Plus assay, an ATP bioluminescent assay kit that measures cytoplasmic adenosine triphosphate (ATP) to assess the functional integrity of living cells. This bioluminescent assay utilizes the enzyme luciferase to catalyze the formation of light from ATP and luciferin. The emitted light intensity is linearly related to ATP concentration.<sup>198</sup> Assay was conducted according to the manufacturer's recommendations.<sup>194</sup> Briefly, HUVEC cells were cultured at a seeding concentration of 2 million cells/ml and incubated for 24 hours to reach confluence in a clear 96 well-plate (Falcon, Corning brand). These cells were treated for 20 hours

with 100  $\mu$ l of 100nM monastrol in culture media for the aneuploid group. Both regular and aneuploid (monastrol-treated) HUVEC cells were exposed to serial concentrations (2nM, 5nM, 10nM, 20nM, 50nM) of both CdSe/ZnS and InP/ZnS QDs dispersed in culture media for 24 hours at 37°C and 5% CO<sub>2</sub>. Next, cells were treated with 50 $\mu$ l of cell lysis reagent for 10 minutes before transferring 100 $\mu$ l of the cell lysate to a black clear-bottomed 96-well plate (Falcon, Corning brand) a volume of 100 $\mu$ l of ATP monitoring reagent (AMR) was added. Bioluminescence was measured using a plate reader (BiotekGen5). Experiments were replicated five times, i.e., n = 5.

Cells grown in culture medium only were considered as negative control (100% cell viability), and others incubated with Triton X-100 (1 $\mu$ L/mL) were used as a positive control (0% cell viability). Cells underwent irreversible membrane permeabilization and structural collapse on exposure to Triton X-100 (non-ionic surfactant) at most micellar concentration and lose cytoplasmic ATP.<sup>199</sup> The percentage viability for each replicate was calculated as follows (Equation 2), and the mean  $\pm$  SD was plotted graphically versus QD concentration.<sup>199</sup> The percentage viability for each replicate was calculated as follows (Equation 2), and the mean  $\pm$  SD was plotted graphically versus QD concentration.

$$\% \text{ Cell viability} = \frac{Lum_{exp} - Lum_{positive\ control}}{Lum_{negative\ control} - Lum_{positive\ control}} * 100 \quad \text{(Equation 2)}$$

In parallel, ATP controls in concentrations of 1.5 and 0.015 $\mu$ M were prepared in culture media. Various concentrations of both types of QDs (50 $\mu$ l each) were incubated with 50 $\mu$ l of the two concentrations of ATP controls. Furthermore, upon adding 100 $\mu$ l of AMR, their bioluminescence was measured to check for wavelength interference in the absence of cells. Quantum Dots and AMR interference were also screened to ensure that the optical properties of QDs had no interference with the AMR.

## 6. Dynamic Vessel-On-A-Chip Experiments

### 6.1 Developing a vessel-on-a-chip model:

HUVEC at a cell seeding of approximately 2.5 to 3x10<sup>6</sup> cells/ml were cultured in a tissue culture-treated microfluidic channel, iBidi  $\mu$ -Slide I<sup>0.2</sup>; with a channel height of 0.2mm, a channel length of 50 mm and width of 5 mm, and growth area of 2.5 cm<sup>2</sup> and incubated for 2 hours to ensure cell

attachment, after which the media was changed (Figure 7). The chip reservoir was filled with 100 $\mu$ l of media and incubated at 37°C. The chips were incubated for at least 24 hours to ensure cell attachment. Culture media were then changed once every 24 hours until cells reach 80 – 90% confluence before subjecting them to static or dynamic flow conditions. For aneuploid vessel-on-a-chip experiments, aneuploidy was induced by further treating the cells with 100 $\mu$ M of monastrol in culture media for 20 hours before further experiments (Figure 8). For all vessel-on-a-chip experiments, the viscosity of the cell culture media was increased to mimic that of the human blood (3.0 cP) with 3% of 500,000 MW Dextran.<sup>191</sup>

## **6.2 Setting-up the Flow Circuit:**

The vessel-on-a-chip was placed in a petri-dish, along with two microtubes with 500 $\mu$ l of filtered distilled water to prevent the media from drying out. We assembled a flow system (Figure 9) – the media with 5% dextran (with or without QD) was loaded in Hamilton™ 1000 Series Gastight™ Luer Lock Syringes with TLL Termination (10 ml and 5 ml), the resistance tubing, media reservoir, t – manifold junctions and fittings (Elveflow™ systems) are connected to the system, and it is primed and filled with media. The system is operated with the mechanical power of a syringe pump (KD Scientific).<sup>200</sup>

Now, the HUVEC cells cultured in the chips to confluence are also connected and were exposed to a flow of media for 4 hours at a flow rate of 65 $\mu$ l/min, wall shear stress (WSS) of 1 dyne/cm<sup>2</sup> (within the reported range of 0.1-2Pa), to simulate a physiological ambiance for HUVEC<sup>98,201</sup>, and experiments were compared to others at static conditions. The flowing QDs were dispersed in cell culture media at a molar concentration of 5 or 10nM. Experimental variables (Table 1) are the presence or absence of chromosomal instability, in addition to the type of QDs (InP/ZnS QDs versus CdSe/ZnS QDs). Static experiments were used as controls. Following 4 hours of exposure, cells were analyzed for barrier integrity, cell uptake, and transcriptomics. The detailed protocols for experiments using normal and aneuploid cells are illustrated in Figures 7 and 8.

**Figure 7: Vessel-on-a-Chip with Normal HUVEC**

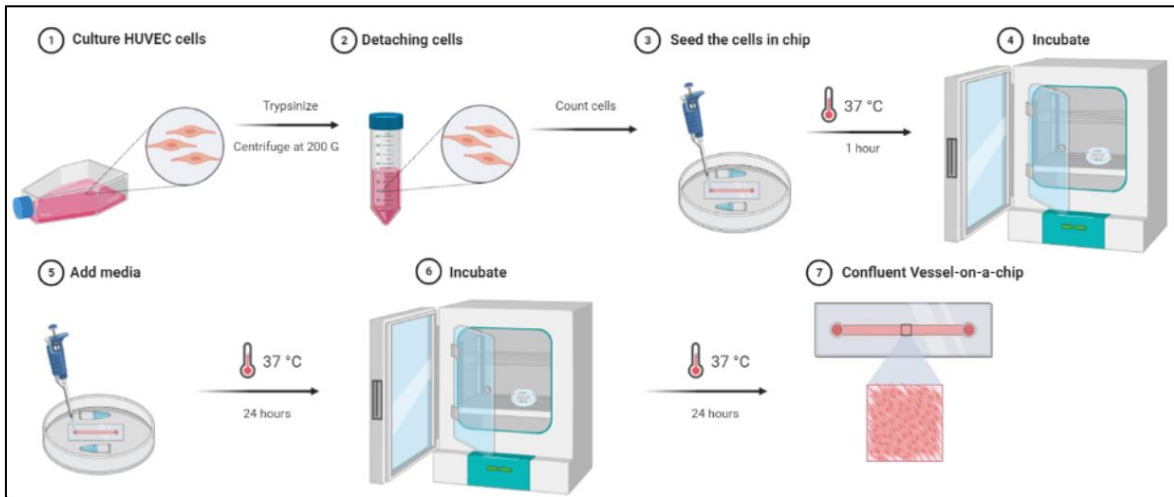


**Figure 8: Vessel-on-a-Chip with Monastrol treatment**

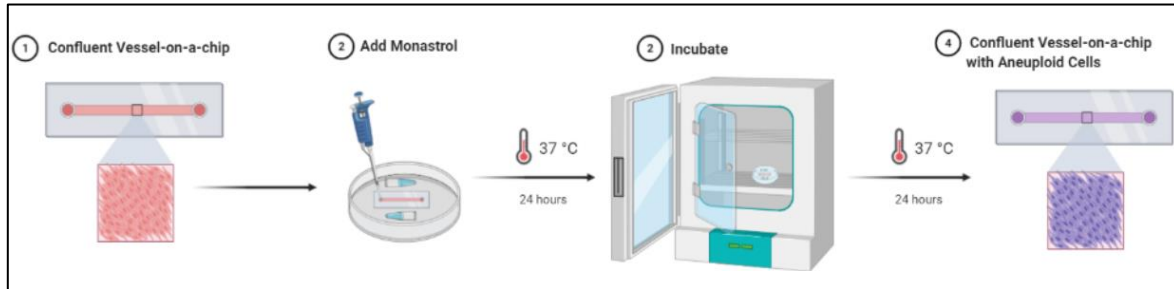
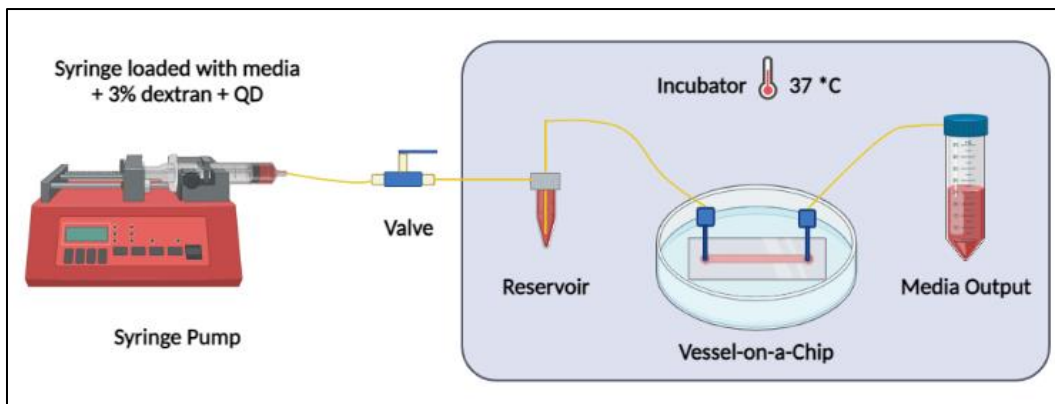


**Figure 9: Vessel-on-a-chip model connected to the flow system** – A vessel-on-a-chip is developed with normal or aneuploid HUVEC cells and connected to the flow system consisting of a syringe pump which delivers the media at a constant flow rate and wall shear stress. The QDs are dispersed in the media at suitable concentrations to study the cellular uptake, and their results are compared to control groups without QD treatment.



### ***Calculation of flow velocity and wall shear stress:***

Flow rate and dynamic viscosity are required in addition to the dimensions of the microfluidic channel to calculate the shear stress. The microfluidic chips that we used came with a pre-determined formula for shear stress calculations which is:

$$\tau = \eta * 512.9 * \phi \quad (\text{Equation 3})$$

Where,  $\tau$  is shear stress (dyn/cm<sup>2</sup>),  $\phi$  is flow rate (ml/min) and  $\eta$  is dynamic viscosity(dyn\*s/cm<sup>2</sup>) of the fluid.

According to the literature survey, we have already determined the desired shear stress to be 1 dyn/cm<sup>2</sup>, so we need to calculate the flow rate required to achieve this. As we want to simulate blood flow, we are also using culture media with blood viscosity, thereby making the dynamic viscosity the same as blood which is 3.0 cP (or) dyn\*s/cm<sup>2</sup>.

Hence, upon calculation using equation 3, we get the flow rate of 0.0649 ml/min, which amounts to 3.89 ml/hr.

### ***Reynold's Number Calculation:***

Reynold's number is the ratio of inertial force to viscous force in a microfluidic channel.

It is represented by  $R_e$  and is calculated using the formula:

$$R_e = \frac{\rho VL}{\mu} \quad (\text{Equation 2})$$

Where  $\rho$  is the fluid density,  $V$  is the flow velocity,  $L$  is the length or diameter of the channel,  $\mu$  is the fluid viscosity. From Equation 3, with a known dimension of channel length as 50 mm, we calculated the  $R_e$  value to be 8.19, which falls in the laminar flow range (<10 is common in microfluidic systems).<sup>52-54</sup>

## **7. HUVEC Cell Morphology**

Cells were checked for morphology via bright-field (BF) imaging using a Bright-field and Fluorescent Microscope – Nikon Eclipse Ti. with 10x and 20x magnification objectives before and after subjecting the chips to the 12 conditions (Table 2).

**Table 2: Groups for Flow Experiment on Vessel-on-a-chip model**

	<b>Normal HUVEC</b>	<b>Aneuploid HUVEC</b>
<b>Control experiments - No QDs</b>	Static	Static
	Dynamic*	Dynamic
<b>Cells exposed to CdSe/ZnS QDs</b>	Static	Static
	Dynamic	Dynamic
<b>Cells exposed to InP/ZnS QDs</b>	Static	Static
	Dynamic	Dynamic

\* Wall shear stress = 1 dyne/cm<sup>2</sup>

## **8. Cell Uptake by Confocal Microscopy**

Confocal imaging (Zeiss LSM700, ZEISS) was used to study the cellular uptake of QDs, following cell exposure to QDs (Table 2). The appropriate controls were also prepared and imaged.

### **8.1 Sample Preparation and Immunofluorescence staining:**

All steps were performed at room temperature. Cells were first formalin-fixed (4% paraformaldehyde / PFA) for 15 minutes, washed thoroughly with a blocking buffer solution (Dulbecco's Phosphate- Buffered Saline (DPBS) containing calcium and magnesium). Next, the cells were incubated for 1 hour in an antibody dilution buffer (1X PBS with 5% bovine serum albumin). Next, the cells were washed thoroughly in DPBS, treated with a nucleus stain solution of DAPI diluted in antibody dilution buffer (diluted according to manufacturer's instructions) - for 30 min in the dark at room temperature. To stain the cell membrane, we used Concanavalin A conjugated with Alexa Fluor 647 for CdSe/ZnS QD treated chips, and Concanavalin A conjugated with Alexa Fluor 488 was used for InP/ZnS/MPA QD treated chips, diluted in antibody dilution buffer to 50 ug/ml (according to manufacturer's instructions) - for 15 min in the dark at room temperature. One last wash with DPBS is done before images are acquired using a confocal laser scanning microscope.

## **8.2 Confocal Imaging:**

We studied the cell uptake of NPs by confocal microscopy using fixed and stained cells (nuclei stain: DAPI and plasma membrane stains – Concanavalin A conjugated with Alexa Fluor 647 or ZO-1 with Alexa Fluor 488. Lasers used in CdSe/ZnS QD experiments are 610 nm for the QD 647 nm for the plasma membrane and 405nm for the Nucleus stained with DAPI. Lasers used in experiments with InP/ZnS/MPA QD are 630 nm for the QD, 488 nm or 647 nm for the plasma membrane, and 405nm for Nucleus stained with DAPI. Z-stacks were sequestered at 1 $\mu$ m steps. At least three Z-stacks in three different areas were imaged per chip, and at least two independent experiments (chips) were run for each experimental condition.<sup>21,154</sup>

## **9. Transcriptomic Analysis**

Following exposure of the cells to QDs and the different controls, cells were trypsinized and extracted from the chips. The RNA was extracted using cell lysate and analyzed for concentration, purity, and quality (n = 3) using a NanoDrop 2000 Spectrophotometer (Thermo Scientific™). According to the manufacturer's instructions, they were processed using RNeasy® Mini Kit (Qiagen) and stored at -80°C. Using this kit, up to 100  $\mu$ g of RNA with 200 bases or longer are separated from the sample. For this, the sample is first lysed and homogenized with specific buffers to isolate the RNA, then purified with ethanol and centrifuged to be rid of contaminants. Purified RNA is then eluted in RNase free water and results in a sample enriched in mRNA as most other RNAs with less than 200 bases like tRNA and rRNA are excluded.

The samples were analyzed using microarray to obtain the complete genetic profile of ECs and the changes seen in each of the 12 conditions. The microarray kit "Clariom™ S Assay, human" (Applied Biosystems™, Thermo Fisher Scientific™) was used as the standard of comparison for this assay. We know the complete gene profile from the kit, and we obtain the gene expression of the ECs under different conditions from the microarray analysis. Upon comparing the gene expression using the kit, we can record the changes in gene expressions seen in the ECs, that is, the gene expressions that were up-regulated and down-regulated under each of those conditions. The data thus generated for the 12 samples were then analyzed by biostatisticians to generate comparisons and highlight those specific genes of interest that have incurred changes and analyze them further.

### ***9.1 Pathway Enrichment Analysis:***

Based on the raw genetic data for each of the 12 conditions (Table 2), a normalized data matrix was generated wherein the data at the log<sub>2</sub> scale was converted to the unlogged or original scale. We identified 12 biological questions where the different conditions were compared. We assigned one as a control group and the other as the case group to compare the two groups. The fold change (FC) was calculated. When  $FC > 1$  (up-regulated genes), the results were kept as it is. When  $FC < 1$  (down-regulated genes), we transformed them into  $-1/FC$ . In this way,  $FC = -1.2$ , downregulated 1.2 folds. We then sorted the absolute fold changes from the largest to the smallest. We selected genes for follow-up analysis using a fold change cut-off of  $FC = 5$  (either up or downregulated). Following this, the normalized data comparisons were further analyzed using the data enrichment software g: Profiler found on the website <http://biit.cs.ut.ee/gprofiler/>.

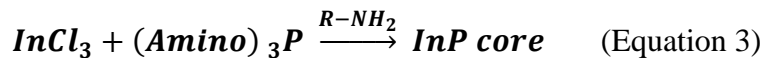
## Chapter 3: RESULTS AND DISCUSSION

The primary goal of this study is to understand the impact of wall shear stress and cell aneuploidy on the interaction of NPs with ECs. Towards this, we used QDs as model NPs. We designed InP/ZnS QDs, characterized them, and conducted a stability study for these newly synthesized NPs. We then investigated their cytotoxicity on ECs in comparison to commercially available CdSe/ZnS QDs. Based on the cytotoxicity experiments, we determined a biologically safe dose for subsequent experiments in which we investigated cell uptake of both QDs and their effect on the cell transcriptome using a vessel-on-chip model developed by us.

### 1. Quantum dots – synthesis, composition, and physicochemical properties:

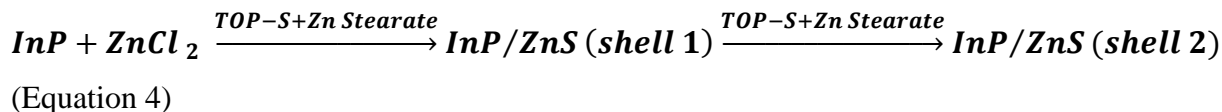
Conventional CdSe/ZnS QDs have been used and studied extensively in the past as a photostable alternative to fluorescent dyes.<sup>27</sup> However, due to the toxicity<sup>153</sup> of cadmium-based QDs, it was essential to design suitable alternative QDs<sup>19,21,161</sup>. To this end, InP/ZnS QDs were developed as an alternative with potentially lower toxicity.<sup>28,197</sup>

As described in the Methods section, we synthesized InP/ZnS QDs under high temperature using a protocol adapted from the work of Tessier et al.<sup>28</sup>. The core precursors InCl<sub>3</sub>, ZnCl<sub>2</sub>, and oleylamine were brought into solution and heated to a very high temperature in an inert atmosphere under nitrogen. InCl<sub>3</sub> is the precursor of indium in the InP core. The reaction occurs in oleylamine (a primary amine) that acts as a solvent and a surface ligand for InP core growth. ZnCl<sub>2</sub> facilitates the Zn shell growth in later stages; it is used in the initial reaction solution to passivate surface defects during InP core growth and has also been shown to reduce the polydispersity of NPs.<sup>28,157,202,203</sup> Tris (diethylamino) phosphine (boiling point 240°C) is the precursor for the phosphide group of InP QD core, which turns the initially colorless reaction mixture into bright red 20 minutes after its addition indicating the formation of InP core (Equation 3).

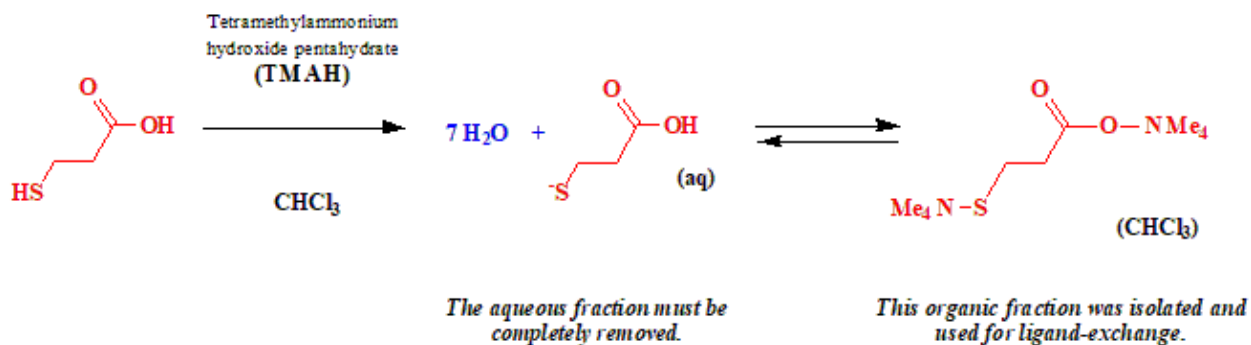


The high-temperature resistance (boiling point about 340°C) of oleylamine is conducive to facilitating shell growth. Aside from ZnCl<sub>2</sub>, the first ZnS shell is formed by slowly adding TOP-S at 180°C and heating to 200°C before adding a mixture of Zn stearate in octadecene. Again, TOP-S and the Zn stearate in octadecene mixture are added at 220°C and 240°C respectively to form

the second shell of ZnS (Equation 4). Finally, the QD dispersion is cooled down and precipitated with ethanol on ice by centrifugation before resuspension of QDs in chloroform to obtain a QD stock.



The InP/ZnS QDs should be rendered dispersible in aqueous media to be suitable for biological applications. For this purpose, we attempted to cap or functionalize the surface of the InP/ZnS QDs with two different polymers: 3-mercaptopropionic acid (MPA) and 11-mercaptoundecanoic acid (MUA) using established ligand exchange reactions.<sup>197</sup> However, capping with MUA did not result in a stable aqueous dispersion of QDs, and aggregation was observed after 48 hours. Capping attempts using MPA were only successful. A mixture of MPA and TMAH in chloroform was used in a 1:1 ratio (for an optimum yield of MPA-capped QD<sup>197</sup>). After removing the water of crystallization (Equation 5) that separates from the equilibrated biphasic mixture, QD stock was added and incubated for 40 hours for the ligand transfer to occur.<sup>197</sup>



(Equation 5)

The InP/ZnS QDs were characterized for size using TEM and zeta potential using dynamic light scattering. The size of the uncapped InP/ZnS QD was measured using TEM (Figure 10), and the three images (115 particles) were analyzed for QD size using ImageJ software to be approximately  $3.3 \pm 0.78$  nm. The surface charge of the InP/ZnS QD stock and MPA-capped InP/ZnS QD were  $-6.9 \pm 2.12$  and  $-15.03 \pm 0.98$ , respectively. Fluorescence correlation spectroscopy was used to

determine the InP/ZnS/MPA QDs concentration to be 400nM, and their fluorescence peak ( $\lambda_{\max}$ ) was at 630 nm as measured using a plate reader (Figure 11).

In our work, we will compare our designed InP/ZnS to commercially available amine(PEG)-terminated CdSe/ZnS QDs (Qdot® 605 ITK™) which were also characterized earlier by our team for diameter, PDI and zeta potential (diameter =  $13.9 \pm 0.6$  nm, PDI =  $0.3 \pm 0.1$ , and zeta potential =  $-1.6 \pm 0.4$ ).<sup>21</sup> These dots have emission maxima of ~ 610 nm, as we measured (Figure 10).<sup>204</sup> The molar concentration of CdSe/ZnS QDs (based on the number of NPs) was determined by the manufacturer and was confirmed by fluorescence correlation experiments, as indicated in an earlier study by our group.<sup>21</sup>

**Figure 10:** Size of InP/ZnS QDs. (A) TEM image of InP/ZnS QDs, (B) Histogram of InP/ZnS QD diameter.

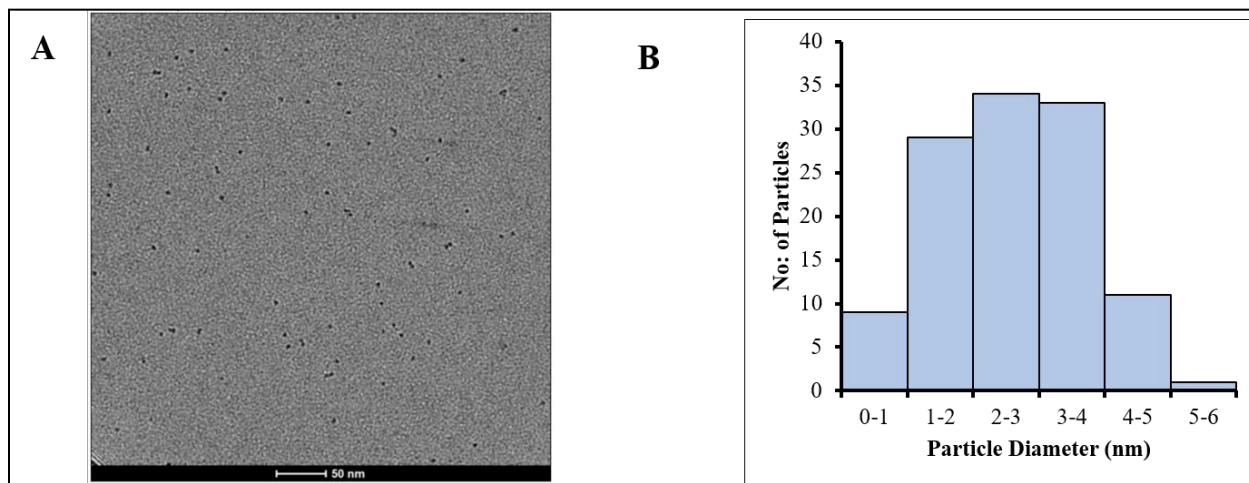
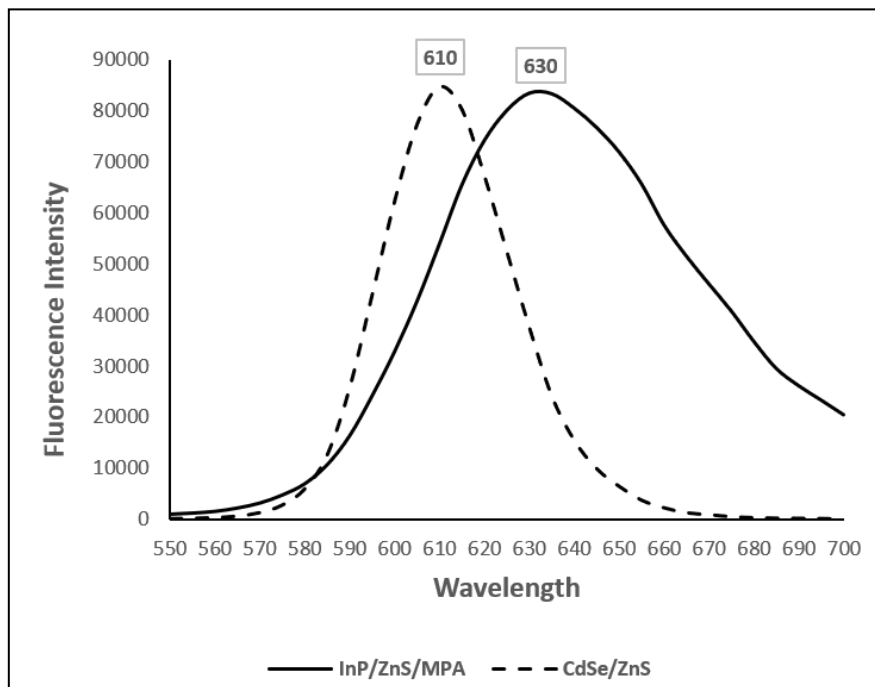


**Figure 11:** Fluorescence curve comparing MPA-capped InP/ZnS QD capped with MPA to conventional CdSe/ZnS QD



## 2. Colloidal stability of MPA-capped InP/ZnS QDs in water and culture media:

The colloidal stability of the capped InP/ZnS/MPA QDs in water and culture media was monitored over a month using fluorescence measurements. To check whether the surface density of the capping agent has any role to play in the stability, we used a series of MPA molar concentrations using the same capping protocol and a 1:1 molar ratio of MPA and TMAH. Tested MPA concentrations were 0.05, 0.25, 0.55, and 0.8 mM resulting in four formulations QD-1 to QD-4 (Table 1).

Capped QDs were centrifuged and dispersed in DI water, and QD dispersions were stored at room temperature in the dark for about 40 days, and their fluorescence was measured periodically. As fluorescence is known to decrease when QDs aggregate<sup>205</sup>, tracking the fluorescence emission of the QDs over time can be considered a reliable method of tracking QD stability, as shown in studies<sup>12,21,206-209</sup>. Figure 12 shows that their fluorescence intensity peak ( $\lambda_{max}$ ) trend was not significantly altered with time, with minimal variations in fluorescence intensities. On comparing

the fluorescence intensities of the different QDs (QD-1 to QD-4), we observed an increase in the fluorescence intensity with an increase in the molar concentration of the capping agent, with QD-4 exhibiting maximum intensity. This increase in intensity can be attributed to an increase in capping efficiency and surface passivation. The shell layers and capping agents act towards increasing fluorescence with increasing MPA concentration, as described by Tessier et al. and other similar studies on QDs.<sup>28,157,202,203,210-213</sup>

For stability in EGM-2 culture media (with supplements - bovine brain extract with heparin, human endothelial growth factor (EGF), hydrocortisone, gentamicin, amphotericin B, fetal bovine serum (FBS)). The InP/ZnS/MPA QD dispersion in water was diluted 1/3 with EGM-2 to obtain a 100nM dispersion, stored in the dark at room temperature, and its fluorescence was tracked over 30 days against a blank of water to media in a 1/3 ratio. It was necessary to dilute the QD as the fluorescence intensity was amplified in the culture media and could not be measured by the plate reader. When the fluorescence curves were plotted (Figure 13) and compared, we observed that the magnitude of fluorescence intensity of the QD increased with time. We attributed this to the deposition of proteins in the culture media on the surface of QDs. This phenomenon where conjugated proteins amplify the fluorescent intensity of QD was previously reported. For instance, several-fold increases in the fluorescence intensities of CdSe and CdSe/ZnS QDs were previously reported in the presence of pseudopeptides<sup>214</sup>. This phenomenon has not yet been observed in the InP/ZnS/MPA QD and is likely the first time.

Overall, InP/ZnS QDs were stable in water (bench storage) and culture media 37°C. Based on these results, we will use QD-4 due to their optimal quantum yield and stability for our subsequent cell experiments, and we will refer to as InP/ZnS QDs in the following experiments and will be compared to commercially available CdSe/ZnS QDs, which were shown earlier by our team as stable in EGM-2 culture media for at 37°C.<sup>21</sup>

**Figure 12: Stability of MPA capped InP/ZnS QD in water over 40 days at 37°C.** Fluorescence emission profiles of (A) QD-1, (B) QD-2, (C) QD-3, (D) QD-4 were prepared using different MPA concentrations of 0.05, 0.25, 0.55, and 0.8 mM, respectively, and dispersed in water.

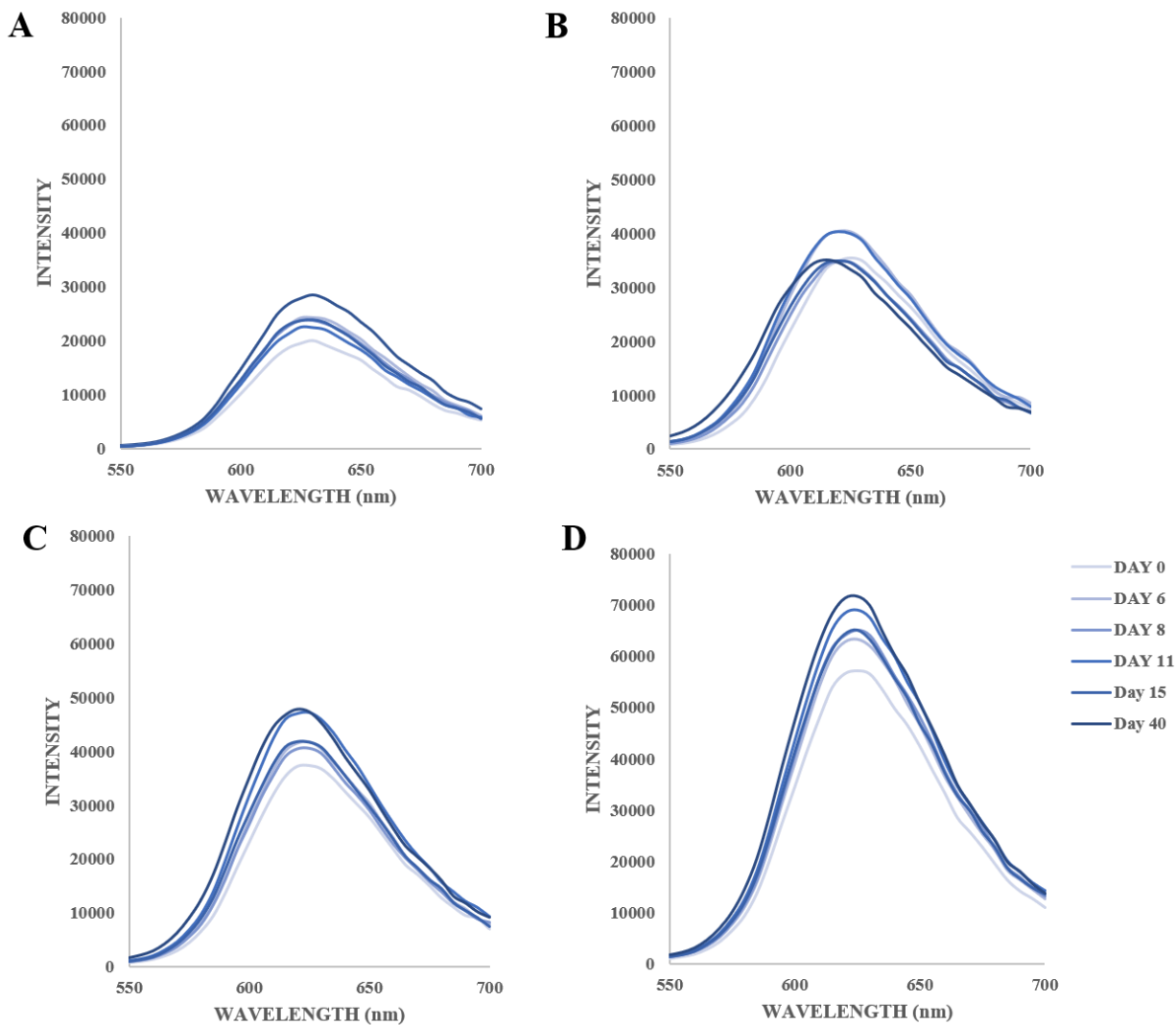
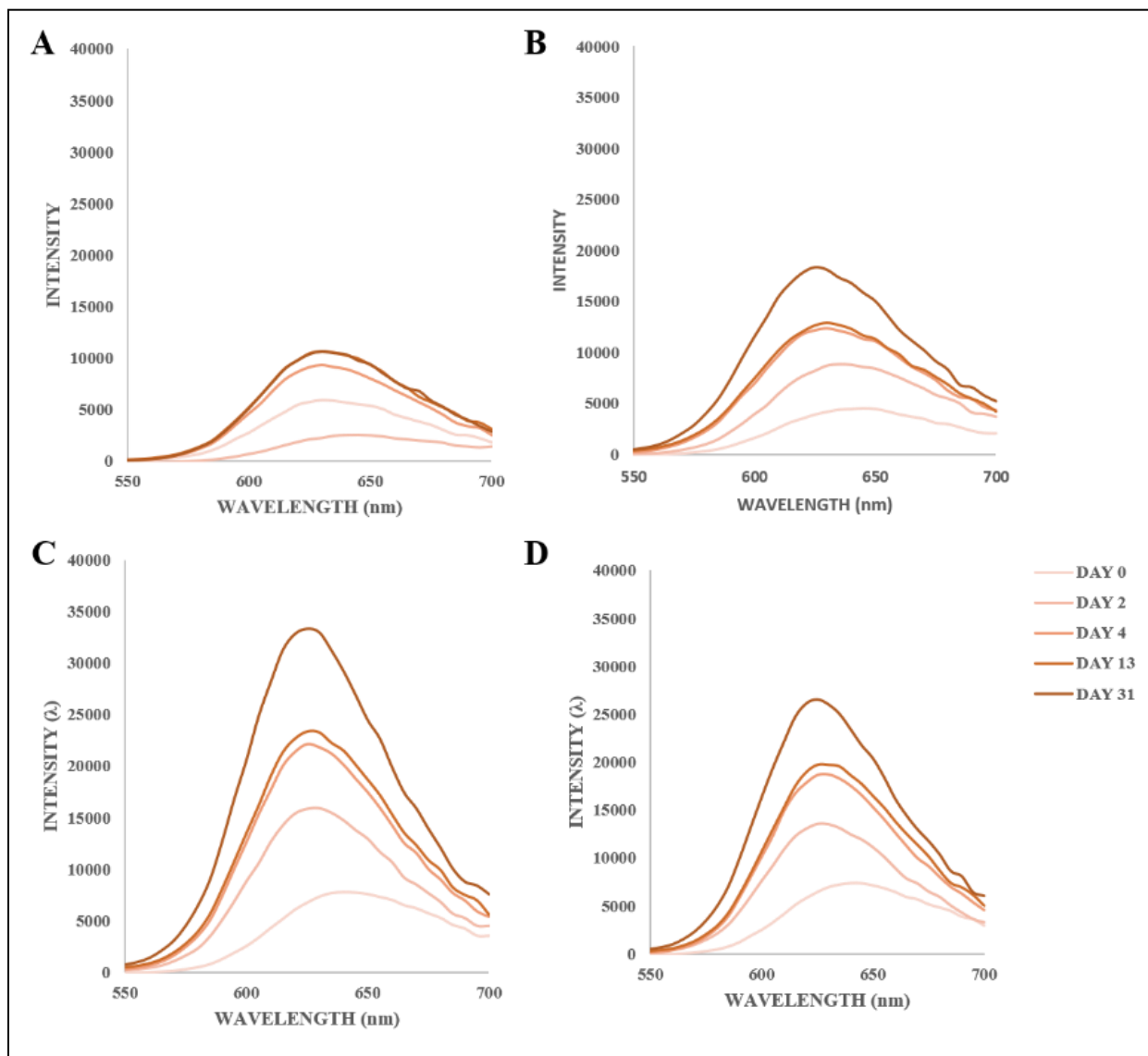


**Figure 13: Stability of MPA capped InP/ZnS QD in EGM-2 media with supplements over 31 days at 37°C.** Fluorescence emission profiles of (A) QD-1, (B) QD-2, (C) QD-3, (D) QD-4 were prepared using different MPA concentrations of 0.05, 0.25, 0.55, and 0.8 mM, respectively and dispersed in EGM-2 media with supplements - bovine brain extract with heparin, human endothelial growth factor (EGF), hydrocortisone, gentamicin, amphotericin B, fetal bovine serum.



### **3. Cell models:**

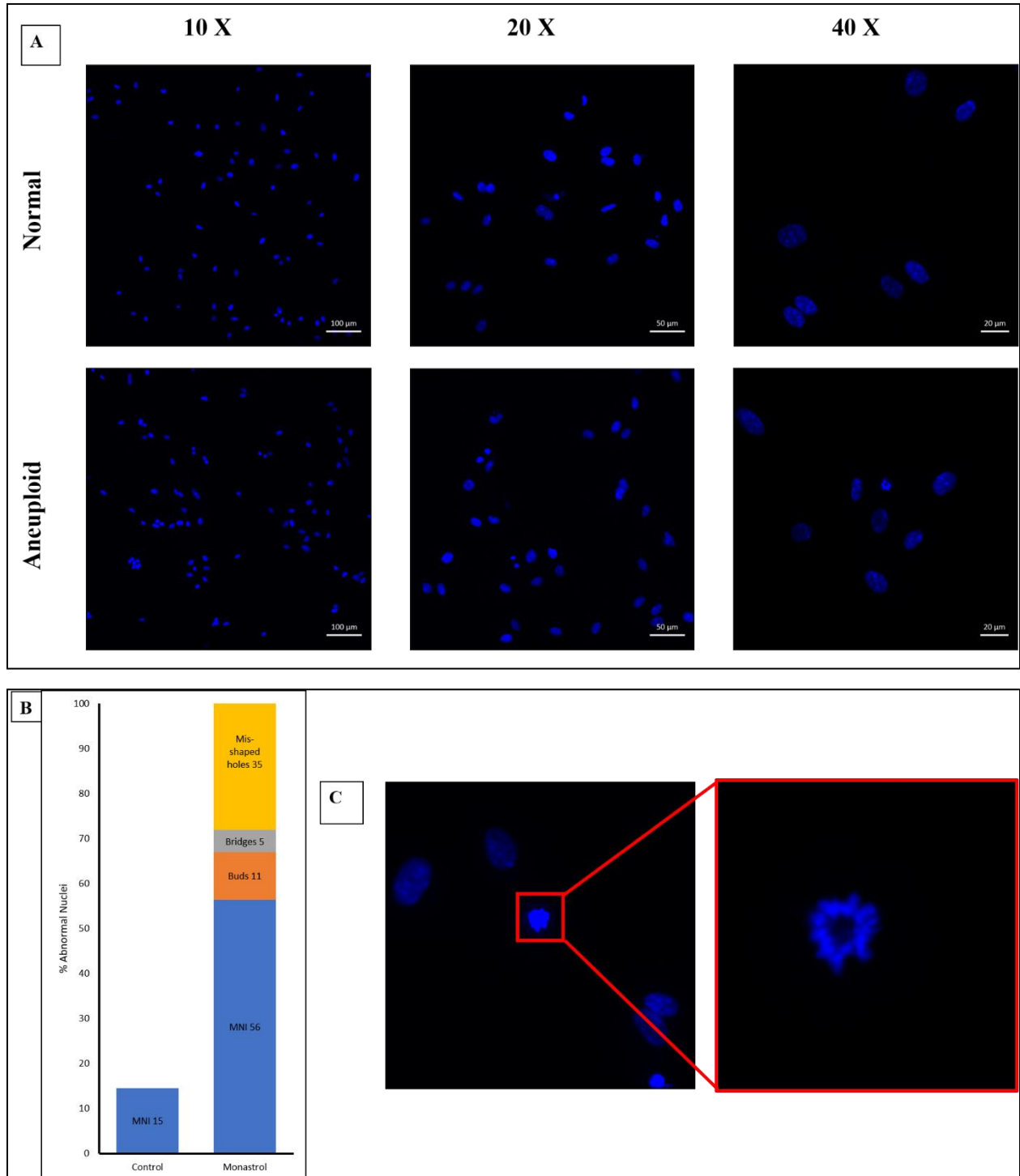
#### ***Selection of cells:***

There are several types of vascular endothelial cell models used to study vasculature.<sup>215,216</sup> However, as we are interested in developing a biomimetic human model, primary human umbilical vein endothelial cells (HUVEC) were chosen from umbilical tissue as a versatile model for endothelial cells.<sup>216</sup> HUVEC cells exhibit all the essential structural and functional characteristics common to all endothelial cells and are easy to culture *in vitro*.<sup>80,90,217-221</sup>

#### ***Induction of aneuploidy in HUVEC cells:***

Aneuploid cells have chromosomal abnormalities and can serve as a model for cancer cells in *in vitro* studies.<sup>192,193</sup> Aneuploidy has been studied, and it has been shown that using kinesin inhibitors like monastrol, we can induce aneuploidy in normal primary cells wherein the mitotic process is inhibited.<sup>192</sup> This inhibition of mitosis is characterized by inhibiting the formation of spindles and other phenotypical changes in the cells. Aneuploid cell nuclei are damaged and are characterized by the formation of micronuclei, bridges, and misshaped holes in the nuclei.<sup>222</sup> On exposure of HUVEC to monastrol for 20 hours, we confirmed aneuploidy using confocal images of DAPI-stained nuclei and quantifying the confocal images for abnormalities from 4 images and 103 nuclei, as shown in Figure 14.

**Figure 14:** (A) Normal and aneuploid HUVEC cells with DAPI stained nuclei at different magnifications, (B) Quantification of abnormal nuclei after monastrol treatment for 20 hours, (C) Monoester formation characteristic of mitosis inhibition by monastrol.



#### 4. Cytotoxicity of Quantum Dots:

Before we studied the NP- EC interactions, the first step was to determine the non-cytotoxic concentration of QDs<sup>21,205</sup>. The toxicity of the QDs is a critical determinant for their potential use in biological studies.<sup>19,21,153,161,205,223,224</sup> This work compares the cytotoxicity of both CdSe/ZnS QDs and InP/ZnS/MPA QDs (referred to as InP/ZnS QDs) on normal and aneuploid HUVEC cells using the ViaLight assay.

ViaLight™ Plus assay is an ATP bioluminescent assay kit that measures cytoplasmic adenosine triphosphate (ATP) to assess the functional integrity of living cells. This bioluminescent assay utilizes the enzyme luciferase to catalyze the formation of light from ATP and luciferin. The emitted light intensity is linearly related to ATP concentration.<sup>198</sup> We treated a group of cells to work as a reference as negative and positive controls to having 100% and 0% cell viability, respectively, as explained in the Methods section, where negative controls were only exposed to culture media and therefore corresponded to 100% cell viability. We induced cell death in positive controls by subjecting them to irreversible cell membrane permeabilization and structural collapse by exposure to Triton X-100, causing the cells to lose cytoplasmic ATP.<sup>199</sup> Therefore, we can note that live cells are capable of ATP synthesis and dead cells will not, and this serves as a comparison to the test group of cells and for the calculation of percentage cell viability using Equation 1.

A critical factor was to rule out optical interferences of QDs with the AMR (test reagent in ViaLight assay) to avoid false-positive and false-negative results<sup>203,225-227</sup>. We incubated both QDs at a series of concentrations (0-50nM) with AMR in the absence of cells, i.e., no source of ATP. No bioluminescence was measured for all QDs with readings corresponding to empty wells and no significant differences between measurements ( $p < 0.05$ ), as shown in Figure 15. Hence, QD and AMR interference screening showed that both QDs do not show luminescence using the assay reagent and conditions. Further, to rule out interference of QDs with the Vialight assay due to surface adsorption of released ATP from the cells, we used the ViaLight assay kit for ATP standards at two concentrations (1.5 and 0.015  $\mu\text{M}$ ) in the presence of either of CdSe/ZnS QD (Figure 16 A) and InP/ZnS QD (Figure 16 B) at a series of concentrations (0 – 50nM). We observed no significant difference ( $p < 0.05$ ) in the luminescence measurements in the absence or presence of CdSe/ZnS QDs and InP/ZnS QDs.

**Figure 15:** Comparing bioluminescence of CdSe/ZnS QDs and InP/ZnS QDs dispersed in culture media for interference, ns denotes statistical non-significance ( $p > 0.05$ ).

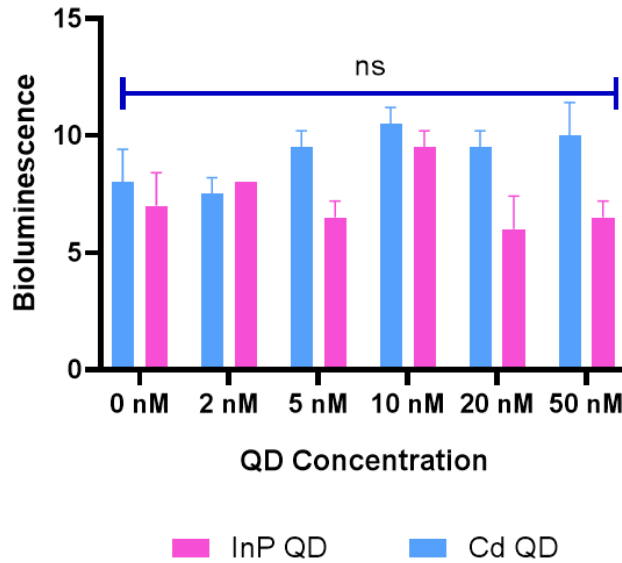
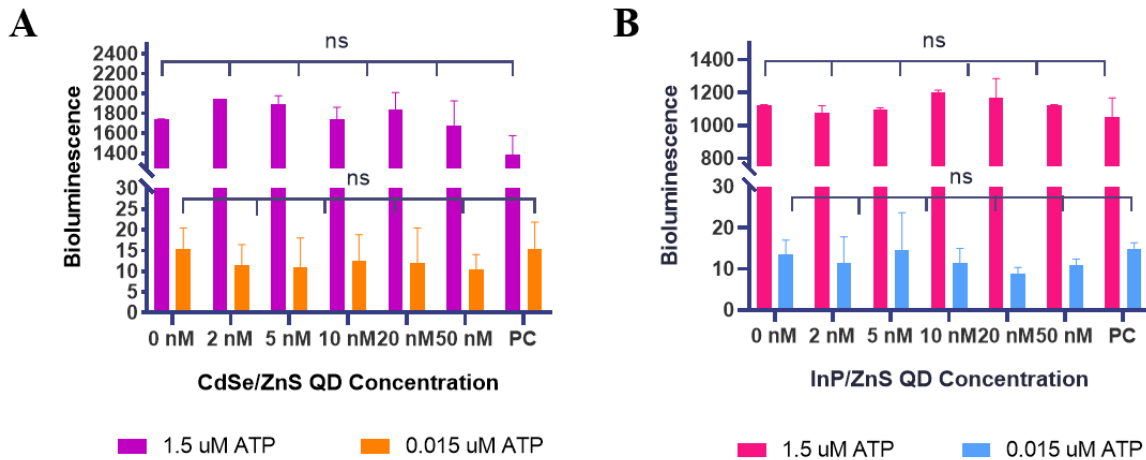


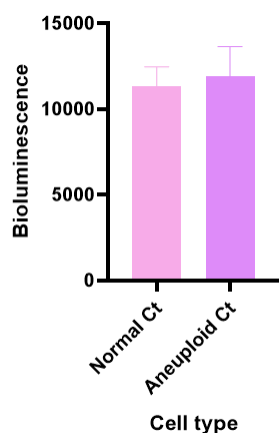
**Figure 16:** ATP Control Assay – (A) CdSe/ZnS QD, (B) InP/ZnS QD capped with MPA, ns denotes statistical non-significance ( $p > 0.05$ ).



Cell viability assays were conducted using normal and aneuploid HUVEC, and the bioluminescence was used to calculate percentage viability using Equation 1. First, we compared the viability of control normal and aneuploid HUVEC at 48 hours following confluence in the absence of QDs. This comparison was to check for the effect of induction of aneuploidy and cellular growth since the induction of aneuploidy required us to incubate HUVEC with monastrol

for an extra 20 hours following confluence. On comparing both cell groups, we observed no significant difference ( $p < 0.05$ ) in the bioluminescence measurements using ViaLight assay, as indicated in Figure 17.

**Figure 17:** Control groups with normal and aneuploid HUVEC cells were compared for Viability to check for any effect of aneuploidy on the bioluminescence.

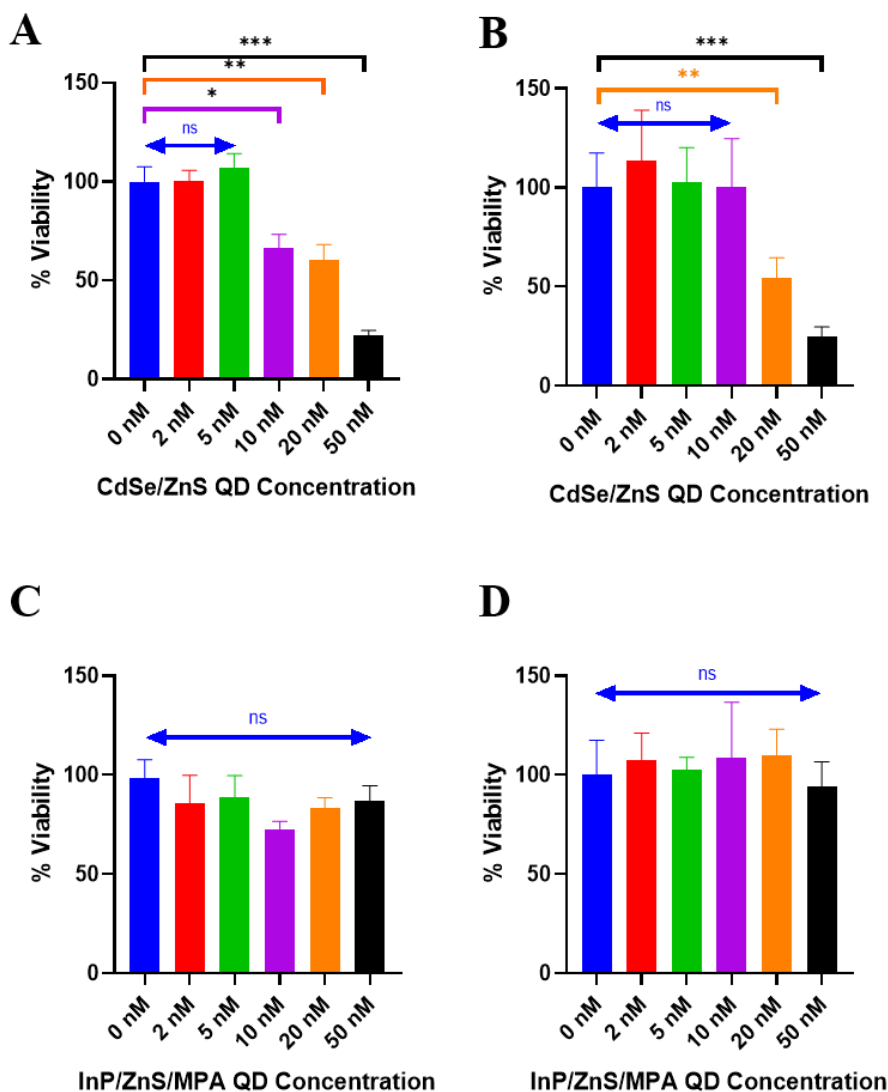


We then conducted a thorough cytotoxicity study to determine the safe concentration range of both QDs on normal and aneuploid HUVEC (Figure 18 A-D). Figures 18 A and B show the viability of CdSe/ZnS QD in normal and aneuploid HUVEC cells, respectively. From Figure 18 A, no significant difference in the viability of the cells exposed to CdSe/ZnS QD concentrations of 2 and 5 nM relative to control HUVEC cells. However, a further increase in the concentration of CdSe/ZnS QDs was accompanied by a significant reduction in cell viability. At 50 nM, cell viability was only 22% indicating high toxicity of CdSe/ZnS QDs to normal HUVEC cells at this concentration. We did the same experiments using aneuploid cells—figure 18 B. On exposing aneuploid HUVEC cells to CdSe/ZnS QDs, no significant change in cell viability was observed up to a concentration of 10 nM, compared to 5 nM in the case of normal cells, indicating that the aneuploid cells could resist the toxicity of CdSe/ZnS QDs to a higher concentration than normal euploid cells. Further increase in CdSe/ZnS QDs concentration similarly resulted in decreased viability of aneuploid cells to around 55% and 25% at 20 and 50 nM, respectively.

We then studied the effect of InP/ZnS QDs on the viability of normal and aneuploid HUVEC. As shown in Figures 18 C, no statistically significant toxicity of InP/ZnS QDs was observed on normal HUVEC relative to the negative control, with percentage viability ranging between 72 – 88%. The

same was observed for aneuploid HUVEC cells (Figure 18 D). However, in aneuploid cells, we see that all the concentrations show viability over 100%. The increase in cell viability over 100% for some experiments following exposure to QDs, especially in InP/Zn QDs, can be attributed to increased cell proliferation over time, as reported for similar studies using NPs.<sup>21</sup> Cell proliferative response was shown as a stress response on induction of aneuploidy as discussed later in the transcriptomic profiling results.

**Figure 18:** Viability of HUVEC cells in the presence of CdSe/ZnS and InP/ZnS QDs. (A) Normal HUVEC cells treated with CdSe/ZnS QD, (B) Aneuploid HUVEC cells treated with CdSe/ZnS QD, (C) Normal HUVEC cells treated with InP/ZnS/MPA QD, and (D) Aneuploid HUVEC treated with InP/ZnS/MPA QD. Mean  $\pm$  SD are plotted for all four groups, n = 5. A statistical significance for



a  $p$ -value  $\leq 0.05$ ,  $\leq 0.001$ , and  $\leq 0.0002$  is denoted by \*, \*\*, \*\*\*, respectively.

Overall, the results confirm our initial hypothesis that InP/ZnS QDs are generally less toxic to endothelial cells than CdSe/ZnS QDs. Also, aneuploid cells were shown to be more resistant to an increasing concentration of the more toxic CdSe/ZnS QDs relative to normal euploid cells. The cell viability study indicates the concentration range of the QD that is safe to use with the cells. Based on this study, we selected 5 nM concentrations of either type QDs for subsequent cell experiments.

## 5. Development of Dynamic Vessel-on-a-Chip Model:

Blood vasculature in the human body is a dynamic regulatory and transport system.<sup>218</sup> This system has vascular endothelial cells at its foundation, and *in vitro* and *in vivo* studies have shown that static conditions do not mimic the phenotypical characteristics of endothelial cells<sup>45,80,228</sup>. ECs subjected to flow exhibit markedly different cell shapes and orientations upon exposure to shear stress.<sup>45</sup> Cell pathways<sup>229,230</sup>, cell uptake<sup>231</sup>, and interaction with and permeability to molecules trafficking the circulation<sup>35</sup> were also reported to be markedly influenced by the presence of dynamic flow. Hence, several studies have been performed to understand and improve the biomimicry of pathophysiology of human microvasculature by studying the endothelial cells in a dynamic flow model.<sup>80,217,221,232</sup>

Several vessel-on-a-chip models have been used for studying ECs.<sup>84,217,233,234</sup> Of these, a simple single-channel vessel slide (iBidi  $\mu$ -Slide I<sup>0.2</sup>) with a channel height of 0.2mm and width of 5 mm was found to be most suitable for this study, as it allowed us to mimic the physiological range of wall shear stress using modified culture media at the dynamic viscosity of blood according to manufacturer's recommendation. The dimensions of this tissue culture pre-treated microfluidic channel allowed for good control of the flow rate of the culture media and the shear stress on the cultured HUVEC cells, calculated using Equation 3, within physiological ranges; we simulated normal physiological shear stress of 1 dyne/cm<sup>243,47</sup>

Following cell culture and confluence, the vessel-on-a-chip was connected to a flow circuit, as depicted in Figure 9. Dextran in 5% w/v concentration was added to the culture media to increase its dynamic viscosity to 3.0 cP, corresponding to blood<sup>191</sup> to mimic blood flow within the blood

vessels under physiological conditions. The chip with HUVEC cells was subjected to a laminar media flow via a syringe pump for 4 hours. This syringe pump cannot withstand the moisture and humidity within the incubator; hence it was placed outside the incubator at room temperature. The media is pumped from the syringe into a reservoir, maintaining the media at 37°C in the incubator before entering the vessel-on-a-chip. As the media from the syringe pump is at room temperature, we have a reservoir for the media inside the incubator to maintain the media passing through to the chips at 37°C. Otherwise, a sudden variation in temperature can cause bubbles that will damage the monolayer of cells. A valve separated the syringe from the media reservoir to maintain backpressure while disconnecting the syringe and replacing it. After circulating the vessel-on-a-chip, the media is collected at the end of the setup in another reservoir.

## **6. Nanoparticle – Endothelial cell interactions:**

### ***6.1 Cell uptake of QDs using confocal microscopy:***

Dynamic models of endothelial cells are vital for studying NP-EC interactions under physiological conditions. Available studies specifically compare NP interactions with cells under static and dynamic conditions resulting in cell uptake.<sup>84,95,99,121,130,135,138,151,231,235</sup> In the presence of laminar flow, the cellular uptake of NPs could be governed by several factors, including flow rate or shear stress, and NP-related parameters, e.g., NP shape, size, and surface chemistry. These factors could influence the margination of NPs flowing through the bloodstream and how many NPs get internalized inside the cells. Not accounting for these factors can cause a discrepancy in the outcomes of *in vitro* and *in vivo* experiments. However, there is a significant gap in our knowledge regarding interactions between different NPs with the different cells under dynamic conditions.<sup>84,99,136,236</sup> For instance, there have been several *in vitro* studies<sup>18-20,149-161</sup> on cell uptake of QDs using different cell types under static conditions. Although several studies examined cadmium based QDs, very few investigated the uptake of InP/ZnS QDs into human endothelial cells under static conditions,<sup>19,20,151,152,154</sup>. However, their cell uptake under dynamic conditions *in vitro* has not been attempted to date.

Further, most applications of NPs include intravenous injection for tumor targeting. Studies show that chromosomal aberrations and missegregation in cancer are not limited to the tumor tissue

itself. It also affects the cells of the tumor microvasculature, including the endothelial cells<sup>105,237-239</sup>. This may affect the association of NPs with endothelial cells. However, the aneuploidy of the angiogenic endothelial cells was not accounted for in previous studies using any NPs, including CdSe/ZnS and InP/ZnS QDs under study. Due to the lack of knowledge on NP interactions with aneuploid cells, our study can be considered a novel and pioneering step in this direction. Understanding the interaction of NPs with aneuploid cells will enable us to design nano diagnostics and delivery systems informed by the tumor tissue's microenvironment and have a high potential for clinical translation in cancer.

In this work, we compared the interaction of CdSe/ZnS and InP/ZnS QDs with normal (euploid) and aneuploid HUVEC cells under dynamic and static conditions using the vessel-on-a-chip model we developed as described earlier in the Methods section; the 12 different experimental conditions are listed in Table 2. At the end of the experiments, we checked for morphology using brightfield microscopy. No significant changes in cell morphology were observed, as shown in Figure 19. After that, we fixed the cells and stained them further to image them using confocal microscopy to investigate the uptake of both QDs into normal and aneuploid HUVEC cells under different static and dynamic conditions. Representative images of the different experiments are shown in Figure 20. For all conditions, we observed higher cell uptake of CdSe/ZnS QDs over InP/ZnS QDs. These differences in cellular uptake of QDs could also justify the differences in cytotoxicity observed earlier, where more CdSe/ZnS QDs are taken up by the cells affecting the intracellular cell machinery than InP/ZnS QDs used at the same concentration. Our group's earlier research findings showed a strong positive correlation between cell uptake of CdSe/ZnS QDs and cytotoxicity that supports this finding.<sup>21</sup>

Differences in the cell uptake of QDs could be attributed to the difference in the physical properties of both QDs, including surface charge (-1.6 for CdSe/ZnS QDs versus -15.03 mV for InP/ZnS QDs), as well as surface chemistry (amine (PEG)-terminated CdSe/ZnS QDs versus MPA-capped InP/ZnS QDs and the size of QDs). Earlier, Chen et al. have observed HCC-15 and RLE-6TN cells uptake of QDs based on their surface functionalization with InP/ZnS-COOH and InP/ZnS-NH<sub>2</sub> QDs being more permeable to cells as compared to InP/ZnS-OH QDs, and the cell uptake of the QDs was directly proportional to their degree of cytotoxicity.<sup>240</sup> However, we must note that the cytotoxicity of these QDs was also concentration-dependent.<sup>241</sup> More recently, Tan et al.

demonstrated that surface-functionalized CdSe/ZnS QDs with polymers acrylic acid and N-(3-aminopropyl)methacrylamide hydrochloride were less prone to non-specific binding and, depending on the surface charge of the ligand, were localized at different cell organelles. However, hydrophobic non-surface functionalized CdSe/ZnS QDs remained at the cell surface. PEGylated QDs penetrated the cells and localized at the lysosomes.<sup>242</sup> Surface charge was also shown earlier to affect cellular uptake of QDs.<sup>243</sup> CdSe/ZnS QDs coated with quaternary amine-modified PMAT with positive zeta potential were shown to be efficiently internalized by Ehrlich Ascites Carcinoma cells, but negatively charged zwitterionic polymer-coated CdSe/ZnS QDs are adsorbed at the cell membrane only under in vitro conditions by Elena et al.<sup>244</sup> Yet another study by Xiao et al. demonstrated that charged CdSe/ZnS QD permeates both breast cancer cells and macrophages while neutral QDs do not, and depending on the type of surface charge, QDs localize at different cell components.<sup>241</sup> Several studies consistently demonstrated that positive charged QDs were cytotoxic while negatively charged QDs were not.<sup>241,242</sup> However, it should be noted that for our study both QDs were negatively charged.

Interestingly, we could observe cell uptake of QDs under all conditions except for aneuploid HUVEC cells under dynamic conditions where 3D analysis of the Z-stacks indicated that InP/ZnS QDs are outside the cells not interact with the cell membrane. Under these conditions, we observed InP/ZnS QDs as aggregates above the resolution limit of the microscope, as shown in Figure 20, which could explain the limited cell uptake of these QDs under these conditions that mimic both physiological shear stress and endothelial cell aneuploidy in a tumor microenvironment. Though we cannot fully understand why InP/ZnS QDs aggregation only under these conditions, these results could have several potential implications that warrant future studies. First, the cell uptake mechanism of both QDs under study could be different, resulting in different cell uptake results under the same conditions. Second, aneuploid cells under dynamic conditions could result in cell excretions that compromise the stability of InP/ZnS QDs but not the CdSe/ZnS QDs in the presence of cells under these conditions. Future studies are required to test the stability of QDs in the presence of cells. To the best of our knowledge, only one study has attempted to test the stability of liposomes in the presence of cells showing no change in the stability of liposomes in the absence or presence of cells.<sup>21</sup> However, this could be different for the different NPs. Importantly, our results lend support and prove our initial hypothesis that shear stress and aneuploidy can dictate NP interaction with endothelial cells. We attributed this to changes in the

cell phenotype under different stress conditions; hence we decided to conduct an extensive transcriptomic study to investigate the cell transcriptome under these conditions using microarray analysis.

**Figure 19:** Bright field images of HUVEC cells in a vessel-on-a-chip model under different conditions (static condition, dynamic flow, and cell aneuploidy) without and following QD exposure.

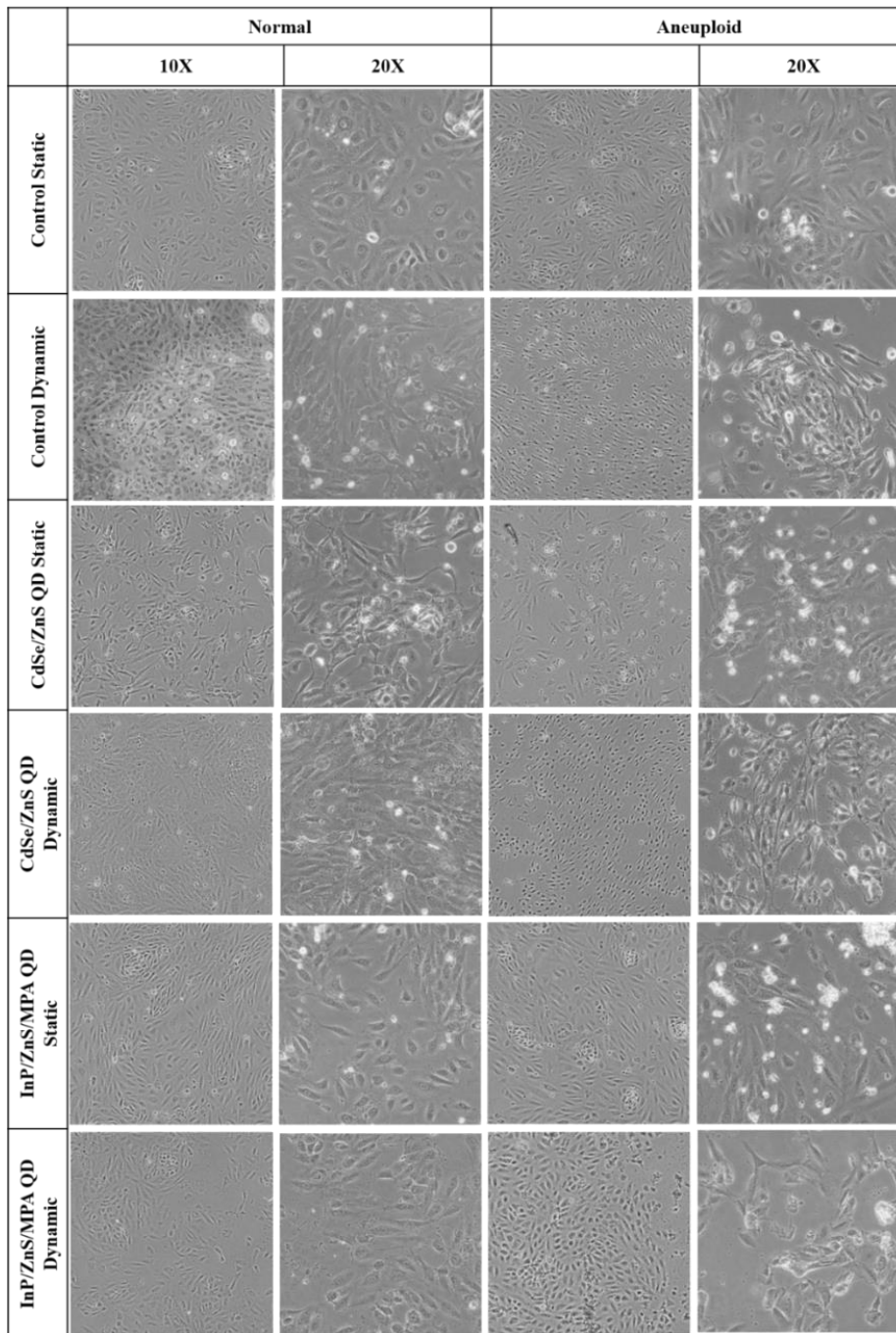
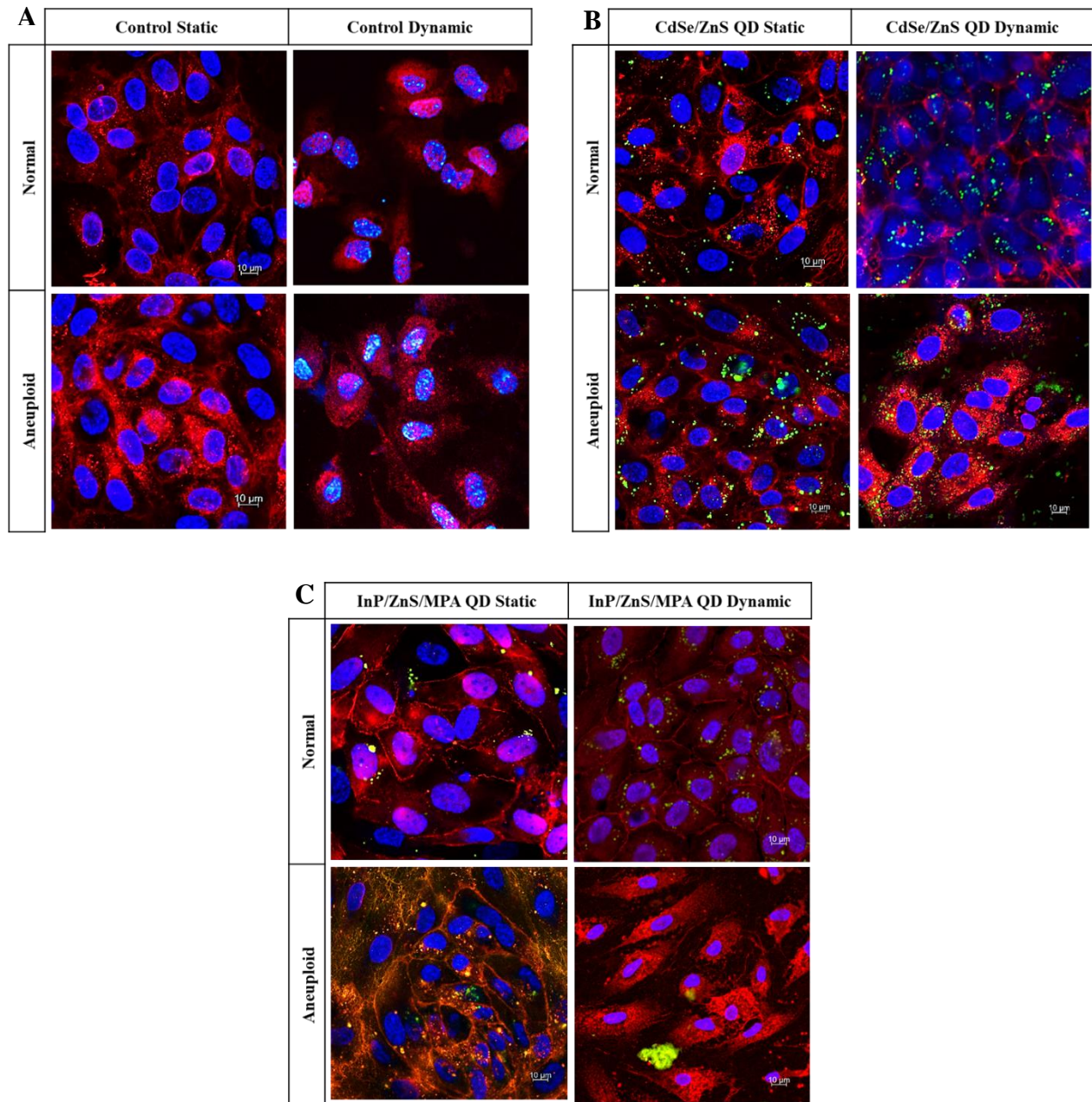


**Figure 20:** Confocal images of HUVEC cells in a vessel-on-a-chip model under different conditions (static condition, dynamic flow, and cell aneuploidy) without and following exposure to QDs. Indicated are DAPI-stained nuclei (blue), Concanavalin-stained cell membranes (red), and QDs (green). A) Control Group with no QD exposure, B) Exposed to CdSe/ZnS QD, and C) Exposed to InP/ZnS/MPA QD.



## 7. Transcriptome Analysis:

The transcriptome is the complete set of all RNA molecules – specifically the mRNAs, translated into proteins via coding transcripts. However, we can also extract useful data on non-coding RNAs such as rRNA, tRNA, lncRNA, siRNA, etc.<sup>245</sup> Transcriptome analysis is the study of the transcriptome or the RNA transcripts produced by a genome in a particular cell using high-throughput techniques. The earliest method for transcriptomic analysis of a cell is microarray, a set of defined sequences arranged on a solid substrate that almost entirely represents the mRNAs.<sup>245</sup> The information thus obtained from the cells comprises data on the gain or loss of cellular function and thereby the change in the cell's overall behavior. It helps identify specific pathways and cellular processes that respond when the cell is subjected to different conditions. In general, the main purpose of the transcriptomic analysis is to compare specific cell samples in pairs to study certain biological questions.<sup>245</sup>

For instance, one study conducted a serial analysis of gene expression using coronary artery endothelial cells (HCAECs) comparing cells exposed to a dynamic laminar shear stress of 15 dyne/cm<sup>2</sup> for 24 hours to cells exposed to all other similar conditions at a static state. The gene expressions from the transcriptomic analysis showed a reduced expression of genes for cell proliferation, angiogenesis, ECM and cell-matrix adhesion, ATP synthesis. An increased expression of stress response proteins and autosomal polycystic kidney disease genes were observed. The stress response was associated with anti-inflammatory and vasodilatory vascular outcomes, and the autosomal polycystic kidney disease genes are associated with a vascular malfunction that causes impairment of the vasoreactivity process.<sup>56</sup>

In another study, the impacts of sustained shear stress for 24 hours on the ECs were studied, and it was established that a selected few genes – TGF  $\beta$ 1, IL-1 $\beta$ , and TNF  $\alpha$ – were flow-responsive.<sup>162</sup> These genes are responsible for tumor growth promotion, inflammatory response, and necrosis, respectively. Moreover, metabolism and signal transduction were most upregulated, whereas cell cycle / growth-related genes were the most downregulated.<sup>162</sup>

Microarray was also used to study the impact of aneuploidy on the physiology of human cells. Diploid cells of colorectal cancer cell line (HCT-116) and retinal epithelial cells (RPE-1) were compared to their counterparts with trisomy and tetrasomy created by microcell fusion from mouse

donor cell lines. Results showed quantitative changes in the genome, transcriptome, and proteome.<sup>165</sup>

The importance of transcriptomics for NP research, in particular, is that it can help us understand the cell's response in the transcriptome upon exposure to specific NP under specific environmental conditions.<sup>245</sup> Incorporating transcriptomic analysis of cells exposed to NPs gives us a more detailed understanding of the exact cellular mechanisms and biological processes at play in the uptake and utilization of the NPs.<sup>246</sup> This can help improve the targeting mechanism for NPs and mitigate any characteristic that can cause undue harm to the cells. Thereby, the main principle of nanomedicine designing – to target specific tissues while mitigating off-target effects – can be achieved with more precision.

Recent transcriptomic studies were conducted to understand the effect of exposure of HUVEC cells to different NPs. In a study by Hu et al., the HUVEC cells were exposed to air pollutants (particulate matter < 2.5µm in aerodynamic diameter) for 24 hours, and their differential gene expression was examined. Microarray analysis of gene expression data showed that the cardiovascular ECs varied largely in cells exposed to laminar shear stress under physiological flow versus static conditions.<sup>247</sup> In a more recent study, Davenport et al. investigated the transcriptome profile of HeLa cells treated with InP/ZnS QDs and found evidence of apoptosis induction.<sup>185</sup> However, it should be noted that they have used an excessively high concentration of QDs, 69 µg/ml (74 µM) and 167 µg/ml (179.25 µM), as opposed to 5 nM (0.5 µg/ml) concentration in our study.<sup>185</sup> Furthermore, their exposure time is 24 hours as opposed to a 4 hour exposure time herein. Chang et al. compared Carbon nanotubes<sup>248</sup> and their impact on transcriptome profiles of HUVECs and alveolar-endothelial co-culture. The direct exposure of HUVECs to carbon nanotubes resulted in cytotoxicity and showed gene expression changes associated with endoplasmic reticulum stress response and autophagy signaling. However, no studies exist on the impact of any QD on the gene expression in HUVEC cells under dynamic conditions.

Our study utilized microarray analysis to understand the impacts of two types of QDs on the HUVEC cells. Microarray analysis is one of the earliest available approaches to study cell transcriptomes, where one experiment is enough to screen hundreds of thousands of genes in the cell.<sup>245,249</sup> First, we exposed the cells to different environmental (static and dynamic) and cell

(euploid and aneuploidy) conditions to compare the effect of both QDs on the cell transcriptome, examine cell phenotypic changes under the different conditions, and develop an understanding of how these transcriptomic changes in the cells under these different conditions result in different impacts of these NPs at the sub-cellular level. The 12 different conditions are listed in Table 2. Extracted RNA was then analyzed using the microarray kit "Clariom™ S Assay, human" (Applied Biosystems™, Thermo Fisher Scientific™). The data obtained comprises the transcriptome data of differentially expressed genes for each condition. The data for each experimental group was then compared to the corresponding control group, and we thus obtained analyzed data with fold changes seen under each of those specific conditions. These fold changes represent the up or down-regulation of a particular gene related to specific processes within the cell. Fold changes  $\geq +5$  (upregulation), and  $\leq -5$  (downregulation) were analyzed and presented, and pathway enrichment was performed on those with  $\geq +2$  or  $\leq -2$  to understand these specific alterations in cellular function.

We will present the expression levels for each condition separately relative to the appropriate control before discussing the results across different groups ending up with overarching conclusions.

### ***7.1 Effect of exposure of Euploid HUVEC cells to dynamic conditions:***

The effect of dynamic conditions on normal HUVEC cells is shown in Figure 21. Panel A shows the upregulated and downregulated genes in response to the dynamic condition compared to the static condition. Two upregulated genes with the highest fold change play a role in the inflammatory response. SMAD6 is upregulated and is one of the genes which acts as a mediator of TGF-beta and BMP anti-inflammatory activity. In addition, it works to suppress IL1R-TLR signaling through its direct interaction with PEL1, which in turn prevents NF-kB activation, nuclear transport, and NF-kB mediated expression of proinflammatory genes.<sup>250</sup> NR4A1 is another gene that is upregulated, and it works to inhibit NF-kB transactivation of IL2 and plays a role in the vascular response to injury.<sup>251</sup> C10orf10 is a gene that is downregulated, and it acts as a critical modulator of FOXO3-induced autophagy through increasing cellular ROS.<sup>252</sup> Another downregulated gene of interest is TNFSF10, also known as Tumor Necrosis Factor Ligand Superfamily Member 10. TNFSF10 is a cytokine that binds to multiple receptors, and it works to induce apoptosis.<sup>253</sup> Overall, the genes discussed above that are downregulated or upregulated all

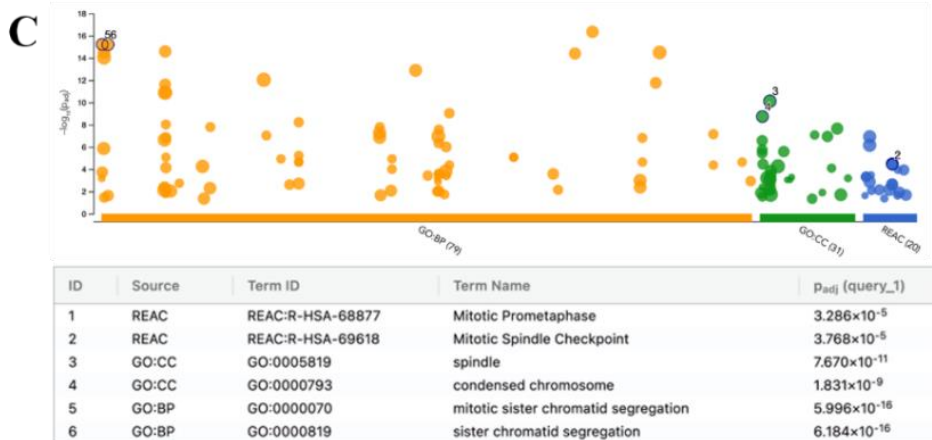
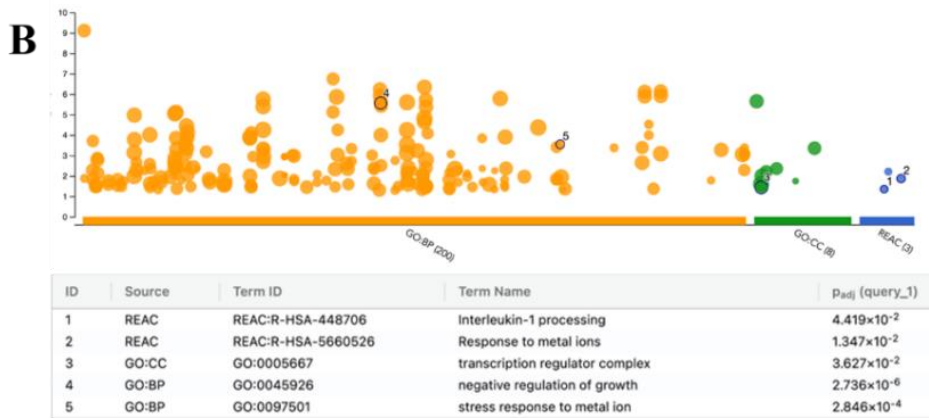
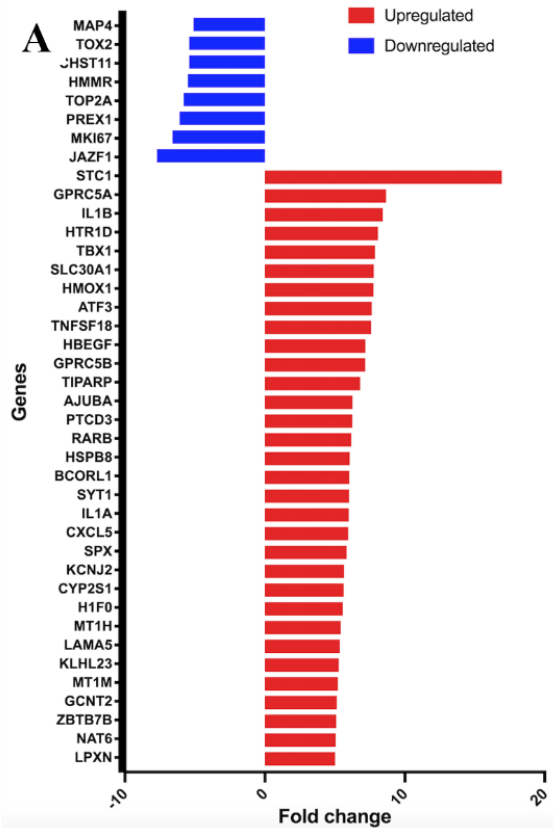
play some role in inflammatory response or act as factors leading to programmed cell death. The downregulated genes, in particular, play a role in inducing cell death and autophagy, but dynamic condition helps in the survival of the cells by downregulating those genes.

To further see the effects of the dynamic condition on the HUVEC cells, pathway enrichment analysis was performed using the g: profiler software. Panel B in Figure 21 shows the biological processes, cellular components, and pathways upregulated when the g: profiler was run using the upregulated genes with the fold change of 2 and more. Two biological processes were upregulated, namely, the SMAD protein complex and adherens junction. SMAD-protein complex is affected by fluid shear stress where shear stress activates SMAD 2/3 and induces their nuclear translocation. Low fluid shear stress also increases SMAD 2/3 gene expression and promotes low flow-induced inward artery remodeling.<sup>254</sup> SMAD-protein complex plays a significant role in regulating artery size, and endothelial cells use SMAD signaling after perceiving the direction of blood flow to control the artery size.<sup>255</sup> The other cellular component which is upregulated is the adherens junction. Adherens junction is affected by shear stress, where shear stress causes reorganization of endothelial adherens junction through pathways involving MAP kinase, Src, and Rho proteins.<sup>256</sup> Both of the upregulated cellular components are affected by fluid shear stress and increased gene expression for these cellular components.

Two biological processes were upregulated, and they were artery morphogenesis and epithelial to mesenchymal transition. Artery morphogenesis is the generation and organization of arteries which are blood vessels built by endothelial cells. These endothelial cells line the interior of the blood vessels through a process named vascular morphogenesis.<sup>257</sup> The biological process of endothelial to mesenchymal transition is induced by low shear stress and causes the transition through the de-differentiation of endothelial cells.<sup>258</sup> Signaling by TGF-beta family members and NGF-stimulated transcription were the two pathways that were upregulated. The TGF-beta members such as TGF-beta 3 are induced due to shear stress on endothelial cells, which leads to the activation of KLF2 and NO signaling, which works to limit endothelial dysfunction and maintain endothelial homeostasis.<sup>259</sup> The TGF-beta members are a superfamily of ligands that bind cell-surface receptor serine/threonine kinases to activate SMAD-dependent and SMAD-independent signaling.<sup>260</sup> TGF-beta has multiple roles, and one of its roles is to stimulate cytotaxis in almost all non-neoplastic epithelial and endothelial cells. It has also been reported to either

induce or suppress programmed cell death in different cell types and plays a role in cell dormancy and autophagy.<sup>261</sup> TGF-beta pathway is upregulated and helps the cells maintain their integrity in dynamic conditions. The nerve growth factor has a role in stimulating endothelial cell invasion, leading to angiogenesis induction.<sup>262</sup> The pathways that are upregulated are working to maintain the homeostasis of the cells under dynamic conditions. Panel C in Figure 21 shows the downregulated processes with the genes of a fold change of -2 and less analyzed using the g: profiler. No significant downregulation was observed for any of the cellular components and biological processes.

**Figure 21: Effect of the dynamic conditions on the Euploid HUVEC cell transcriptome.** (A) Graph showing genes that are upregulated and downregulated on exposure to a dynamic fluid flow of 1 dyne/cm<sup>2</sup> compared to control static group with the upregulated genes having fold change of  $\geq 5$  and downregulated genes with a fold change of  $\leq -5$ . Manhattan plots illustrating the pathway enrichment analysis results of (B) Upregulated genes with the fold change  $\geq 2$ , and (C) downregulated genes with fold change  $\leq -2$  versus the static control group; results are classified into three categories: GO: BP (Biological Process), GO: CC (Cellular Component), and Reactome pathways. The number in the source name in the x-axis labels shows how many significantly enriched terms were found. The circle corresponds to term size. The information underneath the graph lists the terms found in each category with their corresponding term ID and P adjusted value.



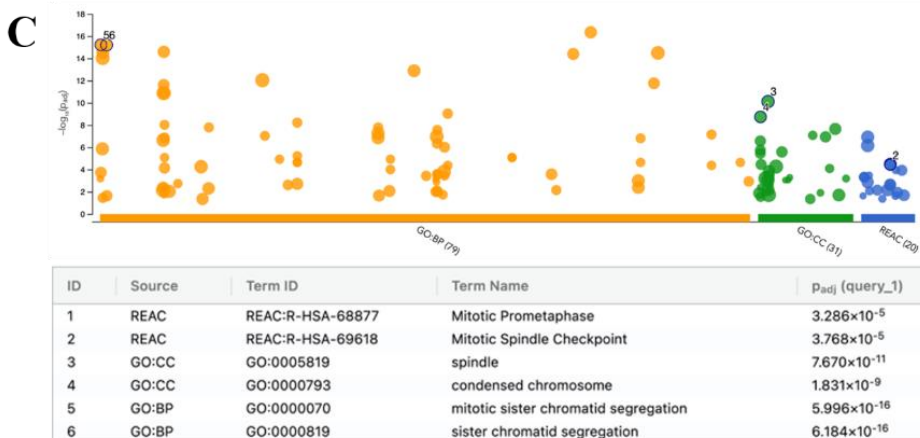
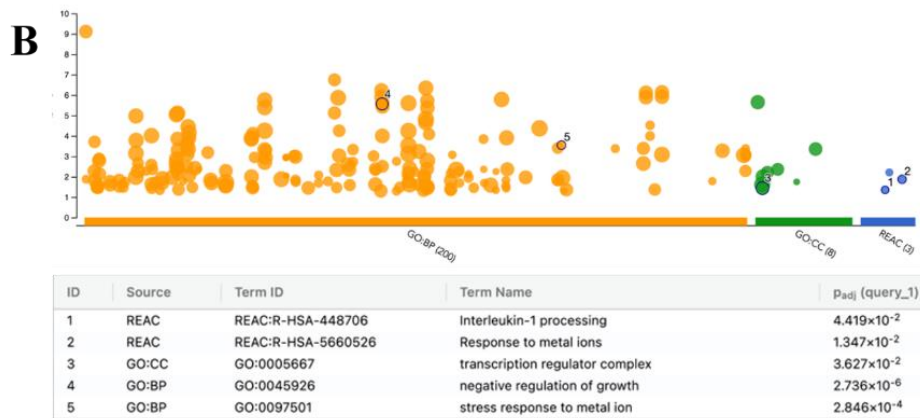
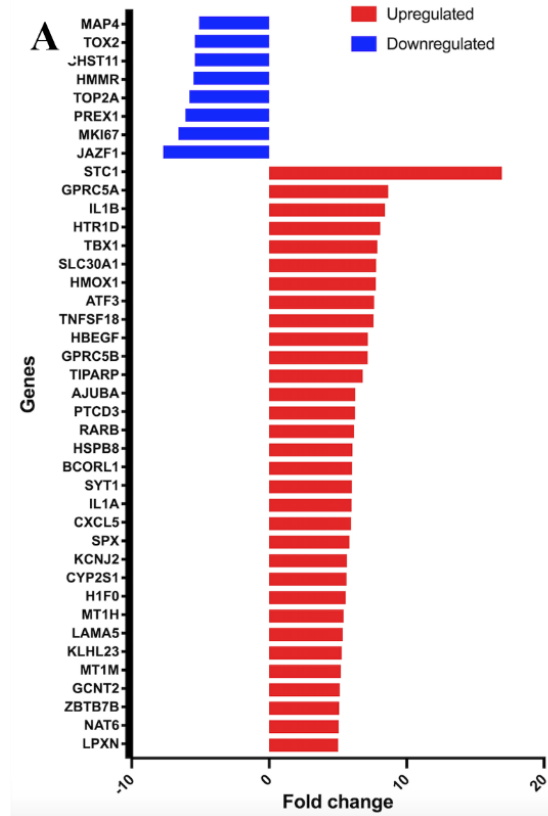
## ***7.2 Effect of Induction of Aneuploidy in HUVEC cells under Static Conditions:***

The effect of induction of aneuploidy in HUVEC cells is shown in Figure 22. Panel A shows the upregulated and downregulated genes in response to aneuploidy in static conditions compared to control euploid HUVEC cells under static conditions. Some of the either upregulated or downregulated genes have a particular role to play in cellular homeostasis. CLDN1 is upregulated and is one of the genes that function as a major constituent of the tight junction complexes. CLDN1 regulates the permeability of epithelia. It is required to prevent the paracellular diffusion of small molecules through the tight junction. Overall, CLDN1 has a barrier function and regulates the permeability of epithelial cells.<sup>263</sup> IFIT1, an interferon-induced protein with tetratricopeptide repeats 1, is an interferon-induced antiviral RNA-binding protein. It provides the cellular response to type 1 interferon to exhibit antiviral activity against multiple viruses such as papilloma and hepatitis C.<sup>264</sup> Another downregulated gene of interest is LYVE1, which acts as a hyaluronan (HA) transporter mediating hyaluronan uptake for catabolism with lymphatic endothelial cells themselves. This gene is important since hyaluronan plays an important role in regulating cell migration and differentiation.<sup>265</sup>

Pathway enrichment analysis was done as described above. Figure 22-B shows the upregulated biological processes, namely the extrinsic apoptotic signaling pathway and stress-activated MAPK cascade. The extrinsic apoptotic pathway, in general, begins outside a cell and depends on the conditions in the extracellular environment. Thus, any changes to the extracellular environment that signal that cell must die lead to activating the extrinsic signaling apoptotic pathway. For instance, the extrinsic apoptotic pathway plays a key role in cancer by selectively killing a diverse range of cancer cells through mediators of the extrinsic apoptotic pathway. Tumor necrosis factor-related apoptosis-inducing ligand (TRAIL/Apo2L) plays an important role in selectively killing various cancer cells. The members of the death receptor family are also key players responsible for the activation of the extrinsic apoptotic pathway and play a role in cancer.<sup>142,266</sup> Stress-activated MAPK cascade is another upregulated biological process that plays a key role in anti-proliferation and is proapoptotic.<sup>267</sup> Thus, it plays a key role in inflammatory responses. Two pathways are also upregulated, and they are interferon signaling and Interferon alpha/beta signaling. Interferons play a role in cancer by inducing tumor cell apoptosis by various mechanisms.<sup>268</sup> Therefore, it can also be a target of interest when it comes to cancer therapy.

Figure 22-C shows the downregulated biological process, including the hyaluronan catabolic process, which has a role in cancer. It has been studied that the catabolism of hyaluronan can be seized by cancer cells in their growth, invasion, and metastasis.<sup>269</sup> Other downregulated pathways were also related to hyaluronan, and they were hyaluronan uptake and degradation and hyaluronan metabolism. Hyaluronan uptake and degradation have been shown to promote endothelial cells' growth due to the fragments generated with the degradation of hyaluronan. The growth of endothelial cells also induces angiogenesis.<sup>270</sup> Hyaluronan also plays a role as a reactive oxygen species (ROS) scavenger. Therefore, hyaluronan helps to remove toxic compounds.<sup>271</sup> Overall, the downregulated pathways and biological processes here are all related to hyaluronan and show the importance of the hyaluronan, highlighting the impact of downregulation on the HUVEC cells due to aneuploidy.

**Figure 22: Effect of aneuploidy induction on the cell transcriptome of HUVEC under static conditions.** (A) Graph showing genes that are upregulated and downregulated on the treatment of HUVEC cells with monastrol to induce aneuploidy compared to control static euploid group with the upregulated genes having fold change of  $\geq 5$  and downregulated genes with a fold change of  $\leq -5$ . Manhattan plots illustrating the pathway enrichment analysis results of (B) Upregulated genes with the fold change  $\geq 2$  and (C) downregulated genes with fold change  $\leq -2$  versus the control static euploid group; results are classified into three categories: GO: BP (Biological Process), GO: CC (Cellular Component), and Reactome pathways. The number in the source name in the x-axis labels shows how many significantly enriched terms were found. The circle corresponds to term size. The information underneath the graph lists the terms found in each category with their corresponding term ID and P adjusted value.



### ***7.3 Effect of Exposure of Aneuploid HUVEC Cells to Dynamic Conditions:***

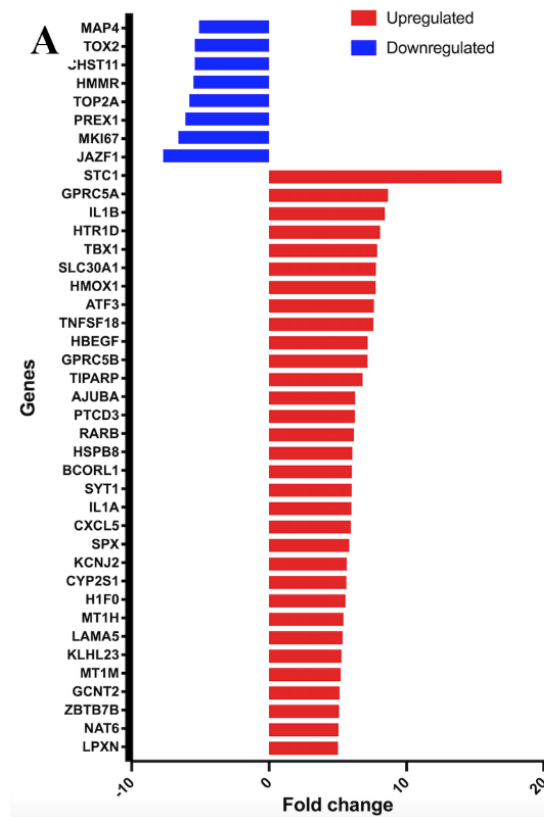
The effect of dynamic conditions on aneuploid HUVEC cells is shown in Figure 23. Panel A shows the upregulated and downregulated genes in HUVEC cells in response to a combination of aneuploidy and dynamic conditions compared to aneuploidy in static conditions. Many different genes are upregulated and downregulated, but some have a vital role in different biological processes. One such upregulated gene is SMAD6, a mediator of the tumor growth factor-beta (TGF-beta) and bone morphogenetic protein (BMP) anti-inflammatory activity. In addition, it suppresses IL1R-TLR signaling, which is involved in an inflammatory response. So overall, SMAD6 is working to suppress or inhibit inflammation due to external or internal stimuli.<sup>272</sup> Another protein of interest is ID2 which is a DNA-binding protein inhibitor ID-2. This protein, in particular, regulates a variety of cellular processes, including differentiation, apoptosis, angiogenesis, and neoplastic transformation. The functions of ID2 are very important since neoplastic transformation leads to progressive tumors.<sup>273</sup> There are two downregulated genes of particular interest - GPRC5B and CSF3. GPRC5B, also known as G-protein coupled receptor family C group 5 member B, regulates inflammatory responses in the glomerulus by modulating the NF-kB signaling pathway. Therefore, GPRC5B is a positive regulator of inflammatory responses.<sup>274</sup> CSF3, also called granulocyte colony-stimulating factor, works to induce granulocytes and controls the production, differentiation, and function of granulocytes and monocyte-macrophages. Therefore, it is involved in inflammation and works as a cytokine that leads to inflammatory cellular response.<sup>275</sup>

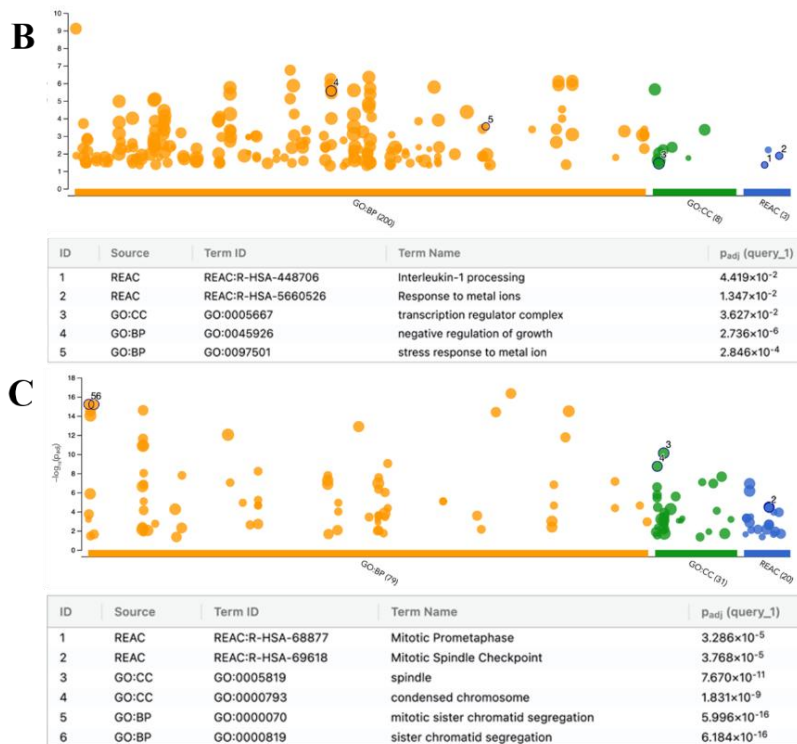
According to pathway enrichment analysis, heart morphogenesis was upregulated (Figure 23-B). It has been found that shear stress caused by the dynamic condition affects the developing heart and vasculature. Shear stress particularly impacts cellular differentiation, proliferation, and growth. Some modulators of cardiomyocytes are also mechanosensitive such as NOS-3, ET-1, and KLF-2, and they increase and decrease in regions of the heart with higher or lower shear stress.<sup>276</sup> Overall, the role of shear stress on heart morphogenesis is a response to an adaptation to environmental demands. Another biological process that was also upregulated was the response to fluid shear stress. It has been found that cancer cells of epithelial origin are more resistant to fluid shear stress than non-transformed epithelial cells.<sup>277</sup> Overall, the upregulated biological processes can lead to changes in the state or activity of cells, such as morphogenesis or resistance in cancer

cells discussed above. The pathways that are upregulated are NGF-stimulated transcription, and the NOTCH4 intracellular domain regulates transcription. The NGF-stimulated transcription plays a role in HUVEC proliferation. Nerve growth factor (NGF) can directly interact with the endothelial cells and lead to angiogenesis.<sup>278</sup> The NOTCH intracellular domain that regulates the transcription pathway is important since NOTCH4 is exclusively expressed in vascular endothelial cells. It promotes proliferation, survival, and migration of endothelial cells. NOTCH4 also regulates angiogenic sprouting.<sup>279</sup> These pathways play a very important role in endothelial cells either through their role in HUVEC proliferation or angiogenesis, making them more suitable for further studies.

The pathways that were found to be downregulated in response to aneuploidy were the resolution of sister chromatid cohesion and mitotic prometaphase (Figure 23-C). Both of these pathways are involved in the cell cycle, which has been affected by induction of aneuploidy with monastrol, a cell-permeable small molecule that is an inhibitor of mitotic kinesin, Eg5.<sup>280</sup> The cellular components that are downregulated are condensed chromosome, centromeric region, and the mitotic spindle. Again, these cellular components are involved in the cell cycle, which is affected by aneuploidy. Chromosome segregation is one of the biological pathways that is downregulated. Chromosome segregation is also another process involved in mitosis, where the genetic material in the form of a chromosome is organized into a specific structure and then physically separated and apportioned to two or more sets.<sup>281</sup> Overall, all the downregulated processes were involved in cell division or cell cycle, and it clearly shows that they are affected by the induction of aneuploidy.

**Figure 23: Effect of the dynamic conditions on Aneuploid HUVEC cell transcriptome. (A)** Graph showing upregulated and downregulated genes when comparing aneuploid HUVEC cells in dynamic condition (CDA) with aneuploid HUVEC cells in static conditions (CSA) with the upregulated genes having fold change of  $\geq 5$  and downregulated genes with a fold change of  $\leq -5$ . **Manhattan plots illustrating the pathway enrichment analysis results of (B) Upregulated genes with the fold change  $\geq 2$  and (C) downregulated genes with fold change  $\leq -2$  versus control; results are classified into three categories: GO: BP (Biological Process), GO: CC (Cellular Component), and Reactome pathways. The number in the source name in the x-axis labels shows how many significantly enriched terms were found. The circle corresponds to term size. The information underneath the graph lists the terms found in each category with their corresponding term ID and P adjusted value.**





#### 7.4 Effect of Induction of Aneuploidy on HUVEC cells under Dynamic Conditions:

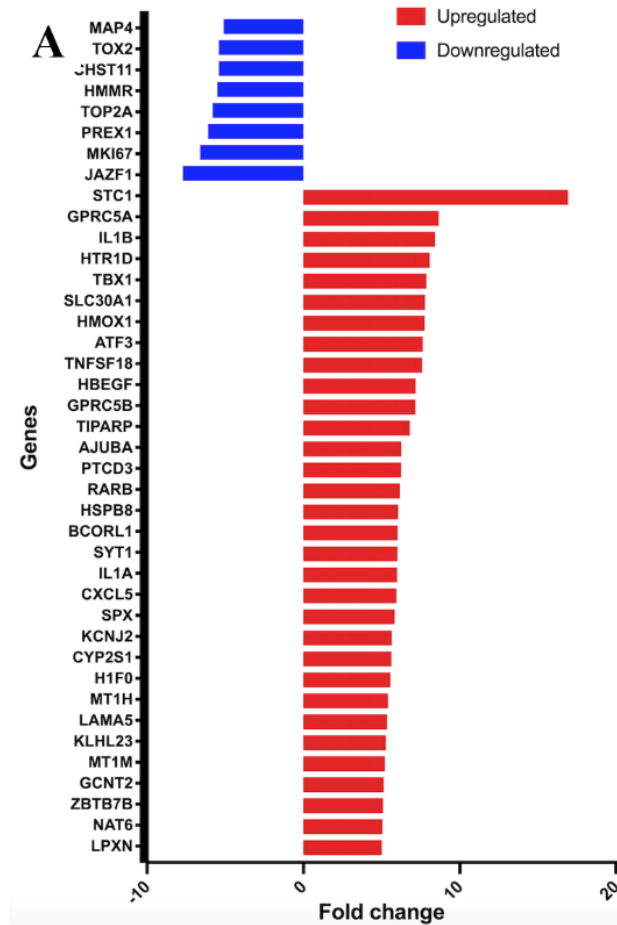
We were also interested in investigating whether induction of aneuploidy under dynamic conditions would result in similar phenotypic changes as in the previously analyzed static group. The effect of induction of aneuploidy on HUVEC cells under dynamic conditions compared to euploid cells of the control group in dynamic conditions is shown in Figure 24. Multiple genes are upregulated and downregulated, each having its unique role and function, of which CDCP1 is an upregulated gene having a particular role in cell adhesion and matrix association. The CUB domain-containing protein 1 (CDCP1) plays a role in regulating anchorage versus migration.<sup>282</sup> This protein has a role in regulating the adhesion and motility of ECs and has been proposed to be involved with metastasis, and it is overexpressed in multiple carcinomas such as colon, lung, and renal cancers.<sup>283</sup> This shows that the role of this protein extends far beyond its normal function of cell adhesion and matrix association.

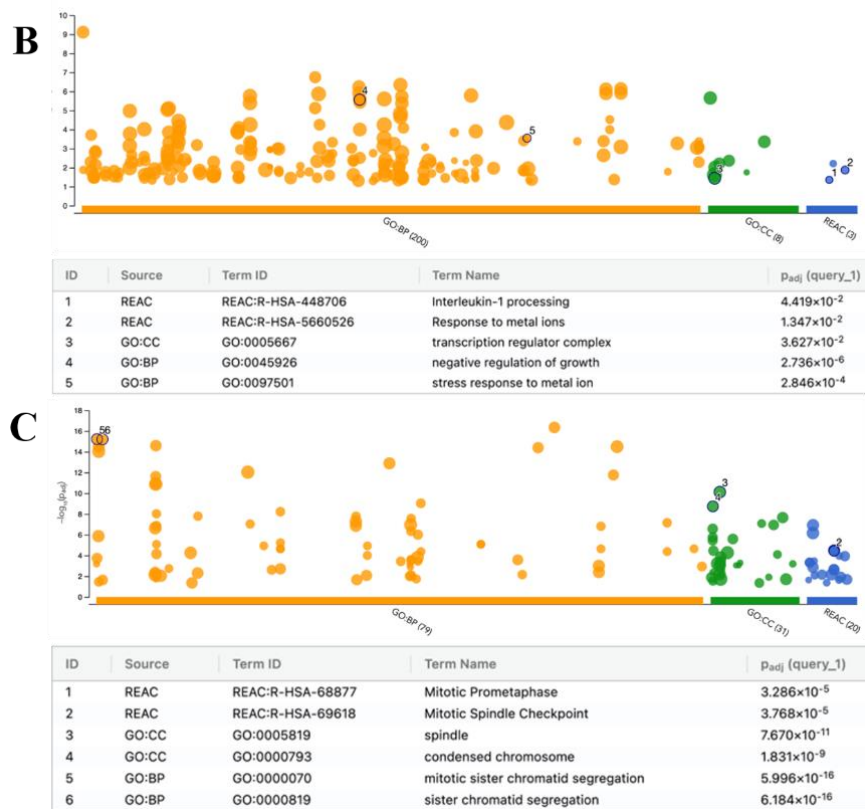
As shown in Figure 24-B, the upregulated biological process is a cellular response to type 1 interferon, which acts on the vascular and lymphatic system to inhibit angiogenesis through downregulation of the Vascular Endothelial Growth Factor (VEGF).<sup>284</sup> The pathway that is

upregulated in interferon signaling. Interferons (IFNs) are cytokines that initiate immune responses in antiviral and anti-tumor effects.<sup>285</sup> The anti-tumor activities of interferon signaling include induction of apoptosis, inhibition of angiogenesis, proliferation, cell terminal differentiation, and immune regulation.<sup>268</sup> This shows that the biological processes and pathways that are upregulated certainly have a role in inhibiting angiogenesis and play an important role in inhibiting the development of tumor growth.

On the other hand, the downregulated biological process is the mitotic nuclear division (Figure 24-C). It is known that in a mitotic nuclear division, chromosomes are organized and then physically separated to be apportioned to two or more sets.<sup>286</sup> The downregulation of this process shows that aneuploidy in HUVEC cells affects their mitotic nuclear division. The spindle is yet another cellular component with a vital role in cell division, which upon downregulation affects mitotic division and is found to have a role in cancer through extracellular force generation.<sup>287</sup> The other key downregulated pathways are cell cycle checkpoints, kinesins, and mitotic prometaphase. In general, a cell cycle checkpoint is a mechanism that halts the progression of the cell cycle until it ensures that the earlier process, for example, DNA replication or mitosis, is complete.<sup>288</sup> As seen before, aneuploidy affects the cell cycle by the downregulation of cellular processes related to the cell cycle. The other downregulated pathway is Kinesins, a superfamily of microtubule-based motor proteins with functions like transport of vesicles, organelles, and chromosomes and regulation of microtubule dynamics.<sup>289</sup> Another downregulated pathway is the mitotic prometaphase, which is the second phase of mitosis, the process by which the duplicated genetic material carried in the nucleus of a parent cell is separated into two identical daughter cells.<sup>290</sup> Again, this shows that a process in cell division is affected due to aneuploidy. Overall, the pathways and processes that are downregulated affect the cell division, potentially due to aneuploidy.

**Figure 24: Effect of induction of aneuploidy on HUVEC cell transcriptome under dynamic conditions.** (A) Graph showing genes that are upregulated and downregulated on the treatment of HUVEC cells with monastrol to induce aneuploidy under dynamic conditions compared to the euploid control group with the upregulated genes having fold change of  $\geq 5$  downregulated genes with a fold change of  $\leq -5$ . Manhattan plots illustrating the pathway enrichment analysis results of: (B) Upregulated genes with the fold change  $\geq 2$  and (C) downregulated genes with fold change  $\leq -2$  versus control; results are classified into three categories: GO: BP (Biological Process), GO: CC (Cellular Component), and Reactome pathways. The number in the source name in the x-axis labels shows how many significantly enriched terms were found. The circle corresponds to term size. The information underneath the graph lists the terms found in each category with their corresponding term ID and P adjusted value.





### 7.5 Effect of CdSe/ZnS QDs on Euploid HUVEC Cells under Static Conditions:

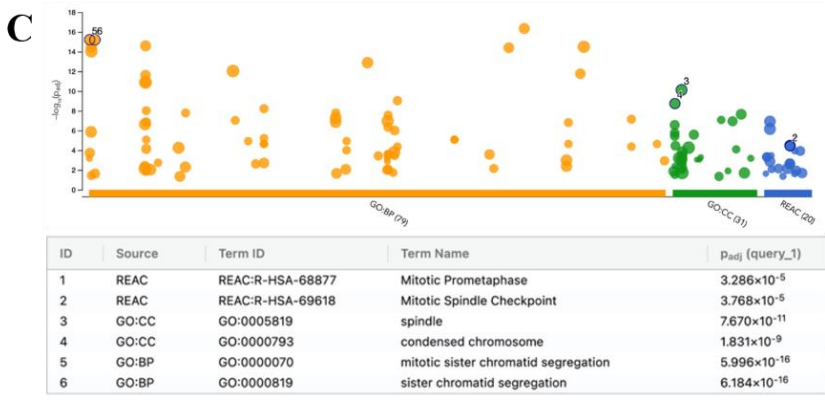
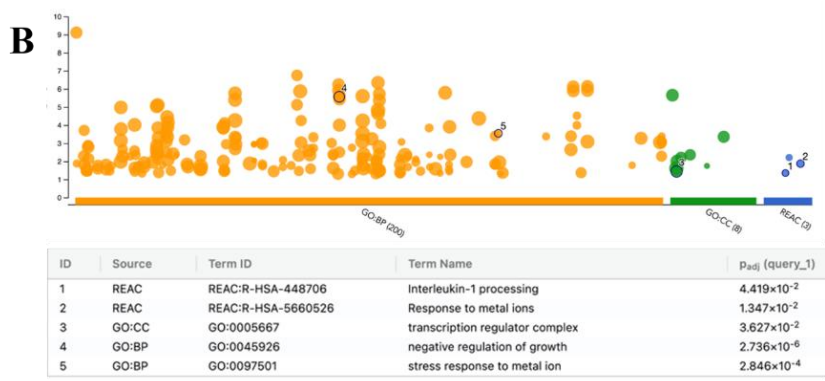
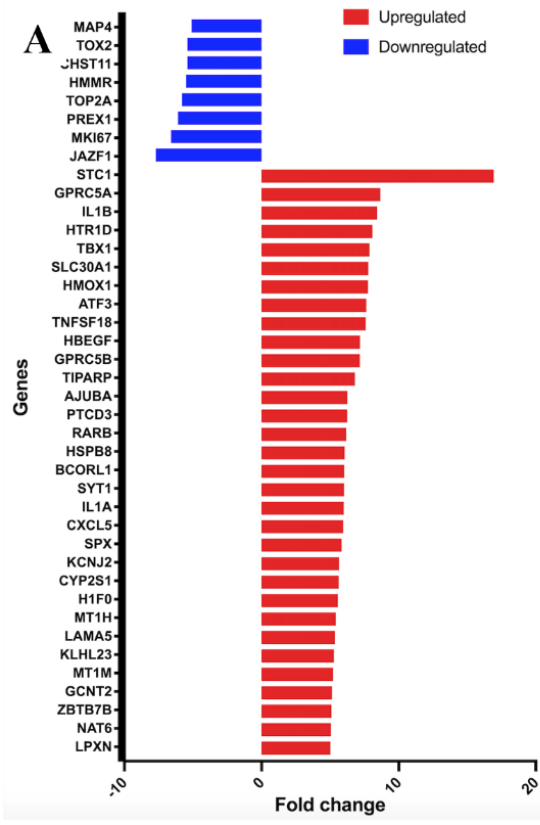
We then investigated the effect of CdSe/ZnS QD on normal HUVEC cells under static conditions (Figure 25). Panel A shows the upregulated and downregulated genes in response to cell exposure to CdSe/ZnS QD under static conditions compared to static HUVEC control. Some upregulated genes have a critical role in the vascular system, like the NR4A1 gene that plays a critical role in the vascular response to injury<sup>291</sup> and ADAMTS1, which works as an angiogenic inhibitor. ADAMTS1 is an active metalloprotease that is also associated with various inflammatory responses.<sup>292</sup> The downregulated gene JAZF1 is a transcriptional corepressor of nuclear receptors such as the nuclear receptor subfamily 2 group C member 2 (NR2C2) involved in embryo development.<sup>293</sup>

Figure 25-B shows the upregulated biological processes, cellular components, and pathways with a fold change of 2 and greater. The biological process upregulated in response to CdSe/ZnS QD is

heat acclimation, a stress response. Heat acclimation response upregulates proteins such as the heat shock protein 72 (HSP72), which inhibits the necrosis factor kappa-B pathway, preserving the epithelial function and reducing inflammation.<sup>294</sup> Cellular components like the aggresome are also found to be upregulated and have been previously shown to take part in the inflammatory stress response.<sup>295</sup> Another important pathway in terminating the stress response is also found, which is the attenuation phase, and it attenuates the heat shock transcriptional response, which occurs with exposure to stress or upon the recovery from stress.<sup>296</sup> Overall, most of the processes and the upregulated pathways are working to resolve a stress response, and, in this case, exposure to CdSe/ZnS QD leads to a stress response in HUVEC cells.

On the other hand, the response to interferon-gamma was downregulated on HUVEC exposure to CdSe/ZnS QDs. Interferon-gamma is a proinflammatory cytokine that is involved in the Th1-driven immune response.<sup>297</sup> On exposure to CdSe/ZnS QDs, this biological process mediated by interferon-gamma is downregulated, which is also the cell's response to stress.

**Figure 25: Effect of exposure to CdSe/ZnS QDs on Euploid HUVEC cell transcriptome under static conditions.** (A) Graph showing genes that are upregulated and downregulated on exposure to CdSe/ZnS QD under static conditions compared to control static group with the upregulated genes with a fold change of  $\geq 5$  and downregulated genes with a fold change of  $\leq -5$ . Manhattan plots illustrating the pathway enrichment analysis results of: (B) Upregulated genes with the fold change  $\geq 2$  and (C) downregulated genes with fold change  $\leq -2$  versus control; results are classified into three categories: GO: BP (Biological Process), GO: CC (Cellular Component), and Reactome pathways. The number in the source name in the x-axis labels shows how many significantly enriched terms were found. The circle corresponds to term size. The information underneath the graph lists the terms found in each category with their corresponding term ID and P adjusted value.



### ***7.6 Effect of InP/ZnS QDs on Euploid HUVEC Cells under Static Conditions:***

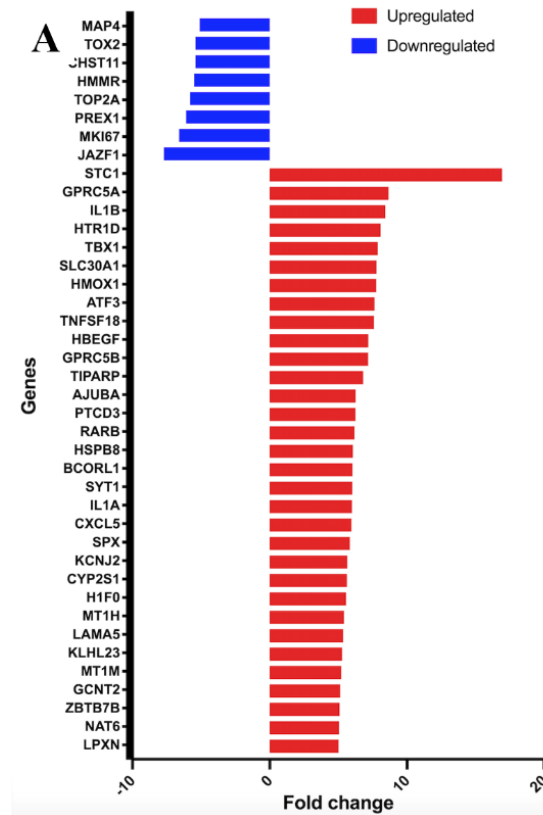
Exposure of normal HUVEC cells to InP/ZnS QDs under static conditions resulted in different outcomes (Figure 26). For example, a gene named GPRC5A was upregulated on exposure to InP/ZnS QDs. GPRC5A is involved in modulating differentiation and maintaining the homeostasis of epithelial cells.<sup>298</sup> The downregulated gene JAZF1 seen in panel A is a transcriptional corepressor of nuclear receptors such as the nuclear receptor subfamily 2 group C member 2 (NR2C2) involved in embryo development.<sup>293</sup> The genes that are either upregulated or downregulated with cell exposure to InP/ZnS QDs all have an important role in endothelial cell maintenance, but some are more affected than the others, as seen in the different fold changes for each gene.

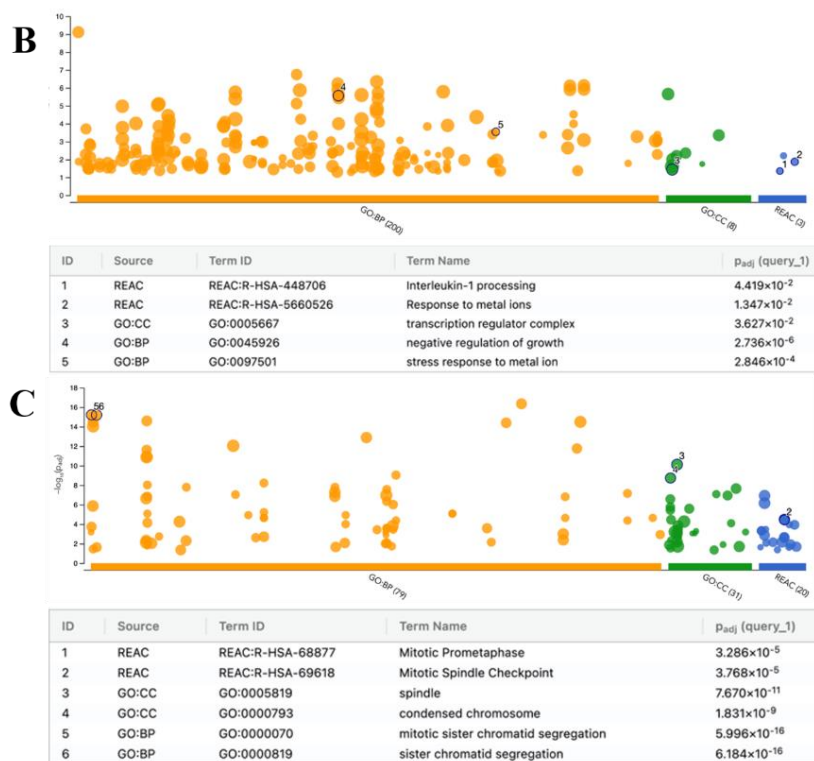
Pathway enrichment analysis showed that the biological process that is found to be upregulated is negative regulation of growth which is any process that reduces the rate or extent of growth by either stopping or preventing growth (Figure 26-B).<sup>299</sup> The cellular component that is upregulated is the transcription regulator complex which regulates the transcription of genes. The pathway that is upregulated with the exposure of InP/ZnS QD is interleukin-1 processing. Interleukin-1 by itself is an inflammatory mediator that acts directly on human vascular endothelial cells (HUVEC) and causes changes to their two functional properties. The first functional property it alters is it induces endothelial cell biosynthesis and surface expression of a tissue factor-like procoagulant activity. The second functional property that it changes is that the IL-1 dramatically increases the adhesiveness of the endothelial surface for human peripheral blood polymorphonuclear leukocytes and monocytes and the related leukocyte cell lines.<sup>300</sup> IL-1 promotes inflammation by inducing the expression of adhesion molecules on endothelial cells, as described before.<sup>301</sup> Another pathway that is also upregulated is a stress response to metal ions, and this process results in changes in the state or activity of a cell in terms of movement, secretion, enzyme production, gene expression, and so on of metal ion stimulus.<sup>302</sup> The upregulated biological process, cellular components, and pathways all show that some changes occur to HUVEC cells with the exposure to InP/ZnS QD, whether it is in terms of gene expression, inflammation, growth, or just cellular homeostasis.

Figure 26-C shows the downregulated genes with a fold change of -2 and less analyzed using the g: profiler. The biological process that affects the cell cycle is also downregulated and is called

mitotic sister chromatid segregation. Overall, the downregulated processes are mostly involved in mitosis; thus, it affects cell growth.

**Figure 26: Effect of exposure to InP/ZnS QDs on Euploid HUVEC cell transcriptome under static conditions.** (A) Graph showing upregulated and downregulated genes on exposure to InP/ZnS QDs under static conditions compared to the control static group with the upregulated genes having fold change of  $\geq 5$  and downregulated genes with a fold change of  $\leq -5$ . Manhattan plots illustrating the pathway enrichment analysis results of: (B) Upregulated genes with the fold change  $\geq 2$  and (C) downregulated genes with fold change  $\leq -2$  versus control; results are classified into three categories: GO: BP (Biological Process), GO: CC (Cellular Component), and Reactome pathways. The number in the source name in the x-axis labels shows how many significantly enriched terms were found. The circle corresponds to term size. The information underneath the graph lists the terms found in each category with their corresponding term ID and P adjusted value.





### 7.7 Effect of CdSe/ZnS QDs in Euploid HUVEC cells under dynamic conditions:

Application of CdSe/ZnS QDs on normal HUVEC cells in dynamic conditions resulted in several upregulated and downregulated responses compared to the dynamic control condition (Figure 27). The upregulated genes with the highest fold change were CHAC1 and ZFAND2A. CHAC1 acts as a pro-apoptotic component of the unfolded response pathway and catalyzes the cleavage of glutathione into 5-oxo-L-proline and a Cys-Gly dipeptide.<sup>303,304</sup> Depletion of glutathione initiates and executes apoptosis, showing that CHAC1 has a clear role in apoptosis.<sup>304</sup> This also means that exposure of HUVEC cells to CdSe/ZnS QD can lead to programmed cell death. In the downregulated set of genes, one particular gene with a key role in the immune system is CCL20. CCL20 acts as a chemotactic factor that mainly attracts lymphocytes to small neutrophils, but not the monocytes.<sup>305</sup> It helps recruit IL-17 which helps produce helper T-cells (th17) and the regulatory T-cells (Treg) to the site of inflammation.<sup>306</sup> This shows that CCL20 plays the role of attracting and recruiting pro-inflammatory factors involved in an inflammatory response.

Two pathways are upregulated, namely Regulation of HSF-1 mediated Heat Shock response and attenuation phase (Figure 27-B). The pathway related to the Heat Shock response is active under a stress response where the heat shock proteins are activated by HSF-1, which prevent or suppress apoptosis by regulating both the mitochondrial and death receptor pathways of apoptosis. The heat shock proteins also interfere with caspase activation at several different levels.<sup>307</sup> This shows that HSF-1 plays a cytoprotective factor under a stressful condition such as the one that cells might experience with exposure to CdSe/ZnS QDs. The attenuation phase is another pathway that is upregulated, which works to attenuate the heat shock transcriptional response. Attenuation occurs due to continuous exposure to intermediate heat shock conditions or upon the recovery from stress.<sup>296</sup> This pathway, in turn, is working towards bringing everything back to normal once the heat shock response has occurred, so overall, it works to modulate the heat shock response. The cellular component which is upregulated is aggresome. An aggresome is defined to be an inclusion body formed by dynein-dependent retrograde transport of an aggregated protein on microtubules.<sup>308</sup> Aggresome has been seen to play a role in inflammatory stress response where it inactivated nitric oxide synthase, which in turn terminates the nitric oxide production. Nitric oxide is an agent of inflammation, so aggresome works to eliminate a factor that can play a role in inflammation.<sup>295</sup>

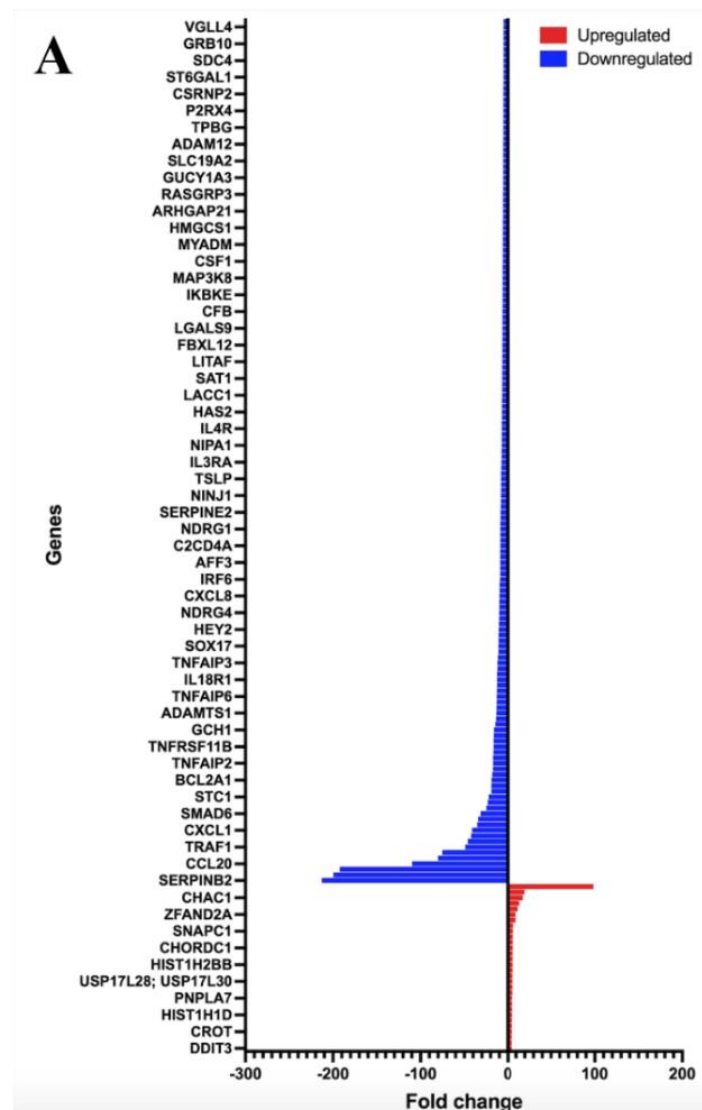
Two biological processes were also upregulated: chaperone-mediated protein folding and the epithelial cell apoptotic process (Figure 27-B). The chaperone-mediated protein folding inhibits aggregation and assists in the covalent and noncovalent assembly of single chain polypeptides or multi-subunit complexes into their correct tertiary structures. This process is dependent on the interaction with a chaperone protein. This process is also important under a stress condition where the proteins are getting denatured and forming aggregates, and chaperone proteins here can help fold the proteins into their correct shape.<sup>308</sup> As previously stated, the stress conditions can lead to an increase in the frequency, rate, or extent of the endothelial cell apoptotic process, which is why the biological process involving positive regulation of the epithelial cell apoptotic process is upregulated.<sup>309</sup> Since endothelial cells are a type of epithelial cells, the results can comparably be interpreted for endothelial cells.

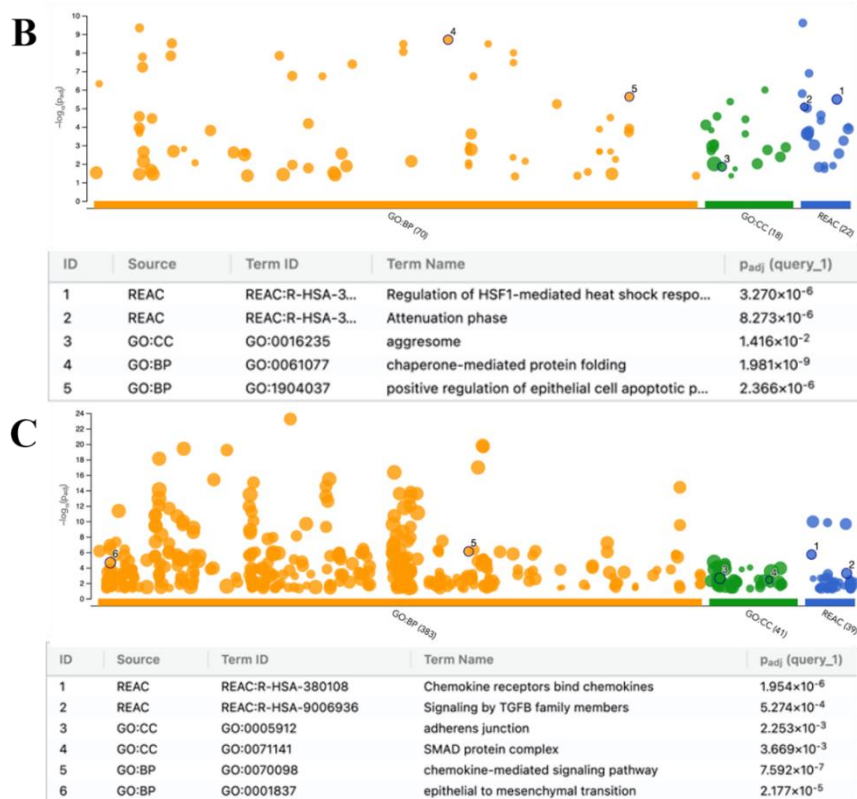
On the other hand, the downregulated pathways were chemokine receptors bind chemokines and signaling by TGF $\beta$  family members (Figure 27-C). The chemokine receptor binds chemokines

pathway causes the flux of intracellular calcium when the chemokine binds the chemokine receptor, leading to chemotaxis. <sup>313</sup> This pathway is downregulated and is probably a feedback mechanism whereby cells are trying to survive under a stress condition where the inflammatory response is upregulated due to the toxic environment created by CdSe/ZnS QD. TGF-beta members such as TGF-beta 3 are induced due to shear stress on endothelial cells, activating KLF2 and NO signaling, limiting endothelial dysfunction, and maintaining endothelial homeostasis.<sup>262</sup> The TGF-beta members are a superfamily of ligands that bind cell-surface receptor serine/threonine kinases to activate SMAD-dependent and SMAD-independent signaling.<sup>263</sup> TGF-beta has multiple roles, and one of its roles is to stimulate cytoskeleton in almost all non-neoplastic epithelial cells and endothelial cells. Their primary role is to facilitate leukocyte adherence on endothelial cells by activating integrins and then inducing chemotaxis of those leukocytes in the tissue environment. It has also been reported to either induce or suppress programmed cell death in different cell types and plays a role in cell dormancy and autophagy.<sup>261</sup> Looking at the number of roles that TGF-beta members play, CdSe/ZnS QD exposure in dynamic conditions has a huge impact on this pathway.

The cellular components that are down-regulated are the adherens junction and SMAD-protein complex. Adherens junction is affected by shear stress, where shear stress causes reorganization of endothelial adherens junction through pathways involving MAP kinase, Src, and Rho proteins.<sup>256</sup> SMAD-protein complex is also affected by fluid shear stress where shear stress-activated SMAD 2/3 induces their nuclear translocation. Low fluid shear stress also increases SMAD 2/3 gene expression and promotes low flow-induced inward artery remodeling.<sup>254</sup> SMAD-protein complex plays a major role in regulating artery size, and endothelial cells use SMAD signaling after perceiving the direction of blood flow to control the artery size.<sup>310</sup> The two biological processes downregulated were the chemokine-mediated signaling pathway and the epithelial to mesenchymal transition. The chemokine-mediated signaling pathway is a series of molecular signals initiated by the binding of chemokine to its cell-surface receptor and ends with regulating a downstream cellular process such as transcription of certain genes.<sup>311</sup> Chemokines are produced by both immune cells and non-immune cells, so cytokines can play a role in chronic inflammation.<sup>312</sup> Low shear stress affects the epithelial to mesenchymal transition and causes dedifferentiation of endothelial cells through this process.<sup>258</sup> Thus, all the downregulated pathways and processes play very important roles and are impacted by exposure to CdSe/ZnS QD.

**Figure 27: Effect exposure to CdSe/ZnS QD on Euploid HUVEC cell transcriptome under dynamic conditions.** (A) Graph showing upregulated and downregulated genes on cell exposure to CdSe/ZnS QD compared to the control group in dynamic conditions with the upregulated genes having fold change of  $\geq 5$  and downregulated genes with a fold change  $\leq -5$ . Manhattan plots illustrating the pathway enrichment analysis results of: (B) Upregulated genes with the fold change  $\geq 2$  and (C) downregulated genes with fold change  $\leq -2$  versus control; results are classified into three categories: GO: BP (Biological Process), GO: CC (Cellular Component), and Reactome pathways. The number in the source name in the x-axis labels shows how many significantly enriched terms were found. The circle corresponds to term size. The information underneath the graph lists the terms found in each category with their corresponding term ID and P adjusted value.





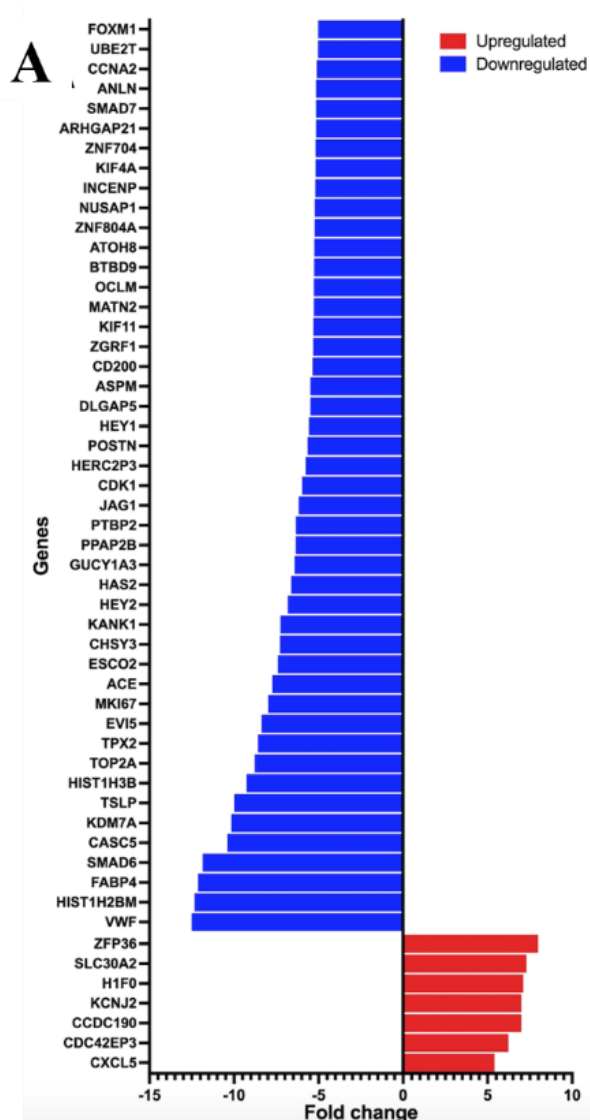
### 7.8 Effect of Exposure to InP/ZnS QDs on Euploid HUVEC cells under Dynamic Conditions:

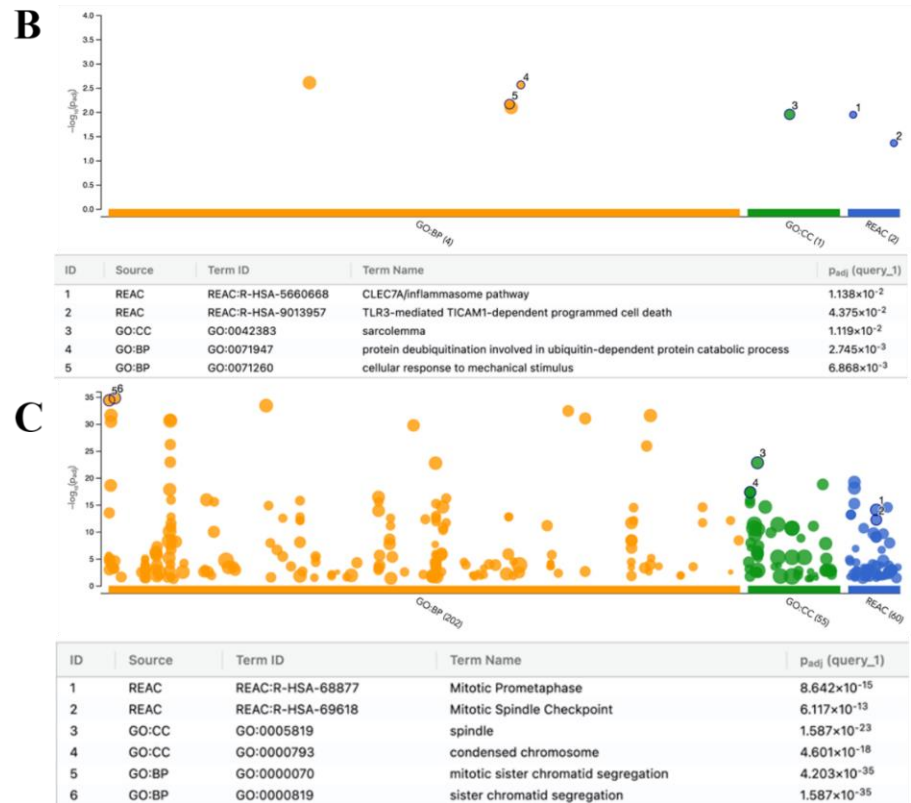
Exposure of normal HUVEC cells to InP/ZnS QDs under dynamic conditions resulted in different upregulated and downregulated responses versus control dynamic conditions compared to results obtained for CdSe/ZnS QDs described above. One of the genes downregulated on exposure to InP/ZnS QDs on HUVEC cells is HIST1H2BM, also called Histone H2B type 1-M, and is found to play a central role in transcription regulation, DNA repair, DNA replication, and chromosomal stability.<sup>313</sup> Some of the genes that are upregulated also have very important functions. ZFP36 is an upregulated gene and is part of the mechanism that attenuates protein synthesis. It also plays a key role in anti-inflammatory responses and suppresses tumor necrosis factor (TNF)- alpha production.<sup>314</sup> We can conclude that the genes are either upregulated or downregulated due to environmental stimuli and respond to these stimuli to maintain the integrity and function of the cells.

To further investigate the effects of the InP/ZnS QDs on HUVEC cells, pathway enrichment analysis was performed. One of the upregulated pathways was CLEC7A/inflammasome pathway. CLEC7A/Inflammasome pathway was shown previously to enable the host immune system to mount a protective TH17 response against infection.<sup>315</sup> Two biological processes were also upregulated: protein deubiquitination involved in ubiquitin-dependent protein catabolic process and cellular response to mechanical stimulus. The protein deubiquitination process is part of the protein catabolism process mediated by ubiquitin, where deubiquitination removes one or more ubiquitin groups from a protein.<sup>316</sup> The cellular response to the mechanical stimulus is a process that causes changes in the structural and functional properties of the cells at the cellular, molecular and genetic levels.<sup>317</sup> The endothelial-related gene expression is increased with the laminar shear stress, which is mechanical stress.<sup>318</sup> Overall, all the pathways and processes that are upregulated have a great effect in many ways on cells, either through changes in gene expression, response to inflammation, or changes in protein metabolism.

Pathways significantly downregulated are mitotic prometaphase and spindle checkpoint. Prometaphase is a process in mitosis whereby duplicated genetic material in the parent cell nucleus is separated into two identical daughter cells.<sup>290</sup> Spindle checkpoint, on the other hand, is a mechanism that ensures that cells with misaligned chromosomes do not exit mitosis and divide to form aneuploidy cells.<sup>319</sup> These two pathways are involved in cell division downregulated by HUVEC exposure to InP/ZnS QDs. During sister chromatid segregation, the replicated homologous chromosomes are organized and are then separated and apportioned to two sets during mitosis.<sup>320</sup> Summarily, we can see a repetitive pattern where the cell cycle is affected by exposure to InP/ZnS QDs, evident by the downregulation of processes and the pathways that are all related to the cell cycle.

**Figure 28: Effect of exposure to InP/ZnS QDs on Euploid HUVEC cell transcriptome under dynamic conditions.** (A) Graph showing upregulated and downregulated genes on cell exposure to InP/ZnS QDs in comparison control group under dynamic conditions. Here, the upregulated genes have a fold change of  $\geq 5$ , and downregulated genes have a fold change of  $\leq -5$ . Manhattan plots illustrating the pathway enrichment analysis results of: (B) Upregulated genes with the fold change  $\geq 2$  and (C) downregulated genes with fold change  $\leq -2$  versus control; results are classified into three categories: GO: BP (Biological Process), GO: CC (Cellular Component), and Reactome pathways. The number in the source name in the x-axis labels shows how many significantly enriched terms were found. The circle corresponds to term size. The information underneath the graph lists the terms found in each category with their corresponding term ID and P adjusted value.





### 7.9 Effect of Exposure to CdSe/ZnS QD on Aneuploid HUVEC Cells in Static Conditions:

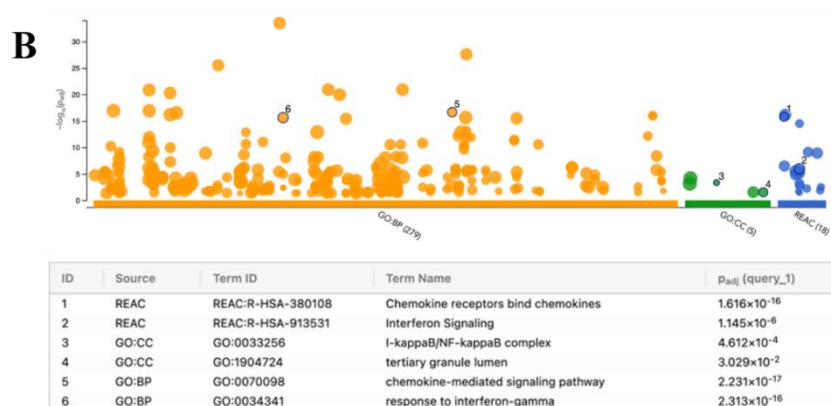
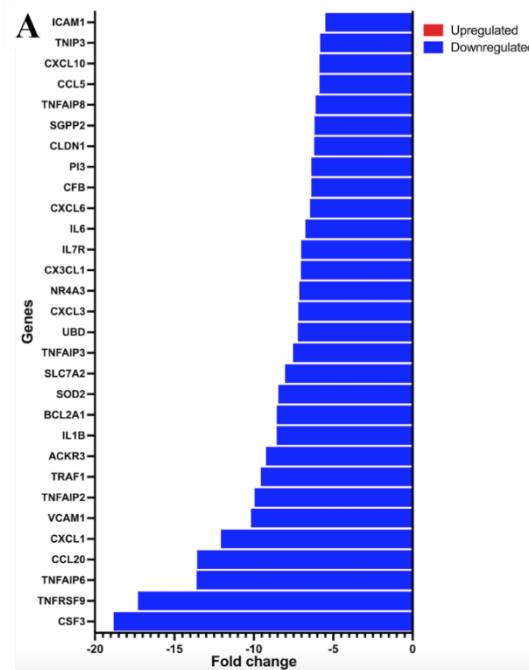
Interestingly, exposure of aneuploid HUVEC cells to CdSe/ZnS QDs did not result in significant gene upregulations. Figure 29-A shows the downregulated genes in response to the CdSe/ZnS QDs in aneuploid cells in static condition compared to control aneuploid cells not exposed to QDs in static condition. Two genes with the higher folded change compared to other genes were downregulated and have been found to play a role in the immune response. The first gene is CSF3, a cytokine that acts in the hematopoiesis by controlling the production, differentiation, and function of two related white cell populations - the granulocytes and the monocytes-macrophages.<sup>321</sup> The second gene is TNFRSF9 (tumor necrosis factor receptor superfamily member 9). This gene expresses a receptor for TNFSF9 and activates mediators of the immune response such as T-cells.<sup>322</sup>

Pathway enrichment analysis shows that Chemokine receptors bind chemokine pathway was downregulated. This pathway causes intracellular calcium flux when the chemokine binds the chemokine receptor, leading to chemotaxis. Their primary role is to facilitate leukocyte adherence

on endothelial cells by activating integrins and then inducing chemotaxis of those leukocytes in the tissue environment.<sup>323</sup> This pathway is also involved in cancer, where the altered expression of the chemokines in malignancies dictates leukocyte recruitment and activation, angiogenesis, cancer cell proliferation, and metastasis in all stages of the disease. Chemokines have also been studied to promote tumor cell survival by preventing apoptosis and regulating the balance between pro-and anti-apoptotic molecules.<sup>324</sup> Overall, chemokines are involved in cancer progression and the inflammation experienced during the disease. Interferon signaling was another downregulated pathway that has been shown to induce tumor cell apoptosis through various mechanisms such as the TRAIL pathway via CD95/Fas members of the Bcl-2 family.<sup>268</sup> The cellular component that was also downregulated was I-kappaB/NF-kappaB complex. This complex contains an inhibitory kappaB protein and one or more copies of NF-kappaB proteins and works to sequester the NF-kappaB in the cytoplasm.<sup>325</sup> This cellular component is important since NF-kB plays an essential role in inflammatory responses where it induces pro-inflammatory genes, including cytokines and chemokines.<sup>326</sup>

The biological processes that were downregulated were chemokine-mediated signaling pathways and response to interferon-gamma. Chemokine-mediated signaling pathway starts with the binding of chemokine to its receptor found on the surface of a cell and ends with regulating a downstream cellular process such as transcription.<sup>327</sup> Chemokines themselves are produced both by the immune and nonimmune cells, and due to this, they may play a pivotal role in orchestrating chronic inflammation. Therefore, the chemokine signaling pathway is one of the pathways which is activated during an inflammatory response.<sup>312</sup> Response to interferon-gamma is another pathway that is also downregulated, and the pathway has plenty of important functions. Interferon-gamma is a pro-inflammatory cytokine that is involved in Th-1 driven immune responses.<sup>297</sup> It also acts directly on vascular muscle cells and induces cellular proliferation and intimal expansion.<sup>328</sup> IFN-gamma also disrupts the epithelial barrier, leading to increased paracellular permeability and endocytosis of tight junction proteins, including JAM-A and claudin-1.<sup>329</sup> IFN-gamma also reduces the immune response and stimulates the progression and metastasis of tumor.<sup>330</sup> Overall, IFN-gamma has various roles, including its participation in inflammation, tumor growth, and increased permeability of barriers.

**Figure 29: Effect of exposure to CdSe/ZnS QDs on Aneuploid HUVEC cell transcriptome in a static condition.** (A) Graph showing downregulated genes on aneuploid HUVEC cell exposure to CdSe/ZnS QDs in the static condition compared to control static aneuploid cells with the downregulated genes having a fold change of  $\leq -5$ . Manhattan plots illustrating the pathway enrichment analysis results of: (B) Upregulated genes with the fold change  $\geq 2$  and (C) downregulated genes with fold change  $\leq -2$  versus control; results are classified into three categories: GO: BP (Biological Process), GO: CC (Cellular Component), and Reactome pathways. The number in the source name in the x-axis labels shows how many significantly enriched terms were found. The circle corresponds to term size. The information underneath the graph lists the terms found in each category with their corresponding term ID and P adjusted value.



### ***7.10 Effect of Exposure to CdSe/ZnS QDs on aneuploid HUVEC cells under dynamic conditions***

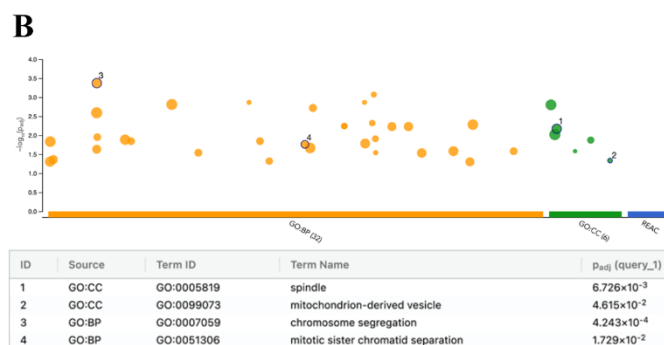
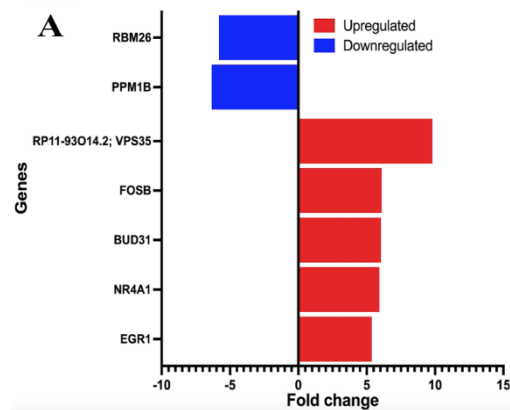
It was then important to determine the effect of CdSe/ZnS QDs on HUVEC cells under conditions capturing the angiogenic vessels in a tumor microenvironment, both endothelial cell aneuploidy, and dynamic conditions. Figure 30-A shows the upregulated and downregulated genes in response to the QDs in aneuploid cells in dynamic conditions compared to control aneuploid cells. The two upregulated genes with the highest fold changes have very important functions. The VPS35 gene, also known as vascular protein sorting-associated protein 35, acts as a retromer cargo-selective complex (CSC) component. The CSC is the core functional component of the retromer or respective retromer complex variant that prevents the mis-sorting of detected transmembrane cargo proteins into the lysosomal degradation pathway.<sup>331</sup> Another gene that is upregulated is FOSB. This gene interacts with jun proteins enhancing their DNA binding activity.<sup>332</sup> The upregulated genes are particularly important in maintaining the cells' normal homeostasis, such as the lysosomal degradation pathway or DNA binding activity required for gene transcription. Two downregulated genes play very important roles. One of them is RBM26 which plays a role in mRNA processing, metal ion binding, and RNA.<sup>333</sup> PPM1B is the second downregulated gene, which plays an important role in the termination of TNF-alpha mediated NF-kappa-B activation through dephosphorylating and inactivating IKBKB/IKKB.<sup>334</sup> The downregulated genes discussed above have multiple roles in normal cells, and their function and role are affected significantly with exposure to QDs, aneuploidy, and dynamic conditions.

Pathway enrichment analysis was performed to investigate further the effects of the CdSe/ZnS QD on aneuploid cells under dynamic conditions. The cellular components that were upregulated were spindle and mitochondrion-derived vesicles. A spindle is a specialized microtubule structure designed to attach and capture chromosomes to partition them evenly to each daughter cell.<sup>335</sup> A study showed that the spindle orientation appeared to be according to the cell elongation along the zero-force direction in response to dynamic shear.<sup>336</sup> This shows that dynamic conditions can impact the orientation of the spindles, which in turn can impact the process of mitosis, during which the spindles take an important part. Mitochondrion-derived vesicle is another upregulated cellular component that is derived via budding from a mitochondrion. Mitochondrion-derived vesicles have been found to play a role in inflammation whereby it prevents inflammation by

controlling the inclusion of mitochondrial proteins into the extracellular vesicles.<sup>336</sup> Mitochondrion-derived vesicles contain inner membrane and, much more and rarely, cristae.<sup>337</sup>

Two biological pathways are upregulated, namely chromosome segregation and mitotic sister chromatid segregation. Chromosome segregation is a process in which the genetic material, in the form of chromosomes, is organized into specific structures and then physically separated and apportioned to two or more sets.<sup>338</sup> A study shows that external forces like mechanical disruptions affect chromosome segregation.<sup>339</sup> Upregulation of chromosome segregation process is related to cell division, which means that with the exposure of CdSe/ZnS QDs on aneuploid cells under dynamic conditions, cell division is enhanced and thus may contribute to the proliferation of aneuploid HUVEC cells. Another pathway that is upregulated and related to mitosis is mitotic sister chromatid separation, a process in which the sister chromatids are physically detached from each other during mitosis.<sup>340</sup> Again, the upregulated biological processes are related to cell division; thus, surprisingly, CdSe/ZnS QDs on aneuploid HUVEC cells under dynamic conditions enhanced cell division and mitosis processes, unlike responses observed earlier for experiments under static conditions.

**Figure 30: Effect of CdSe/ZnS QD exposure on aneuploid HUVEC cell transcriptome under dynamic conditions.** (A) Graph showing upregulated and downregulated genes on aneuploid cell exposure to CdSe/ZnS QDs compared to control aneuploid HUVEC cells under dynamic conditions with the downregulated genes having a fold change of  $\leq -5$ . Manhattan plots illustrating the pathway enrichment analysis results of: (B) Upregulated genes with the fold change  $\geq 2$  and (C) downregulated genes with fold change  $\leq -2$  versus control; results are classified into three categories: GO: BP (Biological Process), GO: CC (Cellular Component), and Reactome pathways. The number in the source name in the x-axis labels shows how many significantly enriched terms were found. The circle corresponds to term size. The information underneath the graph lists the terms found in each category with their corresponding term ID and P adjusted value.



### 7.11 Effect of InP/ZnS QDs on Aneuploid HUVEC cells under static conditions:

Exposing aneuploid HUVEC cells to InP/ZnS QDs under static conditions compared to their corresponding control static group of aneuploid cells resulted in the downregulation of two genes that role in cell survival and inflammation, NR4A3, and BIRC3 (Figure 31-A). NR4A3 regulates the proliferation, survival, and differentiation of many different cell types and is also involved in metabolism and inflammation.<sup>341</sup> BIRC3, on the other hand, is a multi-functional protein that not only regulates caspases and apoptosis but also modulates inflammatory signaling and immunity, mitogenic kinase signaling, and cell proliferation.<sup>342</sup> All of the functions of these two genes are downregulated with the exposure of InP/ZnS QDs in aneuploid cells under static conditions impacts several cell functions.

According to pathway enrichment analysis, the upregulated cellular components were bicellular tight junction and cell leading edge. The bicellular tight junction is an occluding cell-cell junction

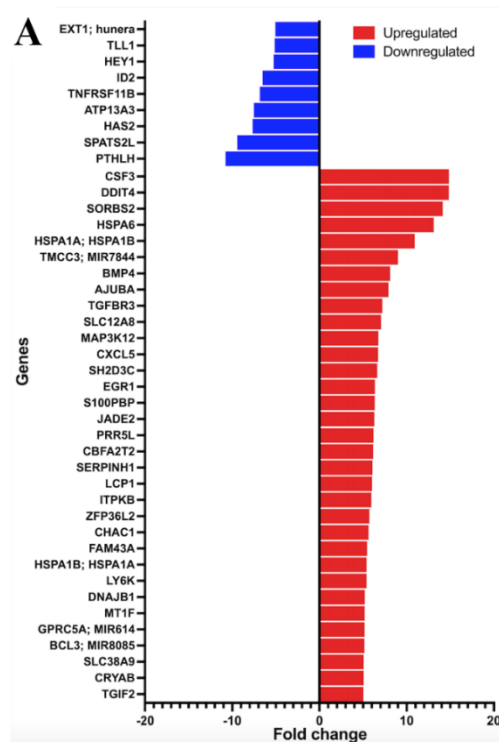
composed of a branching network of sealing strands that encircle each cell's apical end in an epithelial sheet.<sup>343</sup> As such, the bicellular tight junctions are present in all tissues and organs' epithelial and endothelial cells.<sup>344</sup> Cell leading edge is the area of a motile cell closest to the direction of the movement.<sup>345</sup> Both of the cellular components that are upregulated have structural importance in the cell, and as said before, bicellular tight junctions work as a barrier and seal the cell whereas the cell leading edge is more related to the movement of the cell.

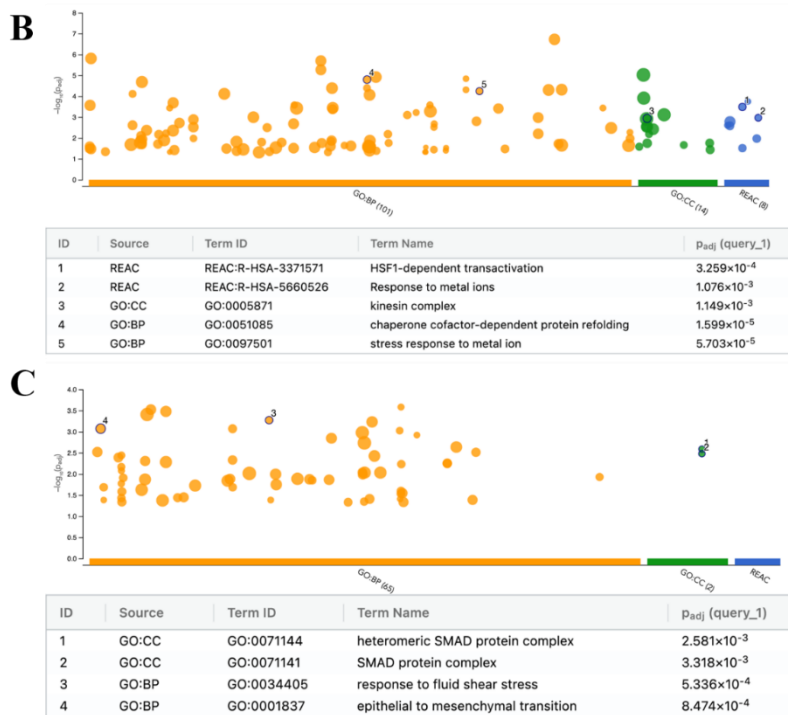
Two biological pathways were upregulated, playing a role in the immune system. Their upregulation is thus important on cell exposure to foreign material such as the InP/ZnS QDs. The first biological process is epithelial cell development. Epithelial cells are non-professional phagocytes that internalize pathogens via “trigger” or “zipper” mechanisms. A “trigger” mechanism causes membrane ruffles and then internalization through the modulation of the actin cytoskeleton, the trigger being when a pathogen secretes effector proteins in the host cell. A “zipper” mechanism is based on the interaction of the host receptor on the plasma membrane with invasion proteins expressed on the pathogen surface, leading to localized cytoskeleton rearrangement and pathogen uptake.<sup>346</sup> This shows the importance of epithelial cells and their role in the immune system. The second is endothelium development, another biological process that is upregulated. Endothelial cells are major participants in and regulators of inflammatory reactions. Resting endothelial cells have been shown to prevent coagulation, control blood flow and passage of proteins into tissues and inhibit inflammation.<sup>347</sup> Endothelial cells studied in the gene analysis have multiple roles, of which inhibiting inflammation is an important one.

Pathway enrichment analysis also shows the downregulation of the chemokine receptors binds chemokines pathway. Chemokines are a large family of cytokines with chemotactic activity, and both cancer and stromal cells express their cognate receptors. Their altered expression in malignancies dictates leukocyte recruitment and activation, angiogenesis, cancer cell proliferation, and metastasis in all the stages of the disease.<sup>324</sup> The two downregulated biological processes were chromosome segregation and mitotic nuclear division. Chromosome segregation is when genetic material in the form of chromosomes is organized into specific structures and then physically separated and apportioned to two or more sets.<sup>348</sup> Mitotic nuclear division is a cell cycle process comprising the steps by which the nucleus of a eukaryotic cell divides. This process involves condensing the chromosomal DNA into a highly compacted form, resulting in two daughter nuclei

whose chromosomes complement is identical to the mother cell.<sup>349</sup> Both of these processes related to cell division are downregulated, which means that the cell cycle is affected by the InP/ZnS QD exposure. Cell division can only happen if the cells are under optimal conditions, with all the resources for cell division, but InP/ZnS QDs introduce a stress situation where the cell is striving to survive rather than proliferate.

**Figure 31: Effect of exposure to InP/ZnS QDs on aneuploid HUVEC cell transcriptome in a static condition.** (A) Graph showing genes downregulated on aneuploid HUVEC cell exposure to InP/ZnS QDs in static condition compared to control static aneuploid cells with the downregulated genes having a fold change of  $\leq -5$ . Manhattan plots illustrating the pathway enrichment analysis results of: (B) Upregulated genes with the fold change  $\geq 2$  and (C) downregulated genes with fold change  $\leq -2$  versus control; results are classified into three categories: GO: BP (Biological Process), GO: CC (Cellular Component), and Reactome pathways. The number in the source name in the x-axis labels shows how many significantly enriched terms were found. The circle corresponds to term size. The information underneath the graph lists the terms found in each category with their corresponding term ID and P adjusted value





### 7.12 Effect of InP/ZnS QDs in aneuploid HUVEC cells in dynamic conditions:

Finally, we investigated the effect of InP/ZnS QDs we designed on aneuploid HUVEC cells under dynamic conditions. Figure 32-A shows the upregulated and downregulated genes in aneuploid HUVEC cells in response to InP/ZnS QDs in the dynamic conditions relative to control aneuploid HUVEC cells present in the dynamic conditions dynamic condition. The gene DDIT4 is upregulated and is called DNA damage-inducible transcript-4 protein, which regulates cell growth, proliferation, and survival by inhibiting the activity of the mammalian target of rapamycin complex-1 (mTORC1). In addition, DDIT4 also regulates the p53/TP53-mediated apoptosis in response to DNA damage by its effect on mTORC1 activity.<sup>350</sup> The PTHLH gene, also called parathyroid hormone-related protein, is downregulated. This protein is a neuroendocrine peptide that is a critical regulator of cellular and organ growth, development, migration, differentiation and survival, and epithelium calcium ion transport.<sup>351</sup> The upregulated gene, DDIT4, is working towards cell survival which is needed since InP/ZnS QDs, which are foreign to the cells, can induce

a stress response, making cell death imminent. The downregulated gene is important for normal homeostasis, a cell mechanism absent in aneuploid cells, and exposure to InP/ZnS QDs.

Pathway enrichment analysis was performed to understand further the effect of InP/ZnS QDs on aneuploid HUVEC cells in a dynamic condition. The upregulated pathways are the HSF1-dependent transactivation and the response to metal ions (Figure 32-B). HSF-1 dependent transactivation is an important pathway for transcription activation of target genes.<sup>352</sup> HSF-1 also appears to have a pleiotropic role in cancer by supporting multiple facets of malignancy, including migration, invasion, proliferation, and cancer cell metabolism.<sup>353</sup> This shows an important role HSF-1 has in cancer and should be studied to target cancer therapy. The response to metal ions involves metal regulatory transcription factor 1 (MTF1), which activates gene expression to upregulate genes encoding proteins, such as metallothioneins and glutamate-cysteine ligase (GCLC) are involved in sequestering metals. Conversely, MTF1 also represses gene expression to down-regulate genes encoding transporters that import the metals into the cell.<sup>354</sup>

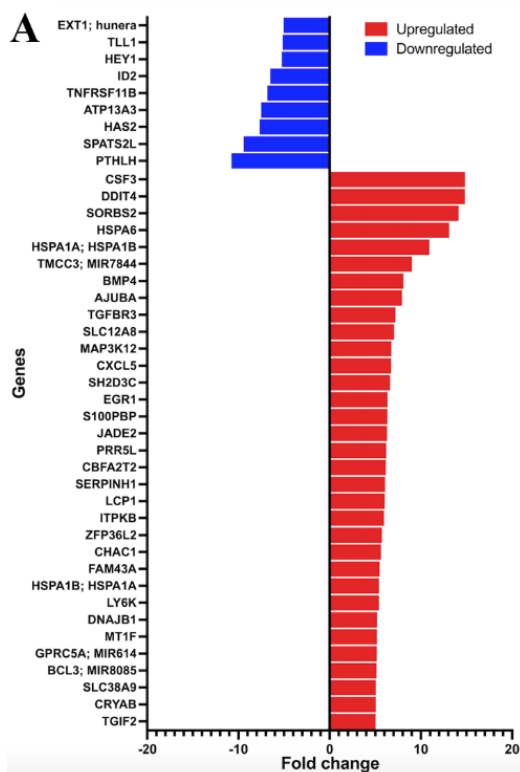
Upregulated biological processes were chaperone cofactor-dependent protein refolding and stress response to metal ions. Chaperone cofactor-dependent protein refolding is the process that assists in the correct posttranslational noncovalent assembly of a protein.<sup>355</sup> The stress response to metal ions is any process that results in a change in the state or activity of a cell or an organism due to disturbances in cellular homeostasis caused by a metal ion stimulus, InP/ZnS QDs herein. The changes experienced are cellular movement, secretion, enzyme production, gene expression, and much more.<sup>356</sup>

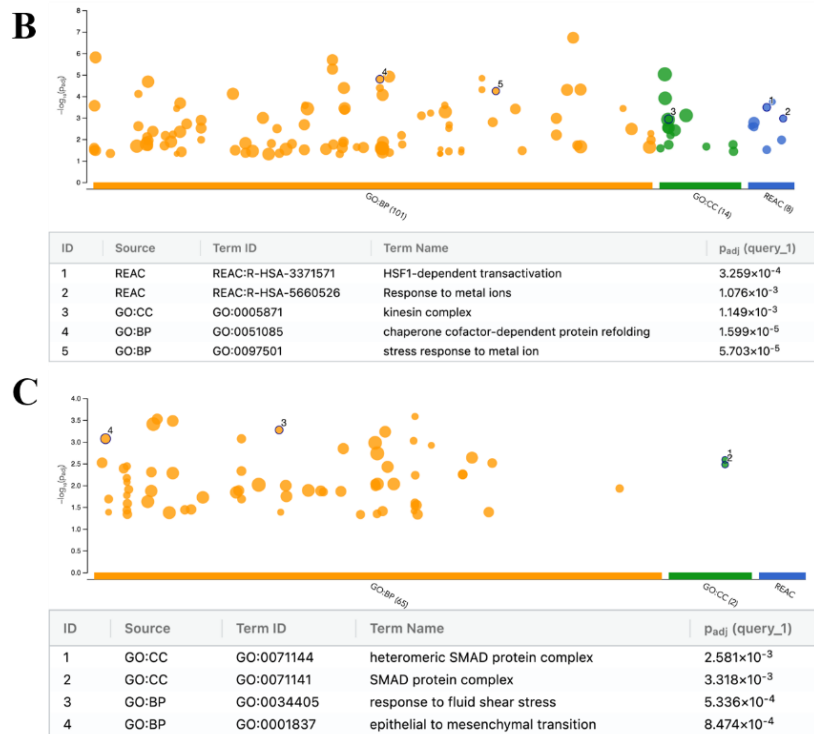
SMAD protein complex is the cellular component that is downregulated. It has been previously shown that fluid shear stress activates the SMAD 2/3 and induces nuclear translocation and gene expression maximally when the shear stress is low, promoting low flow-induced inward artery remodeling.<sup>254</sup> The upregulated biological processes respond to fluid shear stress and epithelial to mesenchymal transition. A study found that cancer cells of epithelial origin are more resistant to fluid shear stress than non-transformed epithelial cells. Fluid shear stress has the same effect on HUVEC cells as seen in cancer cells.<sup>277</sup> The other downregulated biological process is epithelial to mesenchymal transition, which has been influenced by low shear stress. Low shear stress works by inducing dedifferentiation of endothelial cells through the endothelial to mesenchymal

transition (EndMT).<sup>258</sup> Both of these biological processes have been impacted by shear stress which is the dynamic component of the condition applied to the aneuploidy cell. Dynamic condition downregulates shear stress response on cancer cells and dedifferentiation of endothelial cells.

**Figure 32: Effect of exposure to InP/ZnS QDs on aneuploid HUVEC cell transcriptome under dynamic conditions.** (A) Graph showing upregulated and downregulated genes on aneuploid cell exposure to InP/ZnS QDs y to control aneuploid HUVEC cells under dynamic conditions with the downregulated genes having a fold change  $\leq -5$ . Manhattan plots illustrating the pathway enrichment analysis results of:

(B) Upregulated genes with the fold change  $\geq 2$  and (C) downregulated genes with fold change  $\leq -2$  versus control; results are classified into three categories: GO: BP (Biological Process), GO: CC (Cellular Component), and Reactome pathways. The number in the source name in the x-axis labels shows how many significantly enriched terms were found. The circle corresponds to term size. The information underneath the graph lists the terms found in each category with their corresponding term ID and P adjusted value.





In summary, transcriptome sequencing has given us the up and downregulation of genes with corresponding fold-changes in the presence of different conditions (Table 2). Via Pathway enrichment analysis, we could evaluate the up-and down-regulated biological processes, cellular components, and pathways. Our findings confirm observations by cytotoxicity study that indium phosphide-based QDs were less cytotoxic than cadmium-based QDs, as we could see with evidence that the latter, under static and dynamic conditions irrespective of chromosomal stability, showed elevated stress response. Whereas for the indium-based QDs, only pathways and cellular components related to the cell division are impacted, and not many stress-related factors were affected significantly. Furthermore, we can observe a pattern of changes among the dynamic condition and cell aneuploidy compared to those normal euploid cells in the static condition, thus emphasizing the importance of studying both QDs under a dynamic environment simulating the angiogenic blood vessel surrounding solid tumors. In the future, we plan to analyze the data further using hierarchical clustering software to determine the connections between the different pathways to further understand the changes in the cell transcriptome due to the different experimental conditions.

## CHAPTER 4 – SUMMARY

Nanoparticles (NPs) have found great applications, especially for tumor targeting. Cadmium-based QDs such as CdSe/ZnS have as bright fluorophores for diagnostic applications. However, their inherently toxic nature has limited their translation. Several research attempts have resulted in several alternatives, of which the InP/ZnS QDs showed great potential with lower toxicity. So far, these InP/ZnS QDs were only studied under static conditions *in vitro* or using *in vivo* models. These models could potentially be very different and show different results than in actual dynamic physiological conditions of humans. One of our primary goals has been to develop a biomimetic *in vitro* vessel-on-a-chip model that recapitulates the physiological and pathological conditions of angiogenic vessels surrounding solid tumors and thus overcome these discrepancies seen in results obtained from static models or models of different species. Our other aim was to successfully develop InP/ZnS QDs and surface functionalize them to render them suitable for biological applications and evaluate them using the developed microfluidic vessel-on-a-chip model compared to commercial CdSe/ZnS QDs.

To this effect, we synthesized InP/ZnS QDs and characterized them for size ( $3.3\pm 0.78$  nm) and zeta potential ( $6.9\pm 2.12$ ). Using ligand exchange reaction, InP/ZnS QDs were successfully MPA-capped and transferred to the aqueous phase in the presence of TMAH as a catalyst.<sup>28,197</sup> We then conducted a stability study for 40 days in water at room temperature and EGM-2 culture media at 37°C. We tracked the fluorescence of InP/ZnS QDs as a metric for their colloidal stability; a reduction in fluorescence intensity or fluorescence quenching results from QD aggregation and precipitation. MPA-capped InP/ZnS, prepared using an MPA concentration of 400 nM, were shown stable for 40 days in water and 31 days in culture media. Similarly, we referred to previous studies done by our team to establish the stability of CdSe/ZnS QD and deem it as a suitable cadmium-based QD for comparison.<sup>21,357</sup>

Before evaluating the cell uptake of QDs and their impact on the cell transcriptome using the vessel-on-a-chip model, we needed to determine the concentration range that can be used safely without inducing significant cell toxicity. We used Vialight assay to compare the effect of both QDs (2 - 50 nM) on the cell viability of healthy (euploid) and aneuploid HUVEC cells after 24 hours under static conditions. We observed no significant impact of CdSe/ZnS QDs on the viability

of healthy HUVEC cells up to a concentration of 5 nM, whereas higher concentrations of 10 nM and 20 nM reduced cell viability around 66% and 60%, respectively. CdSe/ZnS QDs were extremely toxic to healthy HUVEC cells at 50nM concentration with cell viability of 22%. However, aneuploid HUVEC cells were more resistant to the toxicity of CdSe/ZnS QDs, and no significant changes in cell viability were observed up to a QD concentration of 10 nM. This indicates that the chromosomal stability of the cells could result in different responses to NPs. Unlike the case of CdSe/ZnS QDs, exposure of both normal and aneuploid HUVEC cells to InP/ZnS QDs resulted in no significant changes in cell viability. This confirms our initial hypothesis that InP/ZnS QDs (indium-based cores) are less toxic to HUVEC cells when compared to CdSe/ZnS that are potentially accompanied by the release of toxic cadmium ions.

We then evaluated the cell uptake of QDs and their impact on the cell transcriptome in a dynamic environment using the vessel-on-a-chip system that we developed. HUVEC cells were cultured and subjected to dynamic and aneuploid conditions compared with static and euploid counterparts. These models were then subjected to a combination of conditions that mimic physiological conditions of shear stress and subjected to the presence or absence of the two types of QDs (Table 2). We have come to the following conclusions at each stage of this study that has further informed us on our hypotheses – that wall shear stress and aneuploidy both significantly impact cell phenotype and thereby affect the results of microfluidic *in vitro* models under biomimetic conditions.

Confocal studies for cell uptake of QDs show that overall, higher cell uptake of CdSe/ZnS QDs over InP/ZnS QDs is seen among both euploid and aneuploid groups under both static and dynamic conditions. This variance trend between the two types of QDs reaffirms the similar trend observed in cytotoxicity studies wherein both the concentration and overall tendency for cells to take up more CdSe/ZnS QDs have a massive impact on the ability of cells to survive. Whereas InP/ZnS QDs studied at the same concentrations did not impact the cell viability at any of those concentrations. However, we have strong evidence supporting the direct relationship between cell uptake of CdSe/ZnS QDs and cytotoxicity. The disparity in their cell uptake could also be attributed to the difference in the properties of QDs, including the surface chemistry.

Interestingly, only for aneuploid cells exposed to InP/ZnS QDs under dynamic conditions, no cell uptake of QDs was observed, unlike all other cell uptake experiments (Figure 21). This could be

potentially explained by differences in cell phenotype that resulted in this limited cell uptake of these QDs under a combination of shear stress and aneuploidy. Since these conditions with combined dynamic conditions and cell aneuploidy are the closest in replicating a physiological tumor microenvironment, where aneuploid cells come in contact with the physiological flow of blood, we can estimate that the endothelial cells will take up CdSe/ZnS QDs but not InP/ZnS QDs. So far, our confocal results echo the results of cytotoxicity assay and prove our initial hypothesis that shear stress and aneuploidy can dictate NP interaction with endothelial cells. However, cell transcriptome analysis was needed to confirm changes in cell phenotype under the different experimental conditions and to reveal mechanistic insights on the impact of both QDs under these conditions.

We now examine the transcriptomic results. When comparing HUVEC cells under dynamic to static conditions, the upregulated cellular components, pathways, and biological processes affected the vascular system, such as the SMAD complex, artery morphogenesis, and NGF-stimulated transcription. SMAD complex is activated by fluid shear stress,<sup>254,255</sup> a dynamic condition that promotes inward artery remodeling. The NGF-stimulated transcription pathway can stimulate endothelial cell invasion and induce angiogenesis,<sup>259</sup> illustrating that dynamic conditions lead to changes in the vascular system. The downregulated genes play a part in autophagy and apoptosis, and their downregulation means the reduction of apoptosis and an increase in cell maintenance under dynamic flow similar to physiological conditions.

On the other hand, induction of aneuploidy using monastrol under static conditions resulted in upregulation of the interferon signaling pathway<sup>268</sup>, which induces cell apoptosis and biological pathways such as the extrinsic apoptotic signaling pathway stress-activated MAPK cascade<sup>310</sup> that are anti-proliferative and pro-apoptotic in function. Most downregulated processes and pathways are related to hyaluronan – the hyaluronan catabolic process is usually commandeered by cancer cells for their growth, invasion, and metastasis. Its downregulation means a decrease in cell proliferation. Hyaluronan degradation<sup>270</sup> can promote the growth of the endothelial cells and then induce angiogenesis. The downregulation of the hyaluronan uptake and degradation pathway and the hyaluronan metabolism decreases overall cell proliferation.

After discussing the results obtained after studying dynamic and aneuploidy conditions, some conclusions can be drawn. The dynamic condition affects the vascular system by promoting

angiogenesis and inhibition of apoptosis. At the same time, the aneuploid cells under static conditions upregulate pathways related to apoptosis. When these two conditions – dynamic conditions and cell aneuploidy are combined, the results from the pathway enrichment analysis were unique in some ways but remained similar compared to the static aneuploidy group. The similarities in results for aneuploid cells of the control group subjected to dynamic shear stress compared to aneuploid cells under static conditions showed upregulation of some vascular responses by activating genes such as the NGF-stimulated transcription gene and SMAD6.

In contrast, several phenotypic changes were observed on combining dynamic conditions and cell aneuploidy. The unique upregulated pathway under combined conditions in comparison to the static aneuploidy group was NOTCH4 intracellular Domain Regulates Transcription<sup>279</sup>, which is a pathway that promotes proliferation, survival, and migration of endothelial cells and regulates angiogenic sprouting. Heart morphogenesis and response to fluid shear stress were biological processes unique in combined conditions relative to the static aneuploidy group. Most of these pathways or biological processes directly impact the endothelial cells. Some biological processes such as the response to fluid shear stress also affect the cancer cells, showing that cancer cells of epithelial origin, e.g., endothelial cells, are more resistant to fluid shear stress than normal (euploid) epithelial cells<sup>277</sup>. Overall, when examining the dynamic and aneuploidy conditions concurrently, we found that the results of the combined groups would not have been obtained if the conditions were just studied individually. As mentioned before, the individual models, dynamic and aneuploidy, are important, but the combined conditions provide a better look at pathological conditions such as cancer. Dynamic condition mimics the physiological condition, whereas the aneuploidy condition mimics the pathological condition. The combination allows the pathological conditions to be studied under physiological conditions.

We now compare the impact of both QDs on normal HUVEC cells under static conditions to validate the cytotoxicity results. On exposure to CdSe/ZnS QDs, strong stress and inflammatory response associated with vascular response to injury were elicited. However, exposure to InP/ZnS QDs resulted in a moderate inflammatory response<sup>361</sup> compared to CdSe/ZnS QDs. Most of the upregulated genes had roles in stopping cell growth or regulating transcription or homeostasis maintenance. Cellular pathways related to the mitotic division were downregulated, demonstrating that the cells were more driven towards conserving their energy towards their sustenance and

maintenance. In contrast, this also downregulated proinflammatory cytokine response to counter the effect of upregulated inflammatory responses.

A similar detrimental effect of CdSe/ZnS QDs through a different mechanism was observed under dynamic conditions via upregulation of heat-shock response<sup>294,296</sup>, a type of stress response. Biological processes and pathways related to stress response, such as chaperone-mediated protein folding, were also upregulated. Downregulated pathways, chemokine receptors bind chemokines and signaling by transformer growth factor-beta family members<sup>260,261</sup>, which have cytokines that play multiple roles, such as inflammation, maintaining endothelial cells, and inducing or suppressing apoptosis. The downregulation of these genes causes the stress response to dominate. On the other hand, exposure of normal HUVEC cells to InP/ZnS QDs elicited an upregulation of immune response. Cellular response to a mechanical stimulus due to laminar shear stress was upregulated in addition to the immune response against foreign material and works towards cell survival. Again, like in static conditions, the downregulated pathways are specifically related to a mitotic division<sup>336</sup>. This shows that when exposed to InP/ZnS QDs under both static and dynamic conditions, the cell division is downregulated, and cells are trying to survive and maintain themselves with the aid of the upregulated pathways.

Repeating the same experiments using aneuploid cells, CdSe/ZnS QDs resulted mainly in downregulation of chemokine receptors bind chemokine<sup>323,324</sup> and interferon signaling<sup>268</sup> responsible for cell survival by preventing apoptosis. Downregulation results in an increase in apoptosis of the aneuploid HUVEC cells. Most down-regulated pathways in static aneuploid cells exposed to CdSe/ZnS QD either promote the growth of tumor cells or repress cell growth but do not show any cell death response against cancer cells. Inflammatory response pathways are downregulated as well. However, exposure of aneuploid HUVEC cells to InP/ZnS/MPA QDs caused an upregulation of anti-inflammatory reactions and bicellular tight junctions<sup>344</sup> that control paracellular transport of molecules in static conditions. These mechanisms work to preserve cellular integrity and prevent inflammation. However, mitotic division-related cellular pathways and processes are downregulated, putting the cells in a survival mode by maintaining the integrity and prevention of inflammation.

Under dynamic conditions, aneuploid cells exposed to QDs resulted in different transcriptomic changes than previously examined conditions. CdSe/ZnS QD exposure to aneuploid HUVEC cells under dynamic conditions caused cellular components related to mitosis and pathways and processes that belonged to cell cycle and division to be upregulated. Overall, cell division was upregulated after the exposure to CdSe/ZnS QDs in aneuploid cells under dynamic conditions. Following exposure to InP/ZnS QDs, pathways related to cell proliferation and invasion of cells were upregulated. The DDIT4 gene<sup>307</sup>, which regulates cell survival, proliferation, and regulates apoptotic pathways, was upregulated. The genes that sequester metals were upregulated. Stress responses to metal ions and chaperone cofactor-dependent protein refolding were also upregulated. Overall, the upregulated pathways and processes were working towards cell survival and preventing the aneuploid cells from death caused by exposure to InP/ZnS QDs.

### **Conclusion:**

We could confirm our hypothesis that InP/ZnS QDs were less toxic and were internalized by the HUVEC cells to a lesser extent when compared to CdSe/ZnS QDs. The InP/ZnS QDs showed no statistically significant toxicity of InP/ZnS QDs was observed on normal and aneuploidy HUVEC relative to the negative control at all QD concentrations. However, CdSe/ZnS QDs at a concentration of 10 nM or higher were accompanied by a significant reduction in cell viability. At 50 nM, cell viability was only 22% indicating high toxicity of CdSe/ZnS QDs to normal HUVEC cells at this concentration. Aneuploid responded differently to CdSe/ZnS QDs and were more resistant to the toxicity of CdSe/ZnS QDs than normal euploid cells, where no significant change in cell viability was observed up to a concentration of 10 nM of CdSe/ZnS QDs, compared to 5 nM in the case of normal cells. As confirmed from the microarray data, differences in cell responses to the two types of QDs under the different conditions were attributed to different phenotypic changes, such as cell proliferation, inflammatory response, and cell death. Overall, our results support our hypothesis that dynamic conditions and cell aneuploidy result in differences in cell phenotypes resulting in different cell responses, mainly cell viability and cell uptake of QDs. The groups with combined conditions of aneuploidy and dynamics are the closest in replicating a physiological tumor micro-environment, where aneuploid cells encounter the physiological flow of blood and the impacts of shear stress. Results in this study are believed to direct future research

lines towards minimizing the discrepancies between in vitro and in vivo responses and better defining cell responses of NPs using physiologically relevant in vitro cell-based assays.

## BIBLIOGRAPHY

- 1 Blanco, E., Shen, H. & Ferrari, M. Principles of nanoparticle design for overcoming biological barriers to drug delivery. *Nat Biotechnol* **33**, 941-951, doi:10.1038/nbt.3330 (2015).
- 2 Fang, J., Nakamura, H. & Maeda, H. The EPR effect: Unique features of tumor blood vessels for drug delivery, factors involved, and limitations and augmentation of the effect. *Advanced Drug Delivery Reviews* **63**, 136-151, doi:10.1016/j.addr.2010.04.009 (2011).
- 3 Bertrand, N., Wu, J., Xu, X., Kamaly, N. & Farokhzad, O. C. Cancer nanotechnology: the impact of passive and active targeting in the era of modern cancer biology. *Adv Drug Deliv Rev* **66**, 2-25, doi:10.1016/j.addr.2013.11.009 (2014).
- 4 Xu, X., Ho, W., Zhang, X., Bertrand, N. & Farokhzad, O. Cancer nanomedicine: from targeted delivery to combination therapy. *Trends Mol Med* **21**, 223-232, doi:10.1016/j.molmed.2015.01.001 (2015).
- 5 Uchegbu, I. F. & Siew, A. Nanomedicines and Nanodiagnostics Come of Age. *Journal of Pharmaceutical Sciences* **102**, 305-310, doi:<https://doi.org/10.1002/jps.23377> (2013).
- 6 Wahlich, J. *et al.* Nanomedicines for the Delivery of Biologics. *Pharmaceutics* **11**, doi:10.3390/pharmaceutics11050210 (2019).
- 7 Zhang, C. *et al.* Progress, challenges, and future of nanomedicine. *Nano Today* **35**, 101008, doi:10.1016/j.nantod.2020.101008 (2020).
- 8 Han, X., Xu, K., Taratula, O. & Farsad, K. Applications of nanoparticles in biomedical imaging. *Nanoscale* **11**, 799-819, doi:10.1039/C8NR07769J (2019).
- 9 Patra, J. K. *et al.* Nano based drug delivery systems: recent developments and future prospects. *J Nanobiotechnology* **16**, 71-71, doi:10.1186/s12951-018-0392-8 (2018).
- 10 Teleanu, D. M., Chircov, C., Grumezescu, A. M., Volceanov, A. & Teleanu, R. I. Contrast Agents Delivery: An Up-to-Date Review of Nanodiagnostics in Neuroimaging. *Nanomaterials (Basel)* **9**, doi:10.3390/nano9040542 (2019).
- 11 Brichkin, S. B. Synthesis and properties of colloidal indium phosphide quantum dots. *Colloid Journal* **77**, 393-403, doi:10.1134/s1061933x15040043 (2015).
- 12 Brichkin, S. B. & Razumov, V. F. Colloidal quantum dots: synthesis, properties and applications. *Russian Chemical Reviews* **85**, 1297-1312 (2016).

- 13 Aldeek, F., Balan, L., Lambert, J. & Schneider, R. The influence of capping thioalkyl acid on the growth and photoluminescence efficiency of CdTe and CdSe quantum dots. *Nanotechnology* **19**, 475401, doi:10.1088/0957-4484/19/47/475401 (2008).
- 14 Hardman, R. A Toxicologic Review of Quantum Dots: Toxicity Depends on Physicochemical and Environmental Factors. *Environmental Health Perspectives* **114**, 165-172, doi:10.1289/ehp.8284 (2006).
- 15 Nikazar, S. *et al.* Revisiting the cytotoxicity of quantum dots: an in-depth overview. *Biophysical Reviews* **12**, 703-718, doi:10.1007/s12551-020-00653-0 (2020).
- 16 Tsoi, K. M., Dai, Q., Alman, B. A. & Chan, W. C. W. Are Quantum Dots Toxic? Exploring the Discrepancy Between Cell Culture and Animal Studies. *Accounts of Chemical Research* **46**, 662-671, doi:10.1021/ar300040z (2013).
- 17 Genchi, G., Sinicropi, M. S., Lauria, G., Carocci, A. & Catalano, A. The Effects of Cadmium Toxicity. *International Journal of Environmental Research and Public Health* **17**, 3782, doi:10.3390/ijerph17113782 (2020).
- 18 Brunetti, V. *et al.* InP/ZnS as a safer alternative to CdSe/ZnS core/shell quantum dots: in vitro and in vivo toxicity assessment. *Nanoscale* **5**, 307-317, doi:10.1039/c2nr33024e (2013).
- 19 Yan, M. *et al.* Cytotoxicity of CdTe quantum dots in human umbilical vein endothelial cells: the involvement of cellular uptake and induction of pro-apoptotic endoplasmic reticulum stress. *International Journal of Nanomedicine*, 529, doi:10.2147/ijn.s93591 (2016).
- 20 Mohammadinejad, R. *et al.* Necrotic, apoptotic and autophagic cell fates triggered by nanoparticles. *Autophagy* **15**, 4-33, doi:10.1080/15548627.2018.1509171 (2019).
- 21 Labouta, H. I. *et al.* Understanding and improving assays for cytotoxicity of nanoparticles: what really matters? *RSC Advances* **8**, 23027-23039, doi:10.1039/c8ra03849j (2018).
- 22 Labouta, H. I., Asgarian, N., Rinker, K. & Cramb, D. T. Meta-Analysis of Nanoparticle Cytotoxicity via Data-Mining the Literature. *ACS Nano* **13**, 1583-1594, doi:10.1021/acsnano.8b07562 (2019).

- 23 Lin, G. *et al.* In vivo toxicity assessment of non-cadmium quantum dots in BALB/c mice. *Nanomedicine: Nanotechnology, Biology and Medicine* **11**, 341-350, doi:<https://doi.org/10.1016/j.nano.2014.10.002> (2015).
- 24 Zhong, P. *et al.* Preparation and application of functionalized nanoparticles of CdSe capped with 11-mercaptoundecanoic acid as a fluorescence probe. *Talanta* **70**, 902-906, doi:10.1016/j.talanta.2006.03.015 (2006).
- 25 Spirin, M. G., Brichkin, S. B. & Razumov, V. F. Phosphonic acids as stabilizing ligands for cadmium chalcogenide colloidal quantum dots. *Russ Chem B+* **65**, 1902-1909 (2016).
- 26 Spirin, M. G., Brichkin, S. B. & Razumov, V. F. Features of the influence of stabilizing ligands on luminescence properties of cadmium selenide colloidal quantum dots. *High Energ Chem+* **51**, 38-45 (2017).
- 27 Swift, J. L. & Cramb, D. T. Nanoparticles as fluorescence labels: is size all that matters? *Biophys J* **95**, 865-876, doi:10.1529/biophysj.107.127688 (2008).
- 28 Tessier, M. D., Dupont, D., De Nolf, K., De Roo, J. & Hens, Z. Economic and Size-Tunable Synthesis of InP/ZnE (E = S, Se) Colloidal Quantum Dots. *Chemistry of Materials* **27**, 4893-4898, doi:10.1021/acs.chemmater.5b02138 (2015).
- 29 Chen, B., Li, D. & Wang, F. InP Quantum Dots: Synthesis and Lighting Applications. *Small* **16**, 2002454, doi:10.1002/smll.202002454 (2020).
- 30 Jackson, W. F. in *Muscle* 1197-1206 (2012).
- 31 Li, J. K. *Dynamics of the vascular system*. Vol. 1 (World scientific, 2004).
- 32 Galley, H. F. & Webster, N. R. Physiology of the endothelium. *Br J Anaesth* **93**, 105-113, doi:10.1093/bja/aeh163 (2004).
- 33 Aird, W. C. Phenotypic Heterogeneity of the Endothelium. *Circulation Research* **100**, 158-173, doi:10.1161/01.res.0000255691.76142.4a (2007).
- 34 Pemathilaka, R. L., Reynolds, D. E. & Hashemi, N. N. Drug transport across the human placenta: review of placenta-on-a-chip and previous approaches. *Interface focus* **9**, 20190031, doi:<https://dx.doi.org/10.1098/rsfs.2019.0031> (2019).
- 35 Santaguida, S. *et al.* Side by side comparison between dynamic versus static models of blood-brain barrier in vitro: A permeability study. *Brain Research* **1109**, 1-13, doi:<https://doi.org/10.1016/j.brainres.2006.06.027> (2006).

- 36 Muro, S. *et al.* Endothelial targeting of high-affinity multivalent polymer nanocarriers directed to intercellular adhesion molecule 1. *J Pharmacol Exp Ther* **317**, 1161-1169, doi:10.1124/jpet.105.098970 (2006).
- 37 Artym, V. V. & Matsumoto, K. Imaging cells in three-dimensional collagen matrix. *Curr Protoc Cell Biol* **Chapter 10**, Unit 10 18 11-20, doi:10.1002/0471143030.cb1018s48 (2010).
- 38 al, C. e. *Studies in Mechanobiology, Tissue Engineering and Biomaterials - Mechanical and Chemical Signaling in Angiogenesis*. Vol. 12 (2013).
- 39 Medina-Leyte, D. J., Domínguez-Pérez, M., Mercado, I., Villarreal-Molina, M. T. & Jacobo-Albavera, L. Use of Human Umbilical Vein Endothelial Cells (HUVEC) as a Model to Study Cardiovascular Disease: A Review. *Applied Sciences* **10**, 938, doi:10.3390/app10030938 (2020).
- 40 Nguyen, N. *et al.* Microfluidic models of the human circulatory system: versatile platforms for exploring mechanobiology and disease modeling. *Biophysical Reviews*, doi:10.1007/s12551-021-00815-8 (2021).
- 41 Doddaballapur, A. *et al.* Laminar Shear Stress Inhibits Endothelial Cell Metabolism via KLF2-Mediated Repression of PFKFB3. *Arteriosclerosis, Thrombosis, and Vascular Biology* **35**, 137-145, doi:10.1161/atvbaha.114.304277 (2015).
- 42 Potente, M., Gerhardt, H. & Carmeliet, P. Basic and Therapeutic Aspects of Angiogenesis. *Cell* **146**, 873-887, doi:10.1016/j.cell.2011.08.039 (2011).
- 43 Ballermann, B. J., Dardik, A., Eng, E. & Liu, A. Shear stress and the endothelium. *Kidney Int Suppl* **67**, S100-108, doi:10.1046/j.1523-1755.1998.06720.x (1998).
- 44 Chistiakov, D. A., Orekhov, A. N. & Bobryshev, Y. V. Effects of shear stress on endothelial cells: go with the flow. *Acta Physiologica* **219**, 382-408, doi:10.1111/apha.12725 (2017).
- 45 Dewey, C. F., Bussolari, S. R., Gimbrone, M. A. & Davies, P. F. The Dynamic Response of Vascular Endothelial Cells to Fluid Shear Stress. *Journal of Biomechanical Engineering* **103**, 177-185, doi:10.1115/1.3138276 (1981).
- 46 Caro, C. G. Vascular fluid dynamics and vascular biology and disease. *Mathematical Methods in the Applied Sciences* **24**, 1311-1324, doi:10.1002/mma.181 (2001).

- 47 Seymour, R. S., Hu, Q., Snelling, E. P. & White, C. R. Interspecific scaling of blood flow rates and arterial sizes in mammals. *The Journal of Experimental Biology* **222**, jeb199554, doi:10.1242/jeb.199554 (2019).
- 48 Chen, H. *et al.* Microfluidic models of physiological or pathological flow shear stress for cell biology, disease modeling and drug development. *TrAC Trends in Analytical Chemistry* **117**, 186-199, doi:10.1016/j.trac.2019.06.023 (2019).
- 49 Reneman, R. S. & Hoeks, A. P. Wall shear stress as measured in vivo: consequences for the design of the arterial system. *Med Biol Eng Comput* **46**, 499-507, doi:10.1007/s11517-008-0330-2 (2008).
- 50 Whitesides, G. M. The origins and the future of microfluidics. *Nature* **442**, 368-373, doi:10.1038/nature05058 (2006).
- 51 Sackmann, E. K., Fulton, A. L. & Beebe, D. J. The present and future role of microfluidics in biomedical research. *Nature* **507**, 181-189, doi:10.1038/nature13118 (2014).
- 52 Squires, T. M. & Quake, S. R. Microfluidics: Fluid physics at the nanoliter scale. *Reviews of Modern Physics* **77**, 977-1026, doi:10.1103/revmodphys.77.977 (2005).
- 53 Stone, H. A., Stroock, A. D. & Ajdari, A. Engineering Flows in Small Devices: Microfluidics Toward a Lab-on-a-Chip. *Annual Review of Fluid Mechanics* **36**, 381-411, doi:10.1146/annurev.fluid.36.050802.122124 (2004).
- 54 Wong, K. H., Chan, J. M., Kamm, R. D. & Tien, J. Microfluidic models of vascular functions. *Annu Rev Biomed Eng* **14**, 205-230, doi:10.1146/annurev-bioeng-071811-150052 (2012).
- 55 Akbari, E., Spsychalski, G. B., Rangharajan, K. K., Prakash, S. & Song, J. W. Competing Fluid Forces Control Endothelial Sprouting in a 3-D Microfluidic Vessel Bifurcation Model. *Micromachines (Basel)* **10**, doi:10.3390/mi10070451 (2019).
- 56 Chu, T. J. & Peters, D. G. Serial analysis of the vascular endothelial transcriptome under static and shear stress conditions. *Physiological Genomics* **34**, 185-192, doi:10.1152/physiolgenomics.90201.2008 (2008).
- 57 Folch i Folch, A. *Introduction to bioMEMS*. (CRC Press, 2013).

- 58 Kim, S., Lee, H., Chung, M. & Jeon, N. L. Engineering of functional, perfusable 3D microvascular networks on a chip. *Lab Chip* **13**, 1489-1500, doi:10.1039/c3lc41320a (2013).
- 59 Ahn, J. *et al.* Microfluidics in nanoparticle drug delivery; From synthesis to pre-clinical screening. *Adv Drug Deliv Rev* **128**, 29-53, doi:10.1016/j.addr.2018.04.001 (2018).
- 60 Cavero, I., Guillon, J. M. & Holzgrefe, H. H. Human organotypic bioconstructs from organ-on-chip devices for human-predictive biological insights on drug candidates. *Expert Opin Drug Saf* **18**, 651-677, doi:10.1080/14740338.2019.1634689 (2019).
- 61 Yesil-Celiktas, O. *et al.* Mimicking Human Pathophysiology in Organ-on-Chip Devices. *Advanced Biosystems* **2**, 1800109, doi:10.1002/adbi.201800109 (2018).
- 62 Mastrangeli, M., Millet, S. & Van Den Eijnden-Van Raaij, J. Organ-on-chip in development: Towards a roadmap for organs-on-chip. *ALTEX*, 650-668, doi:10.14573/altex.1908271 (2019).
- 63 Lungu, I. I. & Grumezescu, A. M. Microfluidics – Organ-on-chip. *Biomed Eng Int* **1**, 2-8, doi:<https://doi.org/10.33263/BioMed11.002008> (2019).
- 64 Ahadian, S. *et al.* Organ-On-A-Chip Platforms: A Convergence of Advanced Materials, Cells, and Microscale Technologies. *Adv Healthc Mater* **7**, doi:10.1002/adhm.201700506 (2018).
- 65 Huh, D. *et al.* Microfabrication of human organs-on-chips. *Nat Protoc* **8**, 2135-2157, doi:10.1038/nprot.2013.137 (2013).
- 66 Fetah, K. L. *et al.* Cancer Modeling-on-a-Chip with Future Artificial Intelligence Integration. *Small* **15**, e1901985, doi:10.1002/smll.201901985 (2019).
- 67 Sontheimer-Phelps, A., Hassell, B. A. & Ingber, D. E. Modelling cancer in microfluidic human organs-on-chips. *Nat Rev Cancer* **19**, 65-81, doi:10.1038/s41568-018-0104-6 (2019).
- 68 Benam, K. H. *et al.* Small airway-on-a-chip enables analysis of human lung inflammation and drug responses in vitro. *Nat Methods* **13**, 151-157, doi:10.1038/nmeth.3697 (2016).
- 69 Hassell, B. A. *et al.* Human Organ Chip Models Recapitulate Orthotopic Lung Cancer Growth, Therapeutic Responses, and Tumor Dormancy In Vitro. *Cell Rep* **21**, 508-516, doi:10.1016/j.celrep.2017.09.043 (2017).

- 70 Nawroth, J. C. *et al.* *Breathing on Chip: Biomechanical forces change airway epithelial cell biology in a human Airway Lung-Chip* (Cold Spring Harbor Laboratory, 2021).
- 71 Ragelle, H., Goncalves, A., Kustermann, S., Antonetti, D. A. & Jayagopal, A. Organ-On-A-Chip Technologies for Advanced Blood-Retinal Barrier Models. *J Ocul Pharmacol Ther* **36**, 30-41, doi:10.1089/jop.2019.0017 (2020).
- 72 Falanga, A. P. *et al.* Shuttle-mediated nanoparticle transport across an in vitro brain endothelium under flow conditions. *Biotechnol Bioeng* **114**, 1087-1095, doi:10.1002/bit.26221 (2017).
- 73 Oddo, A. *et al.* Advances in Microfluidic Blood-Brain Barrier (BBB) Models. *Trends Biotechnol* **37**, 1295-1314, doi:10.1016/j.tibtech.2019.04.006 (2019).
- 74 Papademetriou, I., Vedula, E., Charest, J. & Porter, T. Effect of flow on targeting and penetration of angiopep-decorated nanoparticles in a microfluidic model blood-brain barrier. *PLoS One* **13**, e0205158, doi:10.1371/journal.pone.0205158 (2018).
- 75 Blundell, C. *et al.* A microphysiological model of the human placental barrier. *Lab Chip* **16**, 3065-3073, doi:10.1039/c6lc00259e (2016).
- 76 Blundell, C. *et al.* Placental Drug Transport-on-a-Chip: A Microengineered In Vitro Model of Transporter-Mediated Drug Efflux in the Human Placental Barrier. *Advanced healthcare materials* **7**, doi:<https://dx.doi.org/10.1002/adhm.201700786> (2018).
- 77 Horii, M., Touma, O., Bui, T. & Parast, M. M. Modeling human trophoblast, the placental epithelium at the maternal fetal interface. *Reproduction (Cambridge, England)* **160**, R1-R11, doi:<https://dx.doi.org/10.1530/REP-19-0428> (2020).
- 78 Lee, J. S. *et al.* Placenta-on-a-chip: a novel platform to study the biology of the human placenta. *The journal of maternal-fetal & neonatal medicine : the official journal of the European Association of Perinatal Medicine, the Federation of Asia and Oceania Perinatal Societies, the International Society of Perinatal Obstetricians* **29**, 1046-1054, doi:<https://dx.doi.org/10.3109/14767058.2015.1038518> (2016).
- 79 Pemathilaka, R. L., Caplin, J. D., Aykar, S. S., Montazami, R. & Hashemi, N. N. Placenta-on-a-Chip: In Vitro Study of Caffeine Transport across Placental Barrier Using Liquid Chromatography Mass Spectrometry. *Global challenges (Hoboken, NJ)* **3**, 1800112, doi:<https://dx.doi.org/10.1002/gch2.201800112> (2019).

- 80 Hu, C., Chen, Y., Tan, M. J. A., Ren, K. & Wu, H. Microfluidic technologies for vasculature biomimicry. *Analyst* **144**, 4461-4471, doi:10.1039/c9an00421a (2019).
- 81 van Duinen, V., Trietsch, S. J., Joore, J., Vulto, P. & Hankemeier, T. Microfluidic 3D cell culture: from tools to tissue models. *Curr Opin Biotechnol* **35**, 118-126, doi:10.1016/j.copbio.2015.05.002 (2015).
- 82 Kappings, V. *et al.* vasQchip: A Novel Microfluidic, Artificial Blood Vessel Scaffold for Vascularized 3D Tissues. *Advanced Materials Technologies* **3**, doi:10.1002/admt.201700246 (2018).
- 83 Kim, S., Kim, W., Lim, S. & Jeon, J. S. Vasculature-On-A-Chip for In Vitro Disease Models. *Bioengineering (Basel)* **4**, doi:10.3390/bioengineering4010008 (2017).
- 84 Li, Y., Zhu, K., Liu, X. & Zhang, Y. S. Blood-Vessel-on-a-Chip Platforms for Evaluating Nanoparticle Drug Delivery Systems. *Curr Drug Metab* **19**, 100-109, doi:10.2174/1389200218666170925114636 (2018).
- 85 Baker, B. M., Trappmann, B., Stapleton, S. C., Toro, E. & Chen, C. S. Microfluidics embedded within extracellular matrix to define vascular architectures and pattern diffusive gradients. *Lab Chip* **13**, 3246-3252, doi:10.1039/c3lc50493j (2013).
- 86 Wang, X. Y. *et al.* Engineering interconnected 3D vascular networks in hydrogels using molded sodium alginate lattice as the sacrificial template. *Lab Chip* **14**, 2709-2716, doi:10.1039/c4lc00069b (2014).
- 87 Hasan, A. *et al.* Microfluidic techniques for development of 3D vascularized tissue. *Biomaterials* **35**, 7308-7325, doi:10.1016/j.biomaterials.2014.04.091 (2014).
- 88 Park, Y. K. *et al.* In Vitro Microvessel Growth and Remodeling within a Three-dimensional Microfluidic Environment. *Cell Mol Bioeng* **7**, 15-25, doi:10.1007/s12195-013-0315-6 (2014).
- 89 Wang, X., Sun, Q. & Pei, J. Microfluidic-Based 3D Engineered Microvascular Networks and Their Applications in Vascularized Microtumor Models. *Micromachines (Basel)* **9**, doi:10.3390/mi9100493 (2018).
- 90 Cochrane, A. *et al.* Advanced in vitro models of vascular biology: Human induced pluripotent stem cells and organ-on-chip technology. *Adv Drug Deliv Rev* **140**, 68-77, doi:10.1016/j.addr.2018.06.007 (2019).

- 91 Wu, M. A. *et al.* Paroxysmal Permeability Disorders: Development of a Microfluidic Device to Assess Endothelial Barrier Function. *Front Med (Lausanne)* **6**, 89, doi:10.3389/fmed.2019.00089 (2019).
- 92 Zhang, B. *et al.* Microfabrication of AngioChip, a biodegradable polymer scaffold with microfluidic vasculature. *Nat Protoc* **13**, 1793-1813, doi:10.1038/s41596-018-0015-8 (2018).
- 93 Zhang, B. *et al.* Biodegradable scaffold with built-in vasculature for organ-on-a-chip engineering and direct surgical anastomosis. *Nat Mater* **15**, 669-678, doi:10.1038/nmat4570 (2016).
- 94 Chamseddine, I. M., Frieboes, H. B. & Kokkolaras, M. Design Optimization of Tumor Vasculature-Bound Nanoparticles. *Sci Rep* **8**, 17768, doi:10.1038/s41598-018-35675-y (2018).
- 95 Gomez-Garcia, M. J. *et al.* Nanoparticle localization in blood vessels: dependence on fluid shear stress, flow disturbances, and flow-induced changes in endothelial physiology. *Nanoscale* **10**, 15249-15261, doi:10.1039/c8nr03440k (2018).
- 96 Hobson, N. J. *et al.* Clustering superparamagnetic iron oxide nanoparticles produces organ-targeted high-contrast magnetic resonance images. *Nanomedicine (Lond)* **14**, 1135-1152, doi:10.2217/nnm-2018-0370 (2019).
- 97 Peng, F. *et al.* Nanoparticles promote in vivo breast cancer cell intravasation and extravasation by inducing endothelial leakiness. *Nat Nanotechnol* **14**, 279-286, doi:10.1038/s41565-018-0356-z (2019).
- 98 Sarsons, C. D. *et al.* Testing Nanoparticles for Angiogenesis-Related Disease: Charting the Fastest Route to the Clinic. *J Biomed Nanotechnol* **10**, 1641-1676, doi: (2014).
- 99 Shah, P. N. *et al.* Extravasation of Brownian Spheroidal Nanoparticles through Vascular Pores. *Biophys J* **115**, 1103-1115, doi:10.1016/j.bpj.2018.07.038 (2018).
- 100 Tee, J. K. *et al.* Nanoparticles' interactions with vasculature in diseases. *Chem Soc Rev* **48**, 5381-5407, doi:10.1039/c9cs00309f (2019).
- 101 Taylor, A. M. *et al.* Genomic and Functional Approaches to Understanding Cancer Aneuploidy. *Cancer Cell* **33**, 676-689.e673, doi:10.1016/j.ccell.2018.03.007 (2018).
- 102 Gordon, D. J., Resio, B. & Pellman, D. Causes and consequences of aneuploidy in cancer. *Nature Reviews Genetics* **13**, 189-203, doi:10.1038/nrg3123 (2012).

- 103 Molina, O., Abad, M. A., Solé, F. & Menéndez, P. Aneuploidy in Cancer: Lessons from Acute Lymphoblastic Leukemia. *Trends in Cancer* **7**, 37-47, doi:10.1016/j.trecan.2020.08.008 (2021).
- 104 Thompson, S. L. & Compton, D. A. Examining the link between chromosomal instability and aneuploidy in human cells. *Journal of Cell Biology* **180**, 665-672, doi:10.1083/jcb.200712029 (2008).
- 105 Giam, M. & Rancati, G. Aneuploidy and chromosomal instability in cancer: a jackpot to chaos. *Cell Division* **10**, doi:10.1186/s13008-015-0009-7 (2015).
- 106 Orso, F. *et al.* Role of miRNAs in tumor and endothelial cell interactions during tumor progression. *Seminars in Cancer Biology* **60**, 214-224, doi:10.1016/j.semcancer.2019.07.024 (2020).
- 107 Hida, K., Hida, Y. & Shindoh, M. Understanding tumor endothelial cell abnormalities to develop ideal anti-angiogenic therapies. *Cancer Science* **99**, 459-466, doi:10.1111/j.1349-7006.2007.00704.x (2008).
- 108 Ben-David, U. & Amon, A. Context is everything: aneuploidy in cancer. *Nature Reviews Genetics* **21**, 44-62, doi:10.1038/s41576-019-0171-x (2020).
- 109 Lin, P. P. Aneuploid Circulating Tumor-Derived Endothelial Cell (CTEC): A Novel Versatile Player in Tumor Neovascularization and Cancer Metastasis. *Cells* **9**, 1539, doi:10.3390/cells9061539 (2020).
- 110 Thompson, S. L. & Compton, D. A. Proliferation of aneuploid human cells is limited by a p53-dependent mechanism. *Journal of Cell Biology* **188**, 369-381, doi:10.1083/jcb.200905057 (2010).
- 111 Hida, K. *et al.* Tumor-Associated Endothelial Cells with Cytogenetic Abnormalities. *Cancer Research* **64**, 8249-8255, doi:10.1158/0008-5472.can-04-1567 (2004).
- 112 Akino, T. *et al.* Cytogenetic Abnormalities of Tumor-Associated Endothelial Cells in Human Malignant Tumors. *The American Journal of Pathology* **175**, 2657-2667, doi:10.2353/ajpath.2009.090202 (2009).
- 113 Holland, A. J. & Cleveland, D. W. Losing balance: the origin and impact of aneuploidy in cancer. *EMBO reports* **13**, 501-514, doi:10.1038/embor.2012.55 (2012).
- 114 Mailhes, J. B., Mastromatteo, C. & Fuseler, J. W. Transient exposure to the Eg5 kinesin inhibitor monastrol leads to syntelic orientation of chromosomes and aneuploidy in

- mouse oocytes. *Mutation Research/Genetic Toxicology and Environmental Mutagenesis* **559**, 153-167, doi:10.1016/j.mrgentox.2004.01.001 (2004).
- 115 Cao, Y. *et al.* The use of human umbilical vein endothelial cells (HUVECs) as an in vitro model to assess the toxicity of nanoparticles to endothelium: a review. *J Appl Toxicol* **37**, 1359-1369, doi:10.1002/jat.3470 (2017).
- 116 Cicha, I. Strategies to enhance nanoparticle-endothelial interactions under flow. *Journal of Cellular Biotechnology* **1**, 191-208, doi:10.3233/jcb-15020 (2016).
- 117 Galloway, S. M. & Ivett, J. L. Chemically induced aneuploidy in mammalian cells in culture. *Mutation Research/Reviews in Genetic Toxicology* **167**, 89-105, doi:[https://doi.org/10.1016/0165-1110\(86\)90011-4](https://doi.org/10.1016/0165-1110(86)90011-4) (1986).
- 118 Oshimura, M. & Barrett, J. C. Chemically induced aneuploidy in mammalian cells: Mechanisms and biological significance in cancer. *Environmental Mutagenesis* **8**, 129-159, doi:<https://doi.org/10.1002/em.2860080112> (1986).
- 119 Lynch, A. M. *et al.* Targets and mechanisms of chemically induced aneuploidy. Part 1 of the report of the 2017 IWGT workgroup on assessing the risk of aneugens for carcinogenesis and hereditary diseases. *Mutation Research/Genetic Toxicology and Environmental Mutagenesis* **847**, 403025, doi:10.1016/j.mrgentox.2019.02.006 (2019).
- 120 Pacchierotti, F. *et al.* Chemically induced aneuploidy in germ cells. Part II of the report of the 2017 IWGT workgroup on assessing the risk of aneugens for carcinogenesis and hereditary diseases. *Mutation Research/Genetic Toxicology and Environmental Mutagenesis* **848**, 403023, doi:10.1016/j.mrgentox.2019.02.004 (2019).
- 121 Kwak, B., Ozcelikkale, A., Shin, C. S., Park, K. & Han, B. Simulation of complex transport of nanoparticles around a tumor using tumor-microenvironment-on-chip. *J Control Release* **194**, 157-167, doi:10.1016/j.jconrel.2014.08.027 (2014).
- 122 Martins, J. P. *et al.* The solid progress of nanomedicine. *Drug Deliv Transl Res*, doi:10.1007/s13346-020-00743-2 (2020).
- 123 Jie, M., Xian-da, Y., Lee, J., Xing-Jie, L. & Chen, W. Impacts of Nanoparticles on Cardiovascular Diseases: Modulating Metabolism and Function of Endothelial Cells. *Current Drug Metabolism* **13**, 1123-1129, doi:<http://dx.doi.org.uml.idm.oclc.org/10.2174/138920012802850056> (2012).

- 124 Geys, J. *et al.* Acute toxicity and prothrombotic effects of quantum dots: impact of surface charge. *Environmental health perspectives* **116**, 1607-1613, doi:10.1289/ehp.11566 (2008).
- 125 Farokhzad, O. C. *et al.* Microfluidic System for Studying the Interaction of Nanoparticles and Microparticles with Cells. *Analytical Chemistry* **77**, 5453-5459, doi:10.1021/ac050312q (2005).
- 126 Martínez-Jothar, L. *et al.* Endothelial Cell Targeting by cRGD-Functionalized Polymeric Nanoparticles under Static and Flow Conditions. *Nanomaterials-Basel* **10**, 1353, doi:10.3390/nano10071353 (2020).
- 127 Yin Win, K. & Feng, S.-S. Effects of particle size and surface coating on cellular uptake of polymeric nanoparticles for oral delivery of anticancer drugs. *Biomaterials* **26**, 2713-2722, doi:10.1016/j.biomaterials.2004.07.050 (2005).
- 128 <Federico - Unknown - Engineered microfluidic platforms for microenvironment control and cell culture.pdf>.
- 129 Lin, A. *et al.* Shear-regulated uptake of nanoparticles by endothelial cells and development of endothelial-targeting nanoparticles. *J Biomed Mater Res. Part A* **93**, 833-842, doi:10.1002/jbm.a.32592 (2010).
- 130 Klingberg, H., Loft, S., Oddershede, L. B. & Moller, P. The influence of flow, shear stress and adhesion molecule targeting on gold nanoparticle uptake in human endothelial cells. *Nanoscale* **7**, 11409-11419, doi:10.1039/c5nr01467k (2015).
- 131 Park, J. H. *et al.* Biomimetic nanoparticle technology for cardiovascular disease detection and treatment. *Nanoscale Horiz* **5**, 25-42, doi:10.1039/c9nh00291j (2020).
- 132 Barua, S. & Mitragotri, S. Challenges associated with Penetration of Nanoparticles across Cell and Tissue Barriers: A Review of Current Status and Future Prospects. *Nano Today* **9**, 223-243, doi:10.1016/j.nantod.2014.04.008 (2014).
- 133 Jia, J. *et al.* Crossing Biological Barriers by Engineered Nanoparticles. *Chem Res Toxicol*, doi:10.1021/acs.chemrestox.9b00483 (2020).
- 134 Prabhakarandian, B., Shen, M. C., Pant, K. & Kiani, M. F. Microfluidic devices for modeling cell-cell and particle-cell interactions in the microvasculature. *Microvasc Res* **82**, 210-220, doi:10.1016/j.mvr.2011.06.013 (2011).

- 135 Yin, F. *et al.* A 3D human placenta-on-a-chip model to probe nanoparticle exposure at the placental barrier. *Toxicol In Vitro* **54**, 105-113, doi:10.1016/j.tiv.2018.08.014 (2019).
- 136 Yin, F. *et al.* A 3D human placenta-on-a-chip model to probe nanoparticle exposure at the placental barrier. *Toxicology in vitro : an international journal published in association with BIBRA* **54**, 105-113, doi:<https://dx.doi.org/10.1016/j.tiv.2018.08.014> (2019).
- 137 Zhang, M., Xu, C., Jiang, L. & Qin, J. A 3D human lung-on-a-chip model for nanotoxicity testing. *Toxicology Research* **7**, 1048-1060, doi:10.1039/c8tx00156a (2018).
- 138 Kim, Y. *et al.* Probing nanoparticle translocation across the permeable endothelium in experimental atherosclerosis. *Proc Natl Acad Sci U S A* **111**, 1078-1083, doi:10.1073/pnas.1322725111 (2014).
- 139 Vu, M. N. *et al.* Rapid Assessment of Nanoparticle Extravasation in a Microfluidic Tumor Model. *ACS Applied Nano Materials* **2**, 1844-1856, doi:10.1021/acsanm.8b02056 (2019).
- 140 Godek, K. M. & Compton, D. A. 15-32 (Elsevier, 2018).
- 141 Aysun, A., Yağmur, K. & Yusuf, B. Cell Proliferation and Cytotoxicity Assays. *Current Pharmaceutical Biotechnology* **17**, 1213-1221, doi:<http://dx.doi.org/10.2174/1389201017666160808160513> (2016).
- 142 Baig, S. *et al.* Potential of apoptotic pathway-targeted cancer therapeutic research: Where do we stand? *Cell Death & Disease* **7**, e2058-e2058, doi:10.1038/cddis.2015.275 (2016).
- 143 Borra, R. C., Lotufo, M. A., Gaglioti, S. M., Barros, F. D. M. & Andrade, P. M. A simple method to measure cell viability in proliferation and cytotoxicity assays. *Brazilian Oral Research* **23**, 255-262, doi:10.1590/s1806-83242009000300006 (2009).
- 144 Crouch, S. P. M., Kozlowski, R., Slater, K. J. & Fletcher, J. The use of ATP bioluminescence as a measure of cell proliferation and cytotoxicity. *Journal of Immunological Methods* **160**, 81-88, doi:[http://dx.doi.org/10.1016/0022-1759\(93\)90011-U](http://dx.doi.org/10.1016/0022-1759(93)90011-U) (1993).
- 145 Shepherd, R. D. & Rinker, K. D. Bioluminescence-based ATP assays using a charge-coupled device imaging system. *BioTechniques* **37**, 208-210 (2004).

- 146 Labouta, H. I., Asgarian, N., Rinker, K. & Cramb, D. T. Meta-Analysis of Nanoparticle Cytotoxicity via Data-Mining the Literature. *ACS Nano* **13**, 1583–1594, doi:10.1021/acsnano.8b07562 (2019).
- 147 Elsaesser, A. *et al.* Quantification of nanoparticle uptake by cells using microscopical and analytical techniques. *Nanomedicine* **5**, 1447-1457, doi:10.2217/nmm.10.118 (2010).
- 148 <Davda, Labhasetwar - 2002 - Characterization of Nanoparticle Uptake by Endothelial Cells.pdf>.
- 149 Glazer, E. S. & Curley, S. A. Radiofrequency Field-Induced Thermal Cytotoxicity in Cancer Cells Treated With Fluorescent Nanoparticles. *Cancer-Am Cancer Soc* **116**, 3285-3293 (2010).
- 150 Zhu, Z. J. *et al.* Stability of quantum dots in live cells. *Nat Chem* **3**, 963-968, doi:10.1038/nchem.1177 (2011).
- 151 Samuel, S. P. *et al.* Multifactorial determinants that govern nanoparticle uptake by human endothelial cells under flow. *Int J Nanomedicine* **7**, 2943-2956, doi:10.2147/IJN.S30624 (2012).
- 152 Pollinger, K. *et al.* Ligand-functionalized nanoparticles target endothelial cells in retinal capillaries after systemic application. *Proc Natl Acad Sci U S A* **110**, 6115-6120, doi:10.1073/pnas.1220281110 (2013).
- 153 Lin, G. M. *et al.* In vivo toxicity assessment of non-cadmium quantum dots in BALB/c mice. *Nanomed-Nanotechnol* **11**, 341-350 (2015).
- 154 Jiang, X.-Y. *et al.* Quantum dot interactions and flow effects in angiogenic zebrafish ( *Danio rerio* ) vessels and human endothelial cells. *Nanomedicine: Nanotechnology, Biology and Medicine* **13**, 999-1010, doi:10.1016/j.nano.2016.12.008 (2017).
- 155 Yong, K. T. *et al.* Imaging Pancreatic Cancer Using Bioconjugated InP Quantum Dots. *Acs Nano* **3**, 502-510 (2009).
- 156 Rosenberg, J. T., Kogot, J. M., Lovingood, D. D., Strouse, G. F. & Grant, S. C. Intracellular Bimodal Nanoparticles Based on Quantum Dots for High-Field MRI at 21.1 T. *Magn Reson Med* **64**, 871-882 (2010).
- 157 Ayupova, D., Dobhal, G., Laufersky, G., Nann, T. & Goreham, R. V. An In Vitro Investigation of Cytotoxic Effects of InP/Zns Quantum Dots with Different Surface Chemistries. *Nanomaterials-Basel* **9** (2019).

- 158 Barba-Vicente, V. *et al.* Detection of Human p53 In-Vitro Expressed in a Transcription-Translation Cell-Free System by a Novel Conjugate Based on Cadmium Sulphide Nanoparticles. *Nanomaterials-Basel* **10** (2020).
- 159 Zhao, J. W., Hu, H. S., Liu, W. Q. & Wang, X. Multifunctional NaYF<sub>4</sub>:Nd/NaDyF<sub>4</sub> nanocrystals as a multimodal platform for NIR-II fluorescence and magnetic resonance imaging. *Nanoscale Adv* **3**, 463-470 (2021).
- 160 Zhao, Y. *et al.* In vivo biodistribution and behavior of CdTe/ZnS quantum dots. *International Journal of Nanomedicine* **Volume 12**, 1927-1939, doi:10.2147/ijn.s121075 (2017).
- 161 Li, L. *et al.* In vivo Comparison of the Biodistribution and Toxicity of InP/ZnS Quantum Dots with Different Surface Modifications. *International Journal of Nanomedicine* **15**, 1951-1965 (2020).
- 162 Wasserman, S. M. *et al.* Gene expression profile of human endothelial cells exposed to sustained fluid shear stress. *Physiological Genomics* **12**, 13-23, doi:<http://10.1152/physiolgenomics.00102.2002> (2002).
- 163 Lowe, R., Shirley, N., Bleackley, M., Dolan, S. & Shafee, T. Transcriptomics technologies. *PLOS Computational Biology* **13**, e1005457, doi:10.1371/journal.pcbi.1005457 (2017).
- 164 Saarimäki, L. A. *et al.* Manually curated transcriptomics data collection for toxicogenomic assessment of engineered nanomaterials. *Scientific Data* **8**, 49, doi:10.1038/s41597-021-00808-y (2021).
- 165 Stingele, S. *et al.* Global analysis of genome, transcriptome and proteome reveals the response to aneuploidy in human cells. *Molecular Systems Biology* **8**, 608, doi:10.1038/msb.2012.40 (2012).
- 166 Bose, D. & Ahuja, N. Genetic Profiling in Colorectal Cancer. *Early Diagnosis and Treatment of Cancer Series: Colorectal Cancer*, 239-249, doi: (2011).
- 167 Lowe, R., Shirley, N., Bleackley, M., Dolan, S. & Shafee, T. Transcriptomics technologies. *PLoS Comput Biol* **13**, e1005457-e1005457, doi:10.1371/journal.pcbi.1005457 (2017).
- 168 Stears, R. L., Martinsky, T. & Schena, M. Trends in microarray analysis. *Nature Medicine* **9**, 140-145, doi:10.1038/nm0103-140 (2003).

- 169 Atkins, G. B. & Jain, M. K. Role of Krüppel-Like Transcription Factors in Endothelial Biology. *Circulation Research* **100**, 1686-1695, doi:10.1161/01.res.0000267856.00713.0a (2007).
- 170 Sakamoto, J. H. *et al.* Enabling individualized therapy through nanotechnology. *Pharmacological Research* **62**, 57-89, doi:10.1016/j.phrs.2009.12.011 (2010).
- 171 Nayak, C., Chandra, I., Singh, P. & Singh, S. K. 227-248 (Springer Singapore, 2018).
- 172 Khodadadian, A. *et al.* Genomics and Transcriptomics: The Powerful Technologies in Precision Medicine. *International Journal of General Medicine* **Volume 13**, 627-640, doi:10.2147/ijgm.s249970 (2020).
- 173 Kroll, A., Pillukat, M. H., Hahn, D. & Schneckeburger, J. Current in vitro methods in nanoparticle risk assessment: Limitations and challenges. *European Journal of Pharmaceutics and Biopharmaceutics* **72**, 370-377, doi:<https://doi.org/10.1016/j.ejpb.2008.08.009> (2009).
- 174 Yan, S.-K. *et al.* “Omics” in pharmaceutical research: overview, applications, challenges, and future perspectives. *Chinese Journal of Natural Medicines* **13**, 3-21, doi:10.1016/s1875-5364(15)60002-4 (2015).
- 175 Shin, T. H. *et al.* Integration of metabolomics and transcriptomics in nanotoxicity studies. *BMB Reports* **51**, 14-20, doi:10.5483/bmbrep.2018.51.1.237 (2018).
- 176 Saarimäki, L. A. *et al.* Manually curated transcriptomics data collection for toxicogenomic assessment of engineered nanomaterials. *Scientific Data* **8**, doi:10.1038/s41597-021-00808-y (2021).
- 177 Kong, L. *et al.* NanoMiner — Integrative Human Transcriptomics Data Resource for Nanoparticle Research. *PLoS ONE* **8**, e68414, doi:10.1371/journal.pone.0068414 (2013).
- 178 Lim, D.-H. *et al.* The effects of sub-lethal concentrations of silver nanoparticles on inflammatory and stress genes in human macrophages using cDNA microarray analysis. *Biomaterials* **33**, 4690-4699, doi:<https://doi.org/10.1016/j.biomaterials.2012.03.006> (2012).
- 179 Akbari, F., Peymani, M., Salehzadeh, A. & Ghaedi, K. Integrative in silico and in vitro transcriptomics analysis revealed new lncRNAs related to intrinsic apoptotic genes in colorectal cancer. *Cancer Cell International* **20**, doi:10.1186/s12935-020-01633-w (2020).

- 180 Alsagaby, S. A. *et al.* Transcriptomics-Based Characterization of the Toxicity of ZnO Nanoparticles Against Chronic Myeloid Leukemia Cells. *International Journal of Nanomedicine* **15**, 7901-7921, doi:10.2147/ijn.s261636 (2020).
- 181 Gurunathan, S. *et al.* Evaluation of Graphene Oxide Induced Cellular Toxicity and Transcriptome Analysis in Human Embryonic Kidney Cells. *Nanomaterials-Basel* **9**, 969, doi:10.3390/nano9070969 (2019).
- 182 Gurunathan, S. *et al.* Anisotropic Platinum Nanoparticle-Induced Cytotoxicity, Apoptosis, Inflammatory Response, and Transcriptomic and Molecular Pathways in Human Acute Monocytic Leukemia Cells. *International Journal of Molecular Sciences* **21**, 440, doi:10.3390/ijms21020440 (2020).
- 183 Chen, J., Lu, L., Zhang, C., Zhu, X. & Zhuang, S. Endothelial dysfunction and transcriptome aberration in mouse aortas induced by black phosphorus quantum dots and nanosheets. *Nanoscale* **13**, 9018-9030, doi:10.1039/d1nr01965a (2021).
- 184 Horstmann, C., Campbell, C., Kim, D. S. & Kim, K. Transcriptome profile with 20 nm silver nanoparticles in yeast. *FEMS Yeast Res* **19**, doi:10.1093/femsyr/foz003 (2019).
- 185 Davenport, V., Horstmann, C., Patel, R., Wu, Q. & Kim, K. An Assessment of InP/ZnS as Potential Anti-Cancer Therapy: Quantum Dot Treatment Increases Apoptosis in HeLa Cells. *Journal of Nanotheranostics* **2**, 16-32, doi:10.3390/jnt2010002 (2021).
- 186 Jiang, T., Jin, K., Liu, X. & Pang, Z. in *Biopolymer-Based Composites* 221-267 (2017).
- 187 Sun, T. *et al.* Engineered nanoparticles for drug delivery in cancer therapy. *Angew Chem Int Ed Engl* **53**, 12320-12364, doi:10.1002/anie.201403036 (2014).
- 188 Goodman, T. T., Ng, C. P. & Pun, S. H. 3-D Tissue Culture Systems for the Evaluation and Optimization of Nanoparticle-Based Drug Carriers. *Bioconjugate Chemistry* **19**, 1951-1959, doi:10.1021/bc800233a (2008).
- 189 Lin, A. *et al.* Shear-regulated uptake of nanoparticles by endothelial cells and development of endothelial-targeting nanoparticles. *J Biomed Mater Res A* **93**, 833-842, doi:10.1002/jbm.a.32592 (2010).
- 190 Zhang, Y. & Yang, W. X. Tight junction between endothelial cells: the interaction between nanoparticles and blood vessels. *Beilstein J Nanotechnol* **7**, 675-684, doi:10.3762/bjnano.7.60 (2016).

- 191 Jutila, M. A., Walcheck, B., Bargatze, R. & Palecanda, A. 239-256 (Humana Press, 2007).
- 192 Cochran, J. C., Gatial, J. E., Kapoor, T. M. & Gilbert, S. P. Monastrol Inhibition of the Mitotic Kinesin Eg5. *Journal of Biological Chemistry* **280**, 12658-12667, doi:10.1074/jbc.m413140200 (2005).
- 193 Chin, G. M. & Herbst, R. Induction of apoptosis by monastrol, an inhibitor of the mitotic kinesin Eg5, is independent of the spindle checkpoint. *Molecular Cancer Therapeutics* **5**, 2580-2591, doi:10.1158/1535-7163.mct-06-0201 (2006).
- 194
- 195 Qdot® 605 ITK™
- 196 iBidi μ-Slide I 0.2.
- 197 Pong, B.-K., Trout, B. L. & Lee, J.-Y. Modified Ligand-Exchange for Efficient Solubilization of CdSe/ZnS Quantum Dots in Water: A Procedure Guided by Computational Studies. *Langmuir* **24**, 5270-5276, doi:10.1021/la703431j (2008).
- 198 Nafee, N., Schneider, M., Schaefer, U. F. & Lehr, C.-M. Relevance of the colloidal stability of chitosan/PLGA nanoparticles on their cytotoxicity profile. *International Journal of Pharmaceutics* **381**, 130-139, doi:10.1016/j.ijpharm.2009.04.049 (2009).
- 199 Koley, D. & Bard, A. J. Triton X-100 concentration effects on membrane permeability of a single HeLa cell by scanning electrochemical microscopy (SECM). *P Natl Acad Sci USA* **107**, 16783-16787, doi:10.1073/pnas.1011614107 (2010).
- 200 Legato Syringe Pump.
- 201 Huang, Q. *et al.* Fluid shear stress and tumor metastasis. *Am J Cancer Res* **8**, 763-777 (2018).
- 202 Lim, M. *et al.* Synthesis of far-red- and near-infrared-emitting Cu-doped InP/ZnS (core/shell) quantum dots with controlled doping steps and their surface functionalization for bioconjugation. *Nanoscale* **11**, 10463-10471 (2019).
- 203 Wegner, K. D. *et al.* Influence of the Core/Shell Structure of Indium Phosphide Based Quantum Dots on Their Photostability and Cytotoxicity. *Front Chem* **7** (2019).
- 204 Yaehe, K. *et al.* Nanoparticle Accumulation in Angiogenic Tissues: Towards Predictable Pharmacokinetics. *Small* **9**, 3118-3127, doi:10.1002/smll.201201848 (2013).

- 205 Chibli, H., Carlini, L., Park, S., Dimitrijevic, N. M. & Nadeau, J. L. Cytotoxicity of InP/ZnS quantum dots related to reactive oxygen species generation. *Nanoscale* **3**, 2552-2559 (2011).
- 206 Lee, S. *et al.* InP-Quantum-Dot-in-ZnS-Matrix Solids for Thermal and Air Stability. *Chemistry of Materials* **32**, 9584-9590, doi:10.1021/acs.chemmater.0c02870 (2020).
- 207 Kuno, M. *et al.* Fluorescence Intermittency in Single InP Quantum Dots. *Nano Letters* **1**, 557-564, doi:10.1021/nl010049i (2001).
- 208 Tamang, S., Beaune, G., Texier, I. & Reiss, P. Aqueous Phase Transfer of InP/ZnS Nanocrystals Conserving Fluorescence and High Colloidal Stability. *ACS Nano* **5**, 9392-9402, doi:10.1021/nn203598c (2011).
- 209 Brichkin, S. B. *et al.* Colloidal quantum dots InP@ZnS: Inhomogeneous broadening and distribution of luminescence lifetimes. *High Energ Chem+* **50**, 395-399 (2016).
- 210 Grandhi, G. K., M, A. & Viswanatha, R. Understanding the Role of Surface Capping Ligands in Passivating the Quantum Dots Using Copper Dopants as Internal Sensor. *The Journal of Physical Chemistry C* **120**, 19785-19795, doi:10.1021/acs.jpcc.6b04060 (2016).
- 211 Chandrasekaran, V. *et al.* Nearly Blinking-Free, High-Purity Single-Photon Emission by Colloidal InP/ZnSe Quantum Dots. *Nano Letters* **17**, 6104-6109 (2017).
- 212 Ding, C. *et al.* Passivation Strategy of Reducing Both Electron and Hole Trap States for Achieving High-Efficiency PbS Quantum-Dot Solar Cells with Power Conversion Efficiency over 12%. *Acs Energy Lett* **5**, 3224-3236 (2020).
- 213 Wang, L. S. *et al.* Surface organic ligand-passivated quantum dots: toward high-performance light-emitting diodes with long lifetimes. *J Mater Chem C* **9**, 2483-2490 (2021).
- 214 Wadhavane, P. D. *et al.* Photoluminescence Enhancement of CdSe Quantum Dots: A Case of Organogel–Nanoparticle Symbiosis. *Journal of the American Chemical Society* **134**, 20554-20563, doi:10.1021/ja310508r (2012).
- 215 Bouïs, D., Hospers, G. A. P., Meijer, C., Molema, G. & Mulder, N. H. Endothelium in vitro: A review of human vascular endothelial cell lines for blood vessel-related research. *Angiogenesis* **4**, 91-102, doi:10.1023/a:1012259529167 (2001).

- 216 Bachetti, T. & Morbidelli, L. ENDOTHELIAL CELLS IN CULTURE: A MODEL FOR STUDYING VASCULAR FUNCTIONS. *Pharmacological Research* **42**, 9-19, doi:10.1006/phrs.1999.0655 (2000).
- 217 Poussin, C. *et al.* 3D human microvessel-on-a-chip model for studying monocyte-to-endothelium adhesion under flow - application in systems toxicology. *ALTEX* **37**, 47-63, doi:10.14573/altex.1811301 (2020).
- 218 Polacheck, W. J., Kutys, M. L., Tefft, J. B. & Chen, C. S. Microfabricated blood vessels for modeling the vascular transport barrier. *Nat Protoc* **14**, 1425-1454, doi:10.1038/s41596-019-0144-8 (2019).
- 219 Takehara, H., Sakaguchi, K., Sekine, H., Okano, T. & Shimizu, T. Microfluidic vascular-bed devices for vascularized 3D tissue engineering: tissue engineering on a chip. *Biomed Microdevices* **22**, 9, doi:10.1007/s10544-019-0461-2 (2019).
- 220 Krüger, G., Blocki, Franke & Jung. Vascular Endothelial Cell Biology: An Update. *International Journal of Molecular Sciences* **20**, 4411, doi:10.3390/ijms20184411 (2019).
- 221 Mannino, R. G., Pandian, N. K., Jain, A. & Lam, W. A. Engineering "Endothelialized" Microfluidics for Investigating Vascular and Hematologic Processes Using Non-Traditional Fabrication Techniques. *Curr Opin Biomed Eng* **5**, 13-20, doi:10.1016/j.cobme.2017.11.006 (2018).
- 222 Janssen, A., Van Der Burg, M., Szuhai, K., Kops, G. J. P. L. & Medema, R. H. Chromosome Segregation Errors as a Cause of DNA Damage and Structural Chromosome Aberrations. *Science* **333**, 1895-1898, doi:10.1126/science.1210214 (2011).
- 223 Zhang, J. *et al.* InP/ZnSe/ZnS quantum dots with strong dual emissions: visible excitonic emission and near-infrared surface defect emission and their application in in vitro and in vivo bioimaging. *J Mater Chem B* **5**, 8152-8160 (2017).
- 224 Hussain, S. *et al.* One-Pot Fabrication of High-Quality InP/ZnS (Core/Shell) Quantum Dots and Their Application to Cellular Imaging. *Chemphyschem* **10**, 1466-1470 (2009).
- 225 Belsey, N. A., Shard, A. G. & Minelli, C. Analysis of protein coatings on gold nanoparticles by XPS and liquid-based particle sizing techniques. *Biointerphases* **10**, 019012, doi:doi:<http://dx.doi.org/10.1116/1.4913566> (2015).

- 226 Wegner, K. D. *et al.* Influence of the Core/Shell Structure of Indium Phosphide Based Quantum Dots on Their Photostability and Cytotoxicity. *Front Chem* **7**, doi:10.3389/fchem.2019.00466 (2019).
- 227 Male, K. B., Lachance, B., Hrapovic, S., Sunahara, G. & Luong, J. H. T. Assessment of Cytotoxicity of Quantum Dots and Gold Nanoparticles Using Cell-Based Impedance Spectroscopy. *Analytical Chemistry* **80**, 5487-5493, doi:10.1021/ac8004555 (2008).
- 228 Qin, K. R. *et al.* Dynamic modeling for shear stress induced ATP release from vascular endothelial cells. *Biomechanics and Modeling in Mechanobiology* **7**, 345-353, doi:10.1007/s10237-007-0088-8 (2008).
- 229 Kaiser, D., Freyberg, M.-A. & Friedl, P. Lack of Hemodynamic Forces Triggers Apoptosis in Vascular Endothelial Cells. *Biochemical and Biophysical Research Communications* **231**, 586-590, doi:<https://doi.org/10.1006/bbrc.1997.6146> (1997).
- 230 Nerem, R. M. *et al.* The Study of the Influence of Flow on Vascular Endothelial Biology. *The American Journal of the Medical Sciences* **316(3)**, 169–175, doi:[http://doi.org/10.1016/s0002-9629\(15\)40397-0](http://doi.org/10.1016/s0002-9629(15)40397-0) (1998).
- 231 Tan, A., Lam, Y. Y., Pacot, O., Hawley, A. & Boyd, B. J. Probing cell–nanoparticle (cubosome) interactions at the endothelial interface: do tissue dimension and flow matter? *Biomater Sci-Uk* **7**, 3460-3470, doi:10.1039/c9bm00243j (2019).
- 232 Yang, Y. *et al.* Pumpless microfluidic devices for generating healthy and diseased endothelia. *Lab Chip* **19**, 3212-3219, doi:10.1039/c9lc00446g (2019).
- 233 Caballero, D., Blackburn, S. M., de Pablo, M., Samitier, J. & Albertazzi, L. Tumour-vessel-on-a-chip models for drug delivery. *Lab Chip* **17**, 3760-3771, doi:10.1039/c7lc00574a (2017).
- 234 Abudupataer, M. *et al.* Bioprinting a 3D vascular construct for engineering a vessel-on-a-chip. *Biomed Microdevices* **22**, 10, doi:10.1007/s10544-019-0460-3 (2019).
- 235 Cooley, M. *et al.* Influence of particle size and shape on their margination and wall-adhesion: implications in drug delivery vehicle design across nano-to-micro scale. *Nanoscale* **10**, 15350-15364, doi:10.1039/c8nr04042g (2018).
- 236 Mannino, R. G., Qiu, Y. & Lam, W. A. Endothelial cell culture in microfluidic devices for investigating microvascular processes. *Biomicrofluidics* **12**, 042203, doi:10.1063/1.5024901 (2018).

- 237 Bussolati, B., Grange, C. & Camussi, G. Tumor exploits alternative strategies to achieve vascularization. *The FASEB Journal* **25**, 2874-2882, doi:10.1096/fj.10-180323 (2011).
- 238 Molema, G., De Leij, L. F. M. H. & Meijer, D. K. F. Tumor Vascular Endothelium: Barrier or Target in Tumor Directed Drug Delivery and Immunotherapy. *Pharmaceutical Research* **14**, 2-10, doi:10.1023/a:1012038930172 (1997).
- 239 Roberts, W. G. *et al.* Host Microvasculature Influence on Tumor Vascular Morphology and Endothelial Gene Expression. *The American Journal of Pathology* **153**, 1239-1248, doi:[https://doi.org/10.1016/S0002-9440\(10\)65668-4](https://doi.org/10.1016/S0002-9440(10)65668-4) (1998).
- 240 Chen, T. *et al.* Cytotoxicity of InP/ZnS Quantum Dots With Different Surface Functional Groups Toward Two Lung-Derived Cell Lines. *Frontiers in Pharmacology* **9**, doi:10.3389/fphar.2018.00763 (2018).
- 241 Xiao, K., Liu, Q., Li, H., Xia, Q. & Liu, Y. Role of surface charge in determining the biological effects of CdSe/ZnS quantum dots. *International Journal of Nanomedicine*, 7073, doi:10.2147/ijn.s94543 (2015).
- 242 Tan, S. J., Jana, N. R., Gao, S., Patra, P. K. & Ying, J. Y. Surface-Ligand-Dependent Cellular Interaction, Subcellular Localization, and Cytotoxicity of Polymer-Coated Quantum Dots. *Chemistry of Materials* **22**, 2239-2247, doi:10.1021/cm902989f (2010).
- 243 Verma, A. & Stellacci, F. Effect of Surface Properties on Nanoparticle-Cell Interactions. *Small* **6**, 12-21, doi:10.1002/sml.200901158 (2010).
- 244 Elena, A. P. *et al.* Luminescent quantum dots encapsulated by zwitterionic amphiphilic polymer: surface charge-dependent interaction with cancer cells. *Journal of the Belarusian State University. Chemistry* (2018).
- 245 Blumenberg, M. in *Transcriptome Analysis* (IntechOpen, 2019).
- 246 Horstmann, C., Davenport, V., Zhang, M., Peters, A. & Kim, K. Transcriptome Profile Alterations with Carbon Nanotubes, Quantum Dots, and Silver Nanoparticles: A Review. *Genes* **12**, 794, doi:10.3390/genes12060794 (2021).
- 247 Hu, H. *et al.* Gene expression profiles and bioinformatics analysis of human umbilical vein endothelial cells exposed to PM 2.5. *Chemosphere* **183**, 589-598, doi:10.1016/j.chemosphere.2017.05.153 (2017).
- 248 Chang, S. *et al.* Cytotoxicity, cytokine release and ER stress-autophagy gene expression in endothelial cells and alveolar-endothelial co-culture exposed to pristine and

- carboxylated multi-walled carbon nanotubes. *Ecotoxicology and Environmental Safety* **161**, 569-577, doi:10.1016/j.ecoenv.2018.06.025 (2018).
- 249 Costouros, N. G. & Libutti, S. K. Microarray technology and gene expression analysis for the study of angiogenesis. *Expert Opinion on Biological Therapy* **2**, 545-556, doi:10.1517/14712598.2.5.545 (2002).
- 250 Choi, K.-C. *et al.* Smad6 negatively regulates interleukin 1-receptor–Toll-like receptor signaling through direct interaction with the adaptor Pellino-1. *Nature Immunology* **7**, 1057-1065, doi:10.1038/ni1383 (2006).
- 251 Harant, H. Negative cross-talk between the human orphan nuclear receptor Nur77/NAK-1/TR3 and nuclear factor- $\kappa$ B. *Nucleic Acids Research* **32**, 5280-5290, doi:10.1093/nar/gkh856 (2004).
- 252 Salcher, S., Hermann, M., Kiechl-Kohlendorfer, U., Ausserlechner, M. J. & Obexer, P. C10ORF10/DEPP-mediated ROS accumulation is a critical modulator of FOXO3-induced autophagy. *Molecular Cancer* **16**, doi:10.1186/s12943-017-0661-4 (2017).
- 253 UniProt. <https://www.uniprot.org/uniprot/P50591> (2021)
- 254 Min, E. *et al.* Activation of Smad 2/3 signaling by low shear stress mediates artery inward remodeling (Cold Spring Harbor Laboratory, 2019).
- 255 Poduri, A. *et al.* Endothelial cells respond to the direction of mechanical stimuli through SMAD signaling to regulate coronary artery size. *Development* **144**, 3241-3252, doi:10.1242/dev.150904 (2017).
- 256 Langille, B. L. Morphologic Responses of Endothelium to Shear Stress: Reorganization of the Adherens Junction. **8**, 195-206, doi:10.1111/j.1549-8719.2001.tb00169.x (2001).
- 257 Fonseca, C. G., Barbacena, P. & Franco, C. A. Endothelial cells on the move: dynamics in vascular morphogenesis and disease. *Vascular Biology* **2**, H29-H43, doi:10.1530/vb-20-0007 (2020).
- 258 Mahmoud, M. M. *et al.* Shear stress induces endothelial-to-mesenchymal transition via the transcription factor Snail. *Scientific Reports* **7**, doi:10.1038/s41598-017-03532-z (2017).
- 259 Walshe, T. E., dela Paz, N. G. & D'Amore, P. A. The role of shear-induced transforming growth factor- $\beta$  signaling in the endothelium. *Arteriosclerosis, thrombosis, and vascular biology* **33**, 2608-2617, doi:10.1161/atvbaha.113.302161 (2013).

- 260 Morikawa, M., Derynck, R. & Miyazono, K. TGF- $\beta$  and the TGF- $\beta$  Family: Context-Dependent Roles in Cell and Tissue Physiology. *Cold Spring Harbor Perspectives in Biology* **8**, a021873, doi:10.1101/cshperspect.a021873 (2016).
- 261 Zhang, Y., Alexander, P. B. & Wang, X.-F. TGF- $\beta$  Family Signaling in the Control of Cell Proliferation and Survival. *Cold Spring Harbor Perspectives in Biology* **9**, a022145, doi:10.1101/cshperspect.a022145 (2017).
- 262 Park, M.-J. *et al.* Nerve Growth Factor Induces Endothelial Cell Invasion and Cord Formation by Promoting Matrix Metalloproteinase-2 Expression through the Phosphatidylinositol 3-Kinase/Akt Signaling Pathway and AP-2 Transcription Factor. *Journal of Biological Chemistry* **282**, 30485-30496, doi:10.1074/jbc.m701081200 (2007).
- 263 Kirschner, N. *et al.* Contribution of Tight Junction Proteins to Ion, Macromolecule, and Water Barrier in Keratinocytes. *Journal of Investigative Dermatology* **133**, 1161-1169, doi:10.1038/jid.2012.507 (2013).
- 264 UniProt. <https://www.uniprot.org/uniprot/P09914> (2021)
- 265 Banerji, S. *et al.* LYVE-1, a New Homologue of the CD44 Glycoprotein, Is a Lymph-specific Receptor for Hyaluronan. *Journal of Cell Biology* **144**, 789-801, doi:10.1083/jcb.144.4.789 (1999).
- 266 Fulda, S. Modulation of Apoptosis by Natural Products for Cancer Therapy. *Planta Medica* **76**, 1075-1079, doi:10.1055/s-0030-1249961 (2010).
- 267 Dhillon, A. S., Hagan, S., Rath, O. & Kolch, W. MAP kinase signalling pathways in cancer. *Oncogene* **26**, 3279-3290, doi:10.1038/sj.onc.1210421 (2007).
- 268 Martin-Hijano, L. & Sainz, B. The Interactions Between Cancer Stem Cells and the Innate Interferon Signaling Pathway. *Frontiers in Immunology* **11**, doi:10.3389/fimmu.2020.00526 (2020).
- 269 Stern, R. Hyaluronan catabolism: a new metabolic pathway. *European Journal of Cell Biology* **83**, 317-325, doi:10.1078/0171-9335-00392 (2004).
- 270 Kobayashi, T., Chanmee, T. & Itano, N. Hyaluronan: Metabolism and Function. *Biomolecules* **10** (2020). <<http://europepmc.org/abstract/MED/33171800>>
- >
- 271 Erickson, M. & Stern, R. Chain Gangs: New Aspects of Hyaluronan Metabolism. *Biochemistry Research International* **2012**, 1-9, doi:10.1155/2012/893947 (2012).

- 272 Hata, A., Lagna, G., Massagué, J. & Hemmati-Brivanlou, A. Smad6 inhibits BMP/Smad1 signaling by specifically competing with the Smad4 tumor suppressor. *Genes Dev* **12**, 186-197, doi:10.1101/gad.12.2.186 (1998).
- 273 UniProt. <https://www.uniprot.org/uniprot/Q02363> (2021)
- 274 Zambrano, S. *et al.* GPRC5b Modulates Inflammatory Response in Glomerular Diseases via NF-κB Pathway. *Journal of the American Society of Nephrology* **30**, 1573-1586, doi:10.1681/asn.2019010089 (2019).
- 275 UniProt. <https://www.uniprot.org/uniprot/P09919> (2021)
- 276 Majkut, S., P.C & Dennis. Stress Sensitivity and Mechanotransduction during Heart Development. *Current Biology* **24**, R495-R501, doi:10.1016/j.cub.2014.04.027 (2014).
- 277 Mitchell, M. J. & King, M. R. Computational and experimental models of cancer cell response to fluid shear stress. *Front Oncol* **3**, 44 (2013).  
<<http://europepmc.org/abstract/MED/23467856>
- <https://www.ncbi.nlm.nih.gov/pmc/articles/pmid/23467856/pdf/?tool=EBI>
- <https://www.ncbi.nlm.nih.gov/pmc/articles/pmid/23467856/?tool=EBI>
- <https://doi.org/10.3389/fonc.2013.00044>
- <https://europepmc.org/articles/PMC3587800>
- <https://europepmc.org/articles/PMC3587800?pdf=render>>.
- 278 Cantarella, G. *et al.* Nerve growth factor–endothelial cell interaction leads to angiogenesis in vitro and in vivo. *The FASEB Journal* **16**, 1307-1309, doi:10.1096/fj.01-1000fje (2002).
- 279 James, A. C. *et al.* Notch4 reveals a novel mechanism regulating Notch signal transduction. *Biochimica et Biophysica Acta (BBA) - Molecular Cell Research* **1843**, 1272-1284, doi:10.1016/j.bbamcr.2014.03.015 (2014).
- 280 Kapoor, T. M., Mayer, T. U., Coughlin, M. L. & Mitchison, T. J. Probing Spindle Assembly Mechanisms with Monastrol, a Small Molecule Inhibitor of the Mitotic Kinesin, Eg5. *Journal of Cell Biology* **150**, 975-988, doi:10.1083/jcb.150.5.975 (2000).
- 281 EMBL-EBI. <https://www.ebi.ac.uk/QuickGO/term/GO:0007059> (2020)
- 282 UniProt. <https://www.uniprot.org/uniprot/Q9H5V8> (2021)

- 283 Benes, C. H., Poulogiannis, G., Cantley, L. C. & Soltoff, S. P. The SRC-associated protein CUB Domain-Containing Protein-1 regulates adhesion and motility. *Oncogene* **31**, 653-663, doi:10.1038/onc.2011.262 (2012).
- 284 Musella, M., Manic, G., De Maria, R., Vitale, I. & Sistigu, A. Type-I-interferons in infection and cancer: Unanticipated dynamics with therapeutic implications. *OncImmunology* **6**, e1314424, doi:10.1080/2162402x.2017.1314424 (2017).
- 285 Plataniias, L. C. Mechanisms of type-I- and type-II-interferon-mediated signalling. *Nature Reviews Immunology* **5**, 375-386, doi:10.1038/nri1604 (2005).
- 286 EMBL-EBI. <https://www.ebi.ac.uk/QuickGO/term/GO:0007059> (2020)
- 287 Chen, Y., Nam, S., Chaudhuri, O. & Huang, H.-C. The evolution of spindles and their mechanical implications for cancer metastasis. *Cell Cycle* **18**, 1671-1675, doi:10.1080/15384101.2019.1632137 (2019).
- 288 Kastan, M. B. & Bartek, J. Cell-cycle checkpoints and cancer. *Nature* **432**, 316-323, doi:10.1038/nature03097 (2004).
- 289 Verhey, K. J. & Hammond, J. W. Traffic control: regulation of kinesin motors. *Nature Reviews Molecular Cell Biology* **10**, 765-777, doi:10.1038/nrm2782 (2009).
- 290 Magidson, V. *et al.* The Spatial Arrangement of Chromosomes during Prometaphase Facilitates Spindle Assembly. *Cell* **146**, 555-567, doi:10.1016/j.cell.2011.07.012 (2011).
- 291 Papac-Milicevic, N. *et al.* The Interferon Stimulated Gene 12 Inactivates Vasculoprotective Functions of NR4A Nuclear Receptors. *Circulation Research* **110**, e50-e63, doi:10.1161/circresaha.111.258814 (2012).
- 292 Vázquez, F. *et al.* METH-1, a Human Ortholog of ADAMTS-1, and METH-2 Are Members of a New Family of Proteins with Angio-inhibitory Activity. *Journal of Biological Chemistry* **274**, 23349-23357, doi:10.1074/jbc.274.33.23349 (1999).
- 293 Nakajima, T., Fujino, S., Nakanishi, G., Kim, Y.-S. & Jetten, A. M. TIP27: a novel repressor of the nuclear orphan receptor TAK1/TR4. *Nucleic acids research* **32**, 4194-4204, doi:10.1093/nar/gkh741 (2004).
- 294 Lee, B. J. & Thake, C. D. Heat and Hypoxic Acclimation Increase Monocyte Heat Shock Protein 72 but Do Not Attenuate Inflammation following Hypoxic Exercise. *Frontiers in Physiology* **8**, doi:10.3389/fphys.2017.00811 (2017).

- 295 Pandit, L., Kolodziejska, K. E., Zeng, S. & Eissa, N. T. The physiologic aggresome mediates cellular inactivation of iNOS. *Proceedings of the National Academy of Sciences* **106**, 1211-1215, doi:10.1073/pnas.0810968106 (2009).
- 296 Abravaya, K., Phillips, B. & Morimoto, R. I. Attenuation of the heat shock response in HeLa cells is mediated by the release of bound heat shock transcription factor and is modulated by changes in growth and in heat shock temperatures. *Genes & Development* **5**, 2117-2127, doi:10.1101/gad.5.11.2117 (1991).
- 297 Lee, S. H., Kwon, J. Y., Kim, S.-Y., Jung, K. & Cho, M.-L. Interferon-gamma regulates inflammatory cell death by targeting necroptosis in experimental autoimmune arthritis. *Scientific Reports* **7**, doi:10.1038/s41598-017-09767-0 (2017).
- 298 UniProt. <https://www.uniprot.org/uniprot/Q8NFI5> (2018)
- 299 EMBL-EBI. <https://www.ebi.ac.uk/QuickGO/term/GO:0045926> (2007)
- 300 Bevilacqua, M. P., Poher, J. S., Wheeler, M. E., Cotran, R. S. & Gimbrone, M. A. Interleukin-1 activation of vascular endothelium. Effects on procoagulant activity and leukocyte adhesion. *The American journal of pathology* **121**, 394-403 (1985).
- 301 Gabay, C., Lamacchia, C. & Palmer, G. IL-1 pathways in inflammation and human diseases. *Nature Reviews Rheumatology* **6**, 232-241, doi:10.1038/nrrheum.2010.4 (2010).
- 302 EMBL-EBI. <https://www.ebi.ac.uk/QuickGO/term/GO:0097501> (2013)
- 303 Kaur, A. *et al.* ChaC2, an Enzyme for Slow Turnover of Cytosolic Glutathione. *Journal of Biological Chemistry* **292**, 638-651, doi:10.1074/jbc.m116.727479 (2017).
- 304 Mungrue, I. N., Pagnon, J., Kohanim, O., Gargalovic, P. S. & Lulis, A. J. CHAC1/MGC4504 Is a Novel Proapoptotic Component of the Unfolded Protein Response, Downstream of the ATF4-ATF3-CHOP Cascade. *The Journal of Immunology* **182**, 466-476, doi:10.4049/jimmunol.182.1.466 (2009).
- 305 Hieshima, K. *et al.* Molecular Cloning of a Novel Human CC Chemokine Liver and Activation-regulated Chemokine (LARC) Expressed in Liver. *Journal of Biological Chemistry* **272**, 5846-5853, doi:10.1074/jbc.272.9.5846 (1997).
- 306 UniProt. <https://www.uniprot.org/uniprot/P78556> (2021)
- 307 Janus, P. *et al.* Pro-death signaling of cytoprotective heat shock factor 1: upregulation of NOXA leading to apoptosis in heat-sensitive cells. *Cell Death & Differentiation* **27**, 2280-2292, doi:10.1038/s41418-020-0501-8 (2020).

- 308 Kopito, R. R. Aggresomes, inclusion bodies and protein aggregation. *Trends Cell Biol* **10**, 524-530, doi:10.1016/s0962-8924(00)01852-3 (2000).
- 309 Cao, Y. *et al.* TGF- $\beta$  repression of Id2 induces apoptosis in gut epithelial cells. *Oncogene* **28**, 1089-1098, doi:10.1038/onc.2008.456 (2009).
- 310 Shepherd, R. D., Kos, S. M. & Rinker, K. D. Flow-dependent Smad2 phosphorylation and TGIF nuclear localization in human aortic endothelial cells. *American Journal of Physiology-Heart and Circulatory Physiology* **301**, H98-H107, doi:10.1152/ajpheart.00668.2010 (2011).
- 311 EMBL-EBI. <https://www.ebi.ac.uk/QuickGO/term/GO:0070098> (2018).
- 312 Keane, M. P. & Strieter, R. M. Chemokine signaling in inflammation. *Critical Care Medicine* **28** (2000).
- 313 UniProt. <https://www.uniprot.org/uniprot/Q99879> (2021).
- 314 UniProt. <https://www.uniprot.org/uniprot/P26651> (2021).
- 315 Garapati, PV. CLEC7A/inflammasome pathway. Reactome. <https://reactome.org/content/detail/R-HSA-5660668> (2015)
- 316 EMBL-EBI. <https://www.ebi.ac.uk/QuickGO/term/GO:0071947> (2015).
- 317 Davies, P. F. & Tripathi, S. C. Mechanical stress mechanisms and the cell. An endothelial paradigm. *Circulation Research* **72**, 239-245, doi:10.1161/01.res.72.2.239 (1993).
- 318 Maul, T. M., Chew, D. W., Nieponice, A. & Vorp, D. A. Mechanical stimuli differentially control stem cell behavior: morphology, proliferation, and differentiation. *Biomechanics and Modeling in Mechanobiology* **10**, 939-953, doi:10.1007/s10237-010-0285-8 (2011).
- 319 Musacchio, A. & Hardwick, K. G. The spindle checkpoint: structural insights into dynamic signalling. *Nature Reviews Molecular Cell Biology* **3**, 731-741, doi:10.1038/nrm929 (2002).
- 320 EMBL-EBI. <https://www.ebi.ac.uk/QuickGO/term/GO:0000070> (2017)
- 321 UniProt. <https://www.uniprot.org/uniprot/P09919> (2021)
- 322 UniProt. <https://www.uniprot.org/uniprot/Q07011> (2021)
- 323 Kim, C. H. Chemokine-chemokine receptor network in immune cell trafficking. *Curr Drug Targets Immune Endocr Metabol Disord* **4**, 343-361, doi:10.2174/1568008043339712 (2004).

- 324 Mollica Poeta, V., Massara, M., Capucetti, A. & Bonecchi, R. Chemokines and Chemokine Receptors: New Targets for Cancer Immunotherapy. *Frontiers in Immunology* **10**, 379 (2019).
- 325 Bundy, D. L. & McKeithan, T. W. Diverse Effects of BCL3 Phosphorylation on Its Modulation of NF- $\kappa$ B p52 Homodimer Binding to DNA. *Journal of Biological Chemistry* **272**, 33132-33139, doi:10.1074/jbc.272.52.33132 (1997).
- 326 Liu, T., Zhang, L., Joo, D. & Sun, S.-C. NF- $\kappa$ B signaling in inflammation. *Signal Transduction and Targeted Therapy* **2**, 17023, doi:10.1038/sigtrans.2017.23 (2017).
- 327 EMBL-EBI. <https://www.ebi.ac.uk/QuickGO/term/GO:0070098> (2018)
- 328 Wang, Y. *et al.* Interferon- $\gamma$  Induces Human Vascular Smooth Muscle Cell Proliferation and Intimal Expansion by Phosphatidylinositol 3-Kinase-Dependent Mammalian Target of Rapamycin Raptor Complex 1 Activation. *Circulation Research* **101**, 560-569, doi:10.1161/circresaha.107.151068 (2007).
- 329 Utech, M. *et al.* Mechanism of IFN- $\gamma$ -induced Endocytosis of Tight Junction Proteins: Myosin II-dependent Vacuolarization of the Apical Plasma Membrane. *Molecular Biology of the Cell* **16**, 5040-5052, doi:10.1091/mbc.e05-03-0193 (2005).
- 330 Jorgovanovic, D., Song, M., Wang, L. & Zhang, Y. Roles of IFN- $\gamma$  in tumor progression and regression: a review. *Biomarker Research* **8**, doi:10.1186/s40364-020-00228-x (2020).
- 331 UniProt. <https://www.uniprot.org/uniprot/Q96QK1> (2021)
- 332 UniProt. <https://www.uniprot.org/uniprot/P53539> (2021)
- 333 UniProt. <https://www.uniprot.org/uniprot/Q5T8P6> (2021)
- 334 Sun, W. *et al.* PPM1A and PPM1B act as IKK $\beta$  phosphatases to terminate TNF $\alpha$ -induced IKK $\beta$ -NF- $\kappa$ B activation. *Cellular Signalling* **21**, 95-102, doi:10.1016/j.cellsig.2008.09.012 (2009).
- 335 UniProt. <https://www.uniprot.org/locations/SL-0251> (2021)
- 336 Fernandez, P. *et al.* Mitotic Spindle Orients Perpendicular to the Forces Imposed by Dynamic Shear. *PLoS ONE* **6**, e28965, doi:10.1371/journal.pone.0028965 (2011).
- 337 EMBL-EBI. <https://www.ebi.ac.uk/QuickGO/term/GO:0099073> (2016)
- 338 EMBL-EBI. <https://www.ebi.ac.uk/QuickGO/term/GO:0007059> (2020)

- 339 Itabashi, T., Takagi, J., Suzuki, K. & Ishiwata, S. I. Responses of chromosome segregation machinery to mechanical perturbations. *BIOPHYSICS* **9**, 73-78, doi:10.2142/biophysics.9.73 (2013).
- 340 EMBL-EBI. <https://www.ebi.ac.uk/QuickGO/term/GO:0016359> (2017)
- 341 UniProt. <https://www.uniprot.org/uniprot/Q92570> (2021)
- 342 UniProt. <https://www.uniprot.org/uniprot/Q13489> (2021)
- 343 EMBL-EBI. <https://www.ebi.ac.uk/QuickGO/term/GO:0005923> (2015)
- 344 Shi, J., Barakat, M., Chen, D. & Chen, L. Bicellular Tight Junctions and Wound Healing. *International Journal of Molecular Sciences* **19**, 3862, doi:10.3390/ijms19123862 (2018).
- 345 EMBL-EBI. <https://www.ebi.ac.uk/QuickGO/term/GO:0031252> (2019)
- 346 Günther, J. & Seyfert, H.-M. The first line of defence: insights into mechanisms and relevance of phagocytosis in epithelial cells. *Seminars in Immunopathology* **40**, 555-565, doi:10.1007/s00281-018-0701-1 (2018).
- 347 Pober, J. S. & Sessa, W. C. Evolving functions of endothelial cells in inflammation. *Nature Reviews Immunology* **7**, 803-815, doi:10.1038/nri2171 (2007).
- 348 EMBL-EBI. <https://www.ebi.ac.uk/QuickGO/term/GO:0007059> (2020)
- 349 EMBL-EBI. <https://www.ebi.ac.uk/QuickGO/term/GO:0140014> (2020)
- 350 UniProt. <https://www.uniprot.org/uniprot/Q9NX09> (2021).
- 351 Mula, R. V., Bhatia, V. & Falzon, M. PTHrP promotes colon cancer cell migration and invasion in an integrin  $\alpha 6 \beta 4$ -dependent manner through activation of Rac1. *Cancer Lett* **298**, 119-127, doi:10.1016/j.canlet.2010.06.009 (2010).
- 352 Reactome. <https://reactome.org/content/detail/R-HSA-3371571> (2021)
- 353 Richard, L. C. & Yesim, G.-P. HSF1 as a Cancer Biomarker and Therapeutic Target. *Current Cancer Drug Targets* **19**, 515-524, doi:<http://dx.doi.org/10.2174/1568009618666181018162117> (2019).
- 354 Laity, J. H. & Andrews, G. K. Understanding the mechanisms of zinc-sensing by metal-response element binding transcription factor-1 (MTF-1). *Archives of Biochemistry and Biophysics* **463**, 201-210, doi:10.1016/j.abb.2007.03.019 (2007).
- 355 EMBL-EBI. <https://www.ebi.ac.uk/QuickGO/term/GO:0051085> (2017).
- 356 EMBL-EBI. <https://www.ebi.ac.uk/QuickGO/term/GO:0097501> (2013).

357 Labouta, H. I. *et al.* Bacteriomimetic invasin-functionalized nanocarriers for intracellular delivery. *Journal of Controlled Release* **220**, 414-424, doi:10.1016/j.jconrel.2015.10.052 (2015).